DOUBLE DATING DETRITAL ZIRCONS IN TILL FROM THE ROSS EMBAYMENT, ANTARCTICA

Bethany Marie Welke

Submitted to the faculty of the University Graduate School
in partial fulfillment of the requirements
for the degree
Master of Science
in the Department of Earth Science,
Indiana University

September 2013

Accepted by the Faculty of Indiana University, in partial fulfillment of the requirements for the degree of Master of Science.

Kathy J. Licht, PhD

Sidney R. Hemming, PhD

Master's Thesis
Committee

Pamela A. Martin, PhD

ACKNOWLEDGEMENTS

I'd like to express my gratitude to my advisor, Dr. Kathy Licht for this opportunity to work on this wonderful project. She was abundantly helpful and offered excellent guidance, encouragement, enthusiasm, and support throughout this research and thesis. I could have not wished for a better or friendlier advisor. Thank you, Kathy, for introducing me to the Antarctic world, and geochronology.

I am also thankful to my committee members, Dr. Sidney Hemming and Dr. Pamela Martin for their useful comments, conversations, and engagement throughout this research.

I would like to thank my fellow lab mates and friends, Nicole Bader and Theresa Dits, for helping me out the past two years, for their assistance and support, for helping me throughout all the good times, bad times, humorous times, and keeping me sane. Thank you for the wonderful memories.

In my daily work at IUPUI, I'm thankful for a friendly group of fellow graduate and undergraduate students including Samapriya Roy, Anna Samuels, Shiva Laden, Fotios Kafantaris, Justin Hodgson and Alex Schnur and others. Without their friendship, support, and numerous coffee trips I would have never pulled through. I would also like to thank the staff in the Earth Sciences Department at IUPUI for their help in the past two years.

In addition, a thank you to Mark Pecha, Clay Loehn and other staff at the University of Arizona Laserchron Center for their assistance in zircon imaging and U/Pb analyses and Erin Abel and Uttam Chowdhury at the Radiogenic Helium Laboratory for their assistance in zircon picking and (U-Th)/He analysis. I'd also like to thank Dr. Stuart

Thomson and Dr. Paul Fitzgerald for their helpful conversations and insightful comments and Dr. Leigh Stearns for constructing an ice flow map of the Ross Embayment.

I would also like to thank my parents, grandparents, and the rest of my family. They have always encouraged me with their constant support.

This research was supported by the National Science Foundation Office of Polar Programs grant NSF OPP-1043572, a 2012 Geological Society of America Graduate Student Research Grant, IUPUI Educational Enhancement Grant and IUPUI School of Science Graduate Student Council Grant.

ABSTRACT

Bethany Marie Welke

DOUBLE DATING DETRITAL ZIRCONS IN TILL FROM THE ROSS EMBAYMENT, ANTARCTICA

U/Pb and (U-Th)/He (ZHe) dating of detrital zircons from glacial till samples in the Ross Embayment, Antarctica records cooling after the Ross/Pan-African orogeny (450-625 Ma) followed by a mid-Jurassic to mid-Cretaceous heating event in the Beacon basin. Zircons were extracted from till samples from heads of major outlet glaciers in East Antarctica, one sample at the mouth of Scott Glacier, and from beneath three West Antarctic ice streams. The Ross/Pan-African U/Pb population is ubiquitous in these Antarctic tills and many Beacon Supergroup sandstones, thus 83 grains were analyzed for ZHe to subdivide this population. Two ZHe age populations are evident in East Antarctic tills, with 64% of grains 115-200 Ma and 35% between 200-650 Ma. The older population is interpreted to be associated with the Ross/Pan-African orogeny including cooling of the Granite Harbour Intrusives and/or exhumation of the older basement rocks to form the Kukri Peneplain. The lag time between zircon U/Pb, ZHe and $^{40}Ar/^{39}Ar$ ages from K-bearing minerals show cooling over 200 My. Grains in East Antarctic tills with a ZHe age of 115-200 Ma likely reflects regional heating following the breakup of Gondwana from the Ferrar dolerite intrusions, subsidence within the rift basin, and a higher geothermal gradient. Subsequent cooling and/or exhumation of the Transantarctic Mountains brought grains below the closure temperature over a span of 80 My. This population may also provide a Beacon Supergroup signature as most of the tills with this age are adjacent to nunataks mapped as Beacon Supergroup and contain an abundance of

Beacon pebbles within the moraine. Nine zircons grains from three Beacon Supergroup sandstones collected from moraines across the Transantarctic Mountains yield ages from 125-180 Ma. West Antarctic tills contain a range of ZHe ages from 75-450 Ma reflecting the diverse provenance of basin fill from East Antarctica and Marie Byrd Land. ZHe and U/Pb ages <105 Ma appear to be distinctive of West Antarctic tills. The combination of U/Pb, ZHe and $^{40}Ar/^{39}Ar$ analyses demonstrates that these techniques can be used to better constrain the tectonic evolution and cooling of the inaccessible subglacial source terrains beneath the Antarctic Ice Sheet.

Kathy J. Licht, PhD

Table of Contents

List of Tables

List of Figures

1. Introduction

Detrital minerals glacially eroded from the interior of Antarctica then transported to the ice sheet surface provide opportunities to study the history and geology of both the continent and the East and West Antarctic ice sheets. Antarctica is 98% ice covered making the subglacial geology difficult to determine. What is known about the geology of Antarctica is based on satellite imagery, geophysical models, aerogeophysical data, ocean sediments, and limited outcrops around the perimeter and in mountain ranges. Glacial till is an additional resource that can be used to characterize provenance signatures of local and far-derived subglacial material to differentiate otherwise unknown geologic terrains in Antarctica. It is important to characterize sediment provenance signatures to trace the origin of sediment from marine sediment cores back to its source region. This is one method used to reconstruct paleo ice flow lines which is essential in modeling future ice sheet dynamics and selecting future coring sites. Furthermore, till provides information about the geological record in Antarctica which contains valuable information to understand the history and tectonic evolution of Antarctica.

An explanation for the development of the Antarctic Ice Sheet beginning in the Oligocene requires consideration of large scale changes, including the breakup of Gondwana and tectonic evolution over time, that created high relief as nucleation points for ice sheet growth [*DeConto and Pollard*, 2003]. However, the late Mesozoic-early Cenozoic history of Antarctica leading up to the period of ice sheet development remains poorly constrained because of the extensive ice sheet cover which limits access into the subglacial bedrock.

The Transantarctic Mountains separate East and West Antarctica (Figure 1) and are unique because they are a non-compressional mountain range thought to have formed as a result of rifting within the Antarctic Plate [*Talarico and Kleinschmidt*, 2009]; mountains associated with rifting do not typically reach heights of over 4,500 m and extend for over 3,500 km. The timing of uplift and exhumation, as well as uplift mechanisms of the Transantarctic Mountains are not well known. Knowledge of the landscape prior to exhumation of the Transantarctic Mountains is also important to consider, but is limited because the sedimentary record and tectonic structure remains ice covered. Low temperature thermochronology can be used to constrain the cooling history

and exhumation of areas like the Transantarctic Mountains and some studies have been done [*Gleadow and Fitzgerald*, 1987; *Fitzgerald and Gleadow*, 1988; *Fitzgerald*, 1992; *Stump and Fitzgerald*, 1992; *Fitzgerald*, 1994; *Fitzgerald and Stump*, 1997]. In the case of Antarctica, this study presents an example of the combination of multiple geochronometers on glacial till which is a powerful tool to extrapolate the subglacial geology of Antarctica.

The marine sediment record in the continental shelf and the deep sea surrounding Antarctica contains a record of fluctuations of the East and West Antarctic ice sheets. Terrigenous sediments eroded from Antarctic bedrock are transported offshore through glacial and marine processes. A variety of provenance tools have been applied to offshore till around the continent and have provided new insights into the geology of the subglacial Antarctic bedrock, the evolution of the Gamburtsev Moutains, and past ice flow paths [e.g., *Licht et al*., 2005; *Roy et al*., 2007; *van de Fliert et al*., 2008; *Cox et al.*, 2009; *Schilling*, 2010; *Williams et al*., 2010; *Pierce et al*., 2011; *Licht and Palmer*, 2013]. When provenance signatures of southern ocean sediment are linked to those of Antarctic bedrock, this provides a method for assessing changes in ice sheet dynamics [*Pierce et al*., 2011]. However, tracing offshore sediment to its source can be difficult when there is either limited information on the subglacial geology or the source terrains lack of distinctive characteristics. Characterizing glacial till in the Transantarctic Mountains and beneath West Antarctic ice streams makes it possible to better fingerprint potential source areas in East and West Antarctica [*Schilling*, 2010; *Licht and Palmer*, 2013].

The Ross Embayment has been one of the main regions for assessing the stability of the Antarctic Ice Sheet because it is one of the major drainage basins of the East and West Antarctic ice sheets and collection of sediment cores is less hampered by ice cover than the Weddell Sea. The sedimentary record on the continental shelf of the Ross Sea contains a record of numerous advances and retreats of the ice sheets [e.g., *Anderson*, 1999; *Naish et al*., 2009]. Comparison of distinctive characteristics from West and East Antarctic tills to Ross Sea tills through sand petrography, geochemistry and geochronology makes it possible to fingerprint inaccessible source terrains and link Ross Sea till to a source, providing constraints for reconstruction of paleo-ice flow lines in the

Ross Embayment for the Last Glacial Maximum [*Licht et al*., 2005; *Schilling et al*., 2010; *Licht and Palmer*, 2013].

The Antarctic Ice Sheet, if entirely melted, would contribute to a 57 m increase in global sea level rise [*Lythe and Vaughan*, 2001], which would have extreme economic and societal impacts, along with influencing weather and climate patterns on a global scale. Stratigraphic records from the continental margin of Antarctica, such as ANDRILL and the Cape Roberts Project, provide valuable information about the Cenozoic paleoclimate and glacial history of Antarctica, which can be used to help constrain predictions of future climate change [e.g., *Barrett et al.*, 2000, 2001; *Naish et al*., 2001; *Harwood et al*., 2002; *Hambrey*, 2002; *Prebble et al*., 2006; *Pollard and DeConto*, 2009]. The need for models that accurately reproduce past ice sheet configurations and project future ice sheet changes are crucial as global temperatures continue to rise [*Alley et al*., 2005].

To constrain ice sheet history in the Ross Embayment as well as the geologic and thermal history of the Transantarctic Mountains, we have utilized detrital materials, with a focus on zircons, contained within till collected from moraines along the Transantarctic Mountains and ice streams in West Antarctica. We applied U/Pb and (U-Th)/He to single zircon grains, as well as $^{40}Ar/^{39}Ar$ of hornblende and micas to create an extensive new dataset that provides insight into the effects of heating associated with the thermal evolution the Ross Embayment since the Ross Orogeny.

1.1 Provenance Tools

1.1.1 U/Pb dating of detrital zircons

Zircon ($ZrSiO_4$) is a trace mineral formed in igneous rocks, potentially overprinted in metamorphic rocks and/or recycled in sedimentary rocks. U/Pb data measured on zircons allow calculation of a formation age, indicating the timing of crystallization from igneous and metamorphic conditions. The closure temperature for zircon U/Pb is >900°C [*Cherniak and Watson*, 2001]. Zircons are resistant to physical and chemical weathering, occur in many rock types, and have the ability to retain U, Th, Pb and intermediate decay products [*Reiners et al*., 2004]; therefore their ages are used to identify thermal events or a high grade metamorphic overprint. These factors make zircon

useful for geochronologic and thermochronologic studies by providing age constraints on a wide variety of geologic terrains [*Reiners et al*., 2004].

Detrital U/Pb zircon geochronology is a valuable tool for provenance studies and has been used to identify source areas of Ross Sea till by comparing age spectra to those in East and West Antarctica [*Palmer*, 2008; *Schilling*, 2010; *Licht and Palmer*, 2013]. While U/Pb ages of zircons are useful to compare the spatial distribution of crystallization ages of zircons across the Ross Embayment, the dominant U/Pb age populations are ubiquitous. In particular, detrital zircons associated with the Ross/Pan-African Orogeny (450-625 Ma) are widespread in East and West Antarctic tills, Permian Beacon Supergroup sandstones, Eocene erratic sandstones, and in offshore sediments [*Elliot and Fanning*, 2008; *Schilling*, 2010; *Paulsen et al*., 2011; *Palmer et al*., 2012; *Licht and Palmer*, 2013], potentially making them of limited use as a provenance tracer. In one case study along the Byrd Glacier, the U/Pb age spectra within this group of Ross/Pan-African age grains were shown to vary spatially from the mouth to the head of Byrd Glacier, and were useful in distinguishing debris eroded at the head versus the walls of the Byrd Glacier trough [*Licht and Palmer*, 2013]. Given the widespread nature of Ross/Pan-African age zircons, other analytical approaches are typically required to better identify source terrains.

1.1.2 (U-Th)/He dating of detrital zircon

(U-Th)/He is one low temperature thermochronometer that records cooling associated with erosion and exhumation. Zircon contains high concentrations of U and Th, suitable for (U-Th)/He (ZHe) dating. ZHe dating is based on the idea that α-particles (He atoms) produced during radioactive decay of U to Th may be ejected from the crystal until the mineral reaches a certain closure temperature. At this closure temperature the rate that He atoms are produced exceeds the amount of He atoms escaping from the crystal, allowing them to build up in the mineral over time. The (U-Th)/He age is the time elapsed since the mineral was last at its closure temperature. The closure temperature for ZHe analysis is 160-200°C [*Reiners et al*., 2004] (~6-8 km crustal depth with a geothermal gradient of 25°C/km).

Zircon double dating that is measurement of U/Pb and (U-Th)/He on the same grain can be used to subdivide a common U/Pb zircon population by identifying a

separate cooling age [*Reiners et al*., 2004]. In this study, we focus on double dating detrital zircons from tills collected from West Antarctic ice streams and the moraines at heads of major outlet glaciers in the Transantarctic Mountains, as well as Beacon Supergroup sandstone samples. All till samples and Beacon sandstones are dominated by zircons with a U/Pb age 450-625 Ma, indicating the grains originated from magmatic processes or metamorphic overprinting during the Ross/Pan-African Orogeny. The aim in this study is to assess whether the ubiquitous Ross/Pan-African age grains (450-625 Ma) can be subdivided based on their ZHe age.

1.1.3 $^{40}Ar/^{39}Ar$ dating of detrital K-bearing minerals

The $^{40}Ar/^{39}Ar$ method is based on the decay of ^{40}K to ^{40}Ar in K-bearing minerals, such as hornblende, biotite and muscovite. These minerals are less resistant to weathering than zircon and so do not typically survive sedimentary recycling. Hornblende has a closure temperature of 400-600°C [*Harrison,* 1982; *Dahl,* 1996], biotite of 350-400°C [*Harrison et al*., 1985; *Grove and Harrison,* 1996] and 300-350°C in muscovite [*Robbins,* 1972; *Hames and Bowring,* 1994] (~12-24 km crustal depth with a geothermal gradient of 25°C/km). This allows analysis of thermal history over a range of cooling temperatures and crustal depths.

$^{40}Ar/^{39}Ar$ studies from marine sediments around Antarctica have similar age distributions to published onshore $^{40}Ar/^{39}Ar$ ages [e.g., *Roy et al.*, 2007; *Pierce et al*., 2011] making this another valuable sedimentary provenance tool for determining the source of ice-rafted debris and fingerprinting regions of the continent. $^{40}Ar/^{39}Ar$ analyses from detrital hornblende grains have been used to identify recycled versus parent populations when compared to detrital zircon U/Pb data from the head of Byrd Glacier for age constraints age of the subglacial bedrock [*Palmer et al*., 2012]. In this study, $^{40}Ar/^{39}Ar$ data from K-bearing minerals will be compared to detrital zircon U/Pb and ZHe data to better constrain the thermal history and provenance signatures of The Ross Embayment.

2. Geologic Setting

2.1 Antarctic Ice Sheet

Antarctica is 98% covered by the East and West Antarctic ice sheets which are more than 5 km thick in some regions [*Fretwell et al*., 2012]. The East Antarctic ice sheet developed in the Mid-Tertiary [*Ehlers and Gibbard*, 2004], a result of rapid global climate change at 34 Ma during the Eocene-Oligocene transition [*Zachos et al*., 2001; *Coxall and Pearson*, 2007]. This included a decrease in atmospheric carbon dioxide [*DeConto and Pollard*, 2003] which led to a global cooling trend throughout Cenozoic [*Bo et al*., 2009]. The Antarctic Circumpolar current developed from the opening of the Tasmanian and Drake Passages [*Kennett and Exon*, 2004], isolating Antarctica from warmer waters. These atmospheric and oceanic changes led to glaciation, first in the upland regions of Antarctica, including Dronning Maud Land, the Transantarctic Mountains and the Gamburtsev Mountains [e.g., *De Conto and Pollard*, 2003; *Jamieson and Sugden*, 2007]. Full-scale development of the West Antarctic Ice Sheet began at approximately 6 Ma [*Zachos et al.*, 2001].

The West Antarctic Ice Sheet is a marine-based ice sheet where the bed lies below sea level, 2,000 m in some regions [*Fretwell et al.*, 2012]. If entirely melted, much of West Antarctica would be below sea level after complete isostatic rebound [*Thiel*, 1959], which would expose an archipelago of islands [*Elliot*, 1985] and large deep seaways that would deepen towards the ice sheet interior [*Joughin and Alley*, 2011]. Discharge of approximately 40% of the West Antarctic Ice Sheet is controlled by fast moving ice streams into the Ross Ice Shelf [*Price et al.*, 2001] influenced by the presence of basal meltwater and deformable till. The ice streams in the Ross Embayment are 30-70 km wide [*Jacobel et al*., 1996], and move >1,000 m/yr, an order of magnitude faster than the surrounding ice [*Joughin and Alley*, 2011].

Although parts of East Antarctica are more than 1,000 m below sea level [*Fretwell et al.*, 2012], the majority of the East Antarctic Ice Sheet is grounded on a bed above sea level that would rise higher after isostatic rebound [*Bamber et al*., 2009]. Discharge of the East Antarctic Ice Sheet into the Ross Embayment is largely controlled by outlet glaciers in the Transantarctic Mountains where ice moves up to 850 m/yr [*Stearns and Hamilton*, 2005] through the Transantarctic Mountains.

2.2 Sediment erosion and transport

West Antarctic ice streams overlie deformable sediments within elongated sedimentary basins. Unlike the surrounding ice separating each ice stream the ice streams are not frozen to the bed [*Bentley et al*., 1998], but rather exhibit fast flow from the existence of a distinct water layer only in some places in and above the soft sediment [*Alley et al.,* 1986; *Blankenship et al.*, 1986; *Kamb*, 2000]. This subglacial water layer lubricates the bed-ice interface and promotes sliding and deformation of the till layer [*Engelhardt et al.,* 1990].

In East Antarctica, where ice is more likely frozen to its bed, various processes can contribute to sediment entrainment and transport. Sediment entrainment occurs from regelation of ice into subglacial sediments [*Iverson and Semmens,* 1995], net freeze on by conductive cooling or glaciohydraulic supercooling, shear planes, and folding of debris rich layers [*Alley et al*., 1997]. Sediment is transported within ice, or can also be transported in water from subglacial floods [*Alley,* 1989].

Clark [1987] states there are two primary controls on the scales of sediment transport including the topography, and basal ice sliding velocity. High velocities are associated with longer sediment transport distances (continental scale) and low sliding velocities are linked to shorter sediment transport distances [*Clark,* 1987]. Gas content and isotopic composition of debris-rich basal layers of Meserve Glacier in South Victoria Land, provides evidence that active debris layers exist at beds of cold glaciers at sub-freezing temperatures (temperatures below the bulk pressure melting point) [*Cuffey et al*., 2000]. These layers consist of glacially eroded material. This may be an analog for similar mechanisms that may take place under the East Antarctic ice sheet. Although little is known about the exact subglacial mechanisms that contribute to bedrock erosion and transport in East Antarctica, which likely change spatially and through time, it is evident the interior bedrock is being eroded and transported offshore or deposited in moraines.

Sediment in East Antarctica travels within the ice and may accumulate adjacent to nunataks, which are ice-free mountain peaks, as ice-cored moraines in areas where ablation rates are high. This process is similar to the transport and accumulation of meteorites in Antarctica [*Whillans and Cassidy*, 1983] (Figure 2). The moraines adjacent to nunataks at the head of major outlet glaciers may be dominated by local lithologies or

consist of a combination of local and farther traveled sediment [*Palmer et al*., 2012]. The catchment basins of East Antarctic outlet glaciers that cut through the Transantarctic Mountains can cover up to one million km^2 [*Stearns et al.,* 2008], having the potential to erode and transport bedrock from the continental interior. Faceting/striations on pebbles, exotic lithologies inconsistent with the local geology and low sand content are typically indicative of subglacial material in ice-covered nunataks moraines [*Palmer*, 2008; *Goodge et al*., 2010; *Schilling,* 2010; *Palmer et al.,* 2012].

2.3 Geologic history

East Antarctic formed during the Paleoproterozoic and Mesoproterozoic [*Goodge and Finn*, 2010] and was a key piece in the formation of two major supercontinents, Rodinia and Gondwana. Rodinia assembled in the Neoproterozoic between 900-1300 Ma, involved most continental blocks, and lasted ~150 million years after assemblage [*Li et al.,* 2007]. The breakup of Rodinia began with a super plume initiating continental rifting [*Li et al.,* 2008] into two parts, Laurentia and East Gondwana. Laurentia drifted from Gondwana, colliding with it on the other side of the world to form Gondwanaland [*Hoffman,* 1991]. West Gondwana aggregated by 600 Ma but was not complete until 530-540 Ma [*Li et al.,* 2008] after the closure of the Mozambique Ocean when East Antarctica collided with the African continent. The configuration of the continents in Gondwana is well known [*Lawver et al.,* 1998] with East Antarctica in the center. The Pan-African orogeny at 550-600 Ma [*Veevers,* 2003] includes the tectonic, magmatic and metamorphic activity associated with the formation of Gondwana [*Kröner and Stern*, 2005].

East Antarctica experienced a transition from a passive to an active subduction margin on the former rift margin of Gondwana [e.g. *Goodge et al*., 2004; *Faure and Mensing,* 2010] when the paleo-Pacific plate subducted under East Antarctica resulting in the Ross Orogeny at 480-550 Ma [*Stump,* 1995; *Goodge,* 2007]. The Ross Orogeny involved compression of sedimentary and volcanic rocks in combination with the emplacement of the Granite Harbour Intrusives at 480-540 Ma [*Goodge et al.,* 2004]. The active subduction stopped at 450-480 Ma [e.g. *Capponi et al.,* 1990; *Stump,* 1995; *Faure and Mensing*, 2010]. Following the Ross Orogeny, exhumation and erosion of the granitic and metamorphic basement of East Antarctica produced the Kukri Peneplain

[*Gunn and Warren*, 1962]. This unconformity sits between the Ordovician and older bedrock of East Antarctica and the overlying Beacon Supergroup.

The Beacon basin was a lowland intracratonic basin which developed between East Antarctica, the Panthalassan Ocean, Ross and Weddell Sea Embayments, and existed from the mid-Paleozoic through the mid-Jurassic [e.g., *Elliot*, 1975; *Barrett*, 1991; *Collinson et al.*, 1994; *Isbell*, 1999; *Elliot and Fanning*, 2008]. The Beacon Supergroup is approximately 2.7-3.5 km thick, and was deposited in the Devonian through the early Jurassic [*Barrett*, 1991]. In the Ross Embayment, the Beacon Supergroup extends from northern Victoria Land near the Ross Sea to the Ohio Range, south of Reedy Glacier [*Barrett*, 1991]. According to *Barrett* [1991] the stratigraphy of the Beacon Supergroup is simple due to the stability of the interior of East Antarctica since the Paleozoic.

Eroded sediment from both East and West Antarctica was deposited into the Beacon basin. This included eroded igneous rocks from the Ross /Pan-African Orogeny in East Antarctica and sediment from volcanic rocks formed along a Permo-Triassic magmatic arc related to subduction of the proto-Pacific Ocean plate [*Elliot and Fanning*, 2008]. One sandstone from the lower Buckley Formation contains exclusively late Permian zircons derived from the West Antarctic magmatic arc [*Elliot and Fanning*, 2008], implying the magmatic arc was higher elevation than the East Antarctic craton during the late Permian. In contrast, sandstone near the top of the Buckley formation and another at the base of the Fremouw Formation contain zircons with U/Pb ages of late Permian-early Triassic and Ross/Pan-African grains derived from local and magmatic sources [*Elliot and Fanning*, 2008]. The upper Buckley sandstone contains more late Permian-early Triassic grains, whereas the Fremouw sandstone contains more Ross/Pan-African grains [*Elliot and Fanning*, 2008]. As the ages show a shift through time from exclusively Permian to increasing numbers of Ross/Pan-African, the topographic elevation of West and East Antarctica must have shifted during the late Paleozoic through the early Mesozoic. Little is known about the environment, landscape and topographic elevation of East Antarctica and the magmatic arc following Beacon deposition.

The Transantarctic rift margin, which extended between the East Antarctic craton and the microplates of West Antarctica, was initiated in the early stages of the break-up

of Gondwana and accompanied by Jurassic magmatism [*Elliot*, 1992; *Elliot and Fleming*, 2004; *Fitzgerald and Baldwin*, 2007]. In Antarctica, this included the extensive intrusion of the Ferrar dolerite and the extrusive equivalent, Kirkpatrick basalts. Emplacement of the Ferrar dolerite sills occurred at approximately 183 Ma [e.g., *Encarnación*, 1996] and lasted less than one million years [*Fleming et al.*, 1997]. The Jurassic Ferrar Supergroup [*Kyle et al.*, 1980] consists of sills and dikes that extend 3,500 km along the Transantarctic Mountains [*Fleming et al*., 1997; *Elliot and Fleming,* 2004]. The sills are variable in thickness throughout the Transantarctic Mountains, ranging from less than 1 meter to hundreds of meters thick [*Elliot and Fleming*, 2008]. Estimates for total sill volume range from 100,000 km^3 [*Kyle et al.*, 1980] up to 170,000 km^3 [*Fleming et al*., 1997].

2.3.1 West Antarctic Rift System and the exhumation of the Transantarctic Mountains

Multiple models have been proposed to explain the elevation and uplift mechanisms of the Transantarctic Mountains and the relationship with the West Antarctic Rift system. The West Antarctic Rift System is the result of various stages of tectonic activity from the Cenozoic to the Cretaceous to the present [e.g., *Fitzgerald*, 1992; *Studinger et al*., 2004]. The models relating the West Antarctic Rift system to the Transantarctic Mountains include uplift as a flexure of the strong East Antarctic lithosphere [*Stern and ten Brink*, 1989], simple shear extension [*Fitzgerald et al.*, 1986]; isostatic rebound from glacial erosion [*Stern and ten Brink*, 1989; *Stern et al.*, 2005], a topographic reversal during Cretaceous extension [*Bialas et al.*, 2007], and asymmetric rifting [*Lawrence et al.*, 2007]. The rift system, which caused displacement between East Antarctica and Marie Byrd Land, is one of the world's largest areas of extended continental crust [e.g., *Fitzgerald*, 2002; *Winberry and Anandakrishnan*, 2004; *Siddoway*, 2008]. Sedimentary basins of the West Antarctic Rift system were formed by extension associated with the breakup of Gondwana [e.g. *Tessensohn and Wörner,* 1991; *Wilson*, 1992; *Bell et al.*, 2006]. The West Antarctic rift basin contains sediment eroded from Marie Byrd Land and the Transantarctic Mountains [*Anandakrishnan et al.*, 1998; *Peters et al.*, 2006, *Kramer*, 2008; *Schilling*, 2010].

Uplift of the Transantarctic Mountains has been constrained using apatite fission track dating (closure temperatures at 90-120°C [*Laslett et al.,* 1987; *Ketcham et al.,* 1999]). *Fitzgerald* [2002] suggested three periods of exhumation. The first period includes an early Cretaceous exhumation at 125-110 Ma possibly caused by rifting between Marie Byrd Land and the Ellsworth Mountain block [*Fitzgerald,* 2002]. Late Cretaceous exhumation between 100-75 Ma is related to extension between West Antarctica and East Antarctica [*Fitzgerald,* 2002]. The last main phase of uplift is constrained to 55-15 Ma, associated with flexural uplift of the East Antarctic lithosphere [*Fitzgerald,* 2002].

3. Materials and Methods

3.1 Sample Acquisition

In West Antarctica, nine subglacial till samples beneath the Whillans, Kamb and Bindschadler ice streams were obtained from cores collected by researchers at the California Institute of Technology during the 1992-1999 field seasons (Figure 1-A, Table 1). In East Antarctica, Beacon Supergroup sandstones and approximately one liter of till were collected from ice-cored moraines at the head of major outlet glaciers from the Byrd to the Reedy by researchers from Indiana University-Purdue University Indianapolis (2005-06, 2006-07, and 2010-2011 field seasons) (Figure 1-A, Table 1). Till was collected after removing the 2-3 cm of surface material in order to minimize effects of wind erosion.

3.2 Geology of site locations

3.2.1 West Antarctica

West Antarctic ice stream sites include tills from beneath Whillans Ice Stream (WIS), Kamb Ice Stream (KIS) and Bindschadler Ice Stream (BIS) (Figure 1). The onset of BIS is nearest Marie Byrd Land, and the onset of WIS is near East Antarctica. The onset of KIS is in-between these ice streams. Each ice stream follows a sedimentary basin parallel to the Transantarctic Mountains (Figure 1) and which appear to have somewhat different sediment inputs based on U/Pb populations [*Schilling,* 2010]. Mid-Cretaceous U/Pb zircon ages found in KIS and BIS are similar to those found in granitoids and dike swarms from the Ruppert and Hobbs coasts of western Marie Byrd Land [*Mukasa and Dalziel,* 2000] suggesting that the catchment of KIS and BIS contain sediment eroded from Marie Byrd Land [*Schilling,* 2010].

3.2.2 East Antarctica

Reedy Glacier

Strickland Nunatak (SN) is located at the head of Reedy Glacier in the Wisconsin Range. SN is mapped as unknown metamorphic rock [*Davis and Blankenship*, 2005]. Till from SN moraine contains a high percentage of sand from particle size analysis and is dominated by quartz in the pebble count data and felsic lithic, quartz grains and quartzite lithic fragments from sand petrography which likely represents sediment erosion from the local bedrock [*Kramer,* 2008; *Schilling,* 2010].

Scott Glacier

The Karo Hills moraine (KH) is located at the mouth, and Mt. Howe (MH) moraine is located at the head of the Scott Glacier in the Queen Maud Mountains. KH is mapped as Granite Harbour Intrusives [*Stump et al.,* 1980; *Stump et al.,* 2007] and the moraine contains metamorphic and felsic to intermediate igneous rocks [unpublished data] reflecting erosion from local sources. In contrast, the Mt. Howe nunatak is mapped as part of the Beacon Supergroup [*Doumani and Minshew*, 1965]. MH till contains up to ~70% faceted/striated pebbles indicating subglacial erosion, and although there is a variation in particle size across the moraine, sand is the dominant size fraction [*Schilling,* 2010; *Dits,* 2013]. The moraines at MH contain exotic rocks but a dominance of pebbles from the Beacon and Ferrar Supergroups [*Dits,* 2013].

Beardmore Glacier

The Beardmore Glacier (BG) and Davis Nunatak (DN) moraines are at the head of Beardmore Glacier in the central Transantarctic Mountains. They are approximately 40 km distance from each other and nunataks adjacent to each moraine are mapped as Beacon Supergroup [*Borg et al*., 1989; *Goodge and Fanning*, 2002; *Goodge et al.,* 2004]. Through particle size analysis, BG contains more evidence for locally eroded material, with a higher sand content and whereas DN contains an equal distribution of sand and silt + clay, reflecting more subglacially derived material from the East Antarctic interior [*Schilling,* 2010]. DN contains a mixture of coarse-grained felsic and sedimentary rocks while BG is dominated with sedimentary pebbles [unpublished data].

Law Glacier

The Mount Achernar (MA) moraine is located on the southeast side of Law Glacier, which lies between the Beardmore and Nimrod Glaciers. The bedrock around MA is mapped as the Buckley Formation of the Beacon Supergroup with Ferrar intrusions [*Bushnell and Craddock,* 1970]. The pebbles at MA are dominantly Ferrar dolerites and Beacon sedimentary rocks but the particle size distribution shows a higher percentage of silt and clay compared to sand possibly reflecting input of subglacially derived material at the site [*Bader,* 2013].

Nimrod Glacier

The three sites at the head of Nimrod Glacier include Milan Ridge (MR), Argo Glacier (AG) and Turret Nunatak (TN). AG and MR are approximately 20 km apart from each other and apart of the Miller Range, which is mapped as mapped as Precambrian Nimrod Group and Granite Harbour Intrusives [*Goodge et al.*, 2004; *Goodge*, 2007; *Goodge and Finn*, 2010]. AG and MR are south of the East Antarctic craton rift margin and the inferred limit of the Ross Orogen identified by *Goodge and Finn* [2010] (Figure 3). TN is located north and west of the other two sites and is adjacent to a nunatak mapped as Beacon Supergroup and Ferrar dolerite [*Brecke,* 2007; *Goodge et al*., 2008].

Byrd Glacier

The Lonewolf (LW) and Bates Nunatak (BN) samples were collected form moraines at the head of Byrd Glacier. The Lonewolf Nunataks and Bates Nunatak are mapped as Devonian rocks of the Beacon Supergroup [*Anderson,* 1979]. The LW nunataks are also south of the East Antarctic craton rift margin and the inferred limit of the Ross Orogen [*Goodge and Finn,* 2010]. The moraine at BN is dominated by Ferrar dolerite and Beacon sandstones, whereas the moraines at LW nunataks contain 44-66% exotic lithologies, and abundant faceted and striated pebbles from LW and LW2 sites. [*Licht and Palmer*, 2013]. The difference in moraine characterization suggests LW contains more subglacially-derived sediment, where BN contains primarily local material [*Palmer et al.,* 2012].

3.3 Zircon Preparation and Imaging

Selected Antarctic till samples were sieved to the 63-150 μm fraction and were sent to the University of Arizona LaserChron Center for zircon separation and mounting. Zircon separation involved the use of a Frantz magnetic separator combined with heavy liquid separation [*Gehrels,* 2000]. The unknown zircons and standard zircons (SL and R33) were mounted in the middle on one inch diameter epoxy pucks and polished to expose the interior of the grains [*Gehrels et al.,* 2006; 2008].

Low resolution back-scatter electron (BSE) images and low resolution cathodoluminescense (CL) images were taken of the grains of interest to identify chemical zonation using a Hitachi 3400N Scanning Electron Microscope (SEM). The SEM bombards the zircon surface with a straight incident electron beam, which interacts

with the nuclei of the atoms in the grain. The detectors in the SEM collect the re-emitted electrons, convert them into a signal and display the re-emitted BSE or CL signal of the zircon. For BSE images, the electrons from the incident beam collide with atoms in the zircon through elastic and inelastic collisions. Larger atoms (higher atomic number 'Z') [*Orloff*, 1997] have a higher probability of scattering these incident electrons. In BSE images, areas that scatter more electrons appear brighter than areas scattering fewer electrons. These variations allow the composition to be estimated based on the brightness of the BSE images. In the case of zircons, the brighter areas are typically interpreted to represent higher Hf and U [*Hanchar and Miller,* 1993]. Zircons also luminesce when the incident electron beam hits the zircon surface [*Crookes*, 1879] and excites electrons to a higher energy state [*Marshall,* 1988]. When the electrons return to a lower energy level, a photon is produced [*Poller et al.,* 2001]. Usually, areas with a higher U content appear brighter in BSE and darker in CL, as U tends to suppress the CL signal. Where possible, grains were imaged with BSE and CL to identify fractures and assess U and Th zonation patterns, which affect the loss of He from α-ejection [*Horigan et al.,* 2005], however the majority of the grains plucked for ZHe analysis were from *Palmer* [2008] and *Schilling* [2010] samples which lacked BSE and CL images.

3.4 U/Pb analysis

U/Pb analysis on zircon crystals was conducted at the University of Arizona LaserChron Center using a Laser ablation multicollector inductively coupled plasma mass spectrometry (LA-MC-ICPMS). A 30 μm diameter pit on the zircon was ablated by a Photon Machines Analyte G2 excimer laser. The ablated material was carried by He into the Nu HR ICPMS where U, Th and Pb isotopes were measured simultaneously. Each measurement was made in static mode, with a 3e11 ohm resistor for ^{238}U, ^{232}Th, ^{208}Pb, ^{206}Pb, and a discrete dynode ion counter for ^{204}Pb and ^{202}Hg. Ion yields were ~0.8 mv per ppm. Each analysis involved one 15-second integration for backgrounds, fifteen 1-second integrations with the laser firing continuously, followed by a 30 second delay to prepare for the next sample. The ages were reported with a precision of 1-2% (2σ) [*Gehrels et al*., 2006; 2008].

For U/Pb analysis, it is vital to use standard zircons, which have been dated by isotope dilution-thermal ionization, to correct for error in the unknown age calculations.

The R33 zircon standards are 419.3 ± 0.4 Ma [*Black et al.*, 2004] and were analyzed at the beginning, middle and end of each sample analysis. The Sri Lanka (SL) zircon standards are 564 ± 4 Ma [*Gehrels* et al., 2006] and were measured after every fifth unknown analysis to correct for any element fractionation [*Gehrels et al*., 2008]. Common Pb correction was made using Hg-corrected ^{204}Pb, assuming an initial Pb composition from *Stacey and Kramers* [1975].

A subset of the grains measured for U/Pb and reported by *Schilling* [2010] and *Palmer* [2008] used similar methods but different instrumentation at the LaserChron Center. Those grains were analyzed with a using a New Wave/Lambda Physik DUV193 Excimer laser and Faraday detectors. Additional details are in *Palmer et al.* [2012]. Isotopic data collected from the LA-MC-ICPMS was reduced using an Excel macro ('Agecalc'). The ^{206}Pb/^{238}U age was selected for <1000 Ma zircons, and ^{206}Pb/^{207}Pb age for >1000 Ma grains [*Gehrels et al.*, 2006]. The data were filtered for discordance (30% cutoff).

3.5 (U-Th)/He analysis

ZHe analysis on select zircon crystals was conducted at the Radiogenic Helium Dating Laboratory at the University of Arizona. At least four to ten representative zircons from each site were chosen for analysis. Grains selected were chosen from dominant U/Pb age populations within the Ross/Pan-African age spectra (Figure 7-B, C]. Euhedral grains without broken tips and inclusions, as well as a homogeneous U/Th distribution indicated by CL and BSE images were considered and selected when possible.

Each zircon was picked from the epoxy puck and photographed in two directions perpendicular to each other at the highest magnification (11x) on a Leica MZ16 stereozoom microscope. Measurements were taken of the maximum length (with tips), perpendicular widths, perpendicular half-widths of the orthorhombic prism or equatorial radii, and the tip heights of the pyramidal terminations of the crystal. These measurements were used to calculate the surface area to volume ratio for α-ejection corrections following a method from *Reiners et al.* [2005]. Each zircon was assigned an abrasion index number, which is a function of the radius of the circle in the crystal constrained by the corners of the grain [*Rahl et al.*, 2003]. Morphological notes (broken

tips/shape) were also taken of each grain, for consideration when calculating the ZHe age.

Each zircon was packed in a ~1mm Nb foil envelope and then transferred to a stainless steel planchet. Here they were individually heated to 1000-1250°C for a 15 minute ^{4}He gas extraction on the Nd:YAG laser with a spot diameter of 150 μm. At least two gas extractions were run on the sample of interest to insure that 98% of ^{4}He was extracted. The standard used for ZHe analysis was a Fish Canyon Tuff (FCT) volcanic zircon [*Reiners et al.,* 2002] which was run after every four unknowns and used to check performance and calibrations. The FCT has an average age of 28.48 ± 0.06 Ma [*Schmitz and Bowring,* 2001]. Next, the envelopes were transferred to teflon vials and spiked with low amounts of isotopically distinct U and Th to determine the amount of parent nuclides. Measuring U and Th was done in the Element2 high-resolution (single-collector) inductively-coupled plasma mass spectrometer (HR-ICP-MS) [*Reiners,* 2004]. The U and Th amounts were compared to the FCT standard for age calibration.

Each zircon required a correction for α-ejection to calculate the ZHe age [*Farley et al.,* 1996]. Since ^{4}He atoms with high kinetic energy may be ejected from their parent nuclides during radioactive decay, the correction accounts for the He atoms that are ejected during decay because of long-stopping distances (i.e., ~15-20 μm) causing spatial a depletion of α-particles near crystal boundaries [*Farley et al.,* 1996; *Rahl et al.,* 2003; *Reiners,* 2005]. The correction factor assumes a homogeneous U-Th distribution [*Reiners et al.,* 2004] and errors occur if U and Th zonation is not accounted for following a calculation from *Hourigan et al*. [2005]. The majority of zircons used for this study had a heterogeneous U/Th distribution observed in the CL images. Because each zircon was polished prior to ZHe analysis for imaging, this also affected the α-ejection correction because the correction factor assumes morphology of an unmodified crystal [*Reiners et al.,* 2005] and requires a modified calculation for plucked grains.

ZHe ages and errors were based on the morphology of the grain after accounting for polishing. For euhedral grains, the α-ejection corrected age was used with 1σ uncertainty on both sides [*Thomson et al.,* 2013]. For irregular grains, a 'plot age' was calculated from the average of the minimum and maximum age [*Thomson et al.,* 2013]. The maximum age was the full α-ejected corrected age plus the 1σ uncertainty, and the

minimum age was the raw age minus its 1σ uncertainty [*Thomson et al.,* 2013]. Errors for irregular grains were calculated from the difference between the plot age and the maximum and minimum age [*Thomson et al.,* 2013].

3.6 $^{40}Ar/^{39}Ar$ Analysis

$^{40}Ar/^{39}Ar$ analysis on detrital minerals was conducted from the same till samples as zircon U/Pb and (U-Th)/He. Samples were sieved to size fractions: 150-500 μm and 63-150 μm, and sent to Lamont-Doherty Earth Observatory for mineral separation and picking.

Hornblende, biotite and muscovite samples and standards were irradiated at the USGS TRIGA reactor in Denver. $^{40}Ar/^{39}Ar$ ages were obtained using single-step CO_2 laser fusion at the Lamont-Doherty Earth Observatory Argon Geochronology Lab. J values used to correct for neutron flux were made using the co-irradiated Mmhb hornblende monitor standard (520.55 Ma [*Samson and Alexander,* 1987]). $^{40}Ar/^{39}Ar$ data were corrected for backgrounds, mass discrimination and nuclear interferences. Background and mass discrimination corrections were based on time series of blanks and air pipettes (respectively) run throughout the interval of the analyses. The nuclear interference corrections were based on published data concerning the production ratios [*Dalrymple et al.,* 1981]. Ages were calculated using the decay constants from *Steiger and Jaeger* [1977]. Analyses were discarded if the ^{39}Ar was less than 2e-16 moles.

4. Results

4.1 U/Pb

Over 500 detrital zircons were analyzed from sites DN, MR, AG, TN, LW2-D and BIS (Figure 5; Appendix A). This adds to the 537 grains previously analyzed by *Palmer* [2008] and *Schilling* [2010] for these sites. Over 300 zircons were analyzed from Beacon Supergroup sandstones previously analyzed by the SHRIMP U-Pb method [*Elliot and Fanning*, 2008]. The goal was to add additional U/Pb dates on sites not yet analyzed and have a larger population of zircons to pick for ZHe analysis. Although at least 117 zircons should be analyzed in order to be 95% confident that no population greater than 0.05 of the population will be missed [*Vermeesch*, 2004], some samples yielded less than 100 zircons. The new U/Pb show ages which span from the Cretaceous through the Archean. The dominant age population occurs within the Ross/Pan-African Orogeny (450-625 Ma), which is consistent with other U/Pb analyses in the Ross Embayment [*Palmer*, 2008; *Schilling*, 2010; *Licht and Palmer*, 2013]. The new data also contain grains within the Grenville Orogeny (950-1250) Ma and a small number of ages spanning the late Archean through the early Proterozoic (2400-3200 Ma).

At the head of Byrd Glacier, 22 grains from LW2-D were analyzed and produced similar age distribution to existing U/Pb data from LW and LW2 (A, B and C), including dominance of grains with ages 550-600 Ma (Figure 5) [*Palmer*, 2008; *Licht and Palmer*, 2013]. At Nimrod Glacier, the three sites (AG, MR and TN) display a similar age distribution to each other with the majority of the grains included in an 550-600 Ma population [*Schilling*, 2010; *Licht and Palmer*, 2013] (Figure 5), similar to sites at nearby catchments (Byrd and Beardmore Glaciers).

An additional 119 grains were analyzed from DN at the head of Beardmore Glacier and added to those of *Schilling* [2010] which increased the total number of measured grains to 170. DN has a large population of grains for the Ross/Pan African Orogeny (550-600 Ma) in addition to a population of late Permian through early Triassic grains (220-290 Ma) (Figure 5).

Eighty-four grains from BIS were analyzed and combined with measurements by *Schilling* [2010], which increased the total number of measured grains to 222. The BIS data display two Neoproterozoic peaks at 525-575 Ma and at 450-500 Ma, and small

populations at 95-120 Ma and 150-250 Ma (Figure 5). These young ages are also seen at KIS [*Schilling,* 2010]. However, BIS contains a population of grains 290-370 Ma, which is absent from the other ice streams.

Zircons analyzed from the Beacon Supergroup sandstones are consistent with results of *Elliot and Fanning* [2008] (Figure 6). The lower Buckley sandstone contains U/Pb ages of only Permian-Triassic grains. The upper Buckley and Fremouw sandstone contain Permian-Triassic grains as well as Ross/Pan-African grains; however the upper Buckley contains more Permian-Triassic grains whereas the Fremouw contains more Ross/Pan-African grains.

4.1.1 Statistical Analysis for U/Pb data

The non-parametric Kolmogorov-Smirnov test (K-S test) was used to compare the similarity of the distribution of detrital zircon U/Pb ages within the dominant Ross/Pan-African age (450-625 Ma) for samples in East and West Antarctica (data combined with data from *Palmer* [2008], *Schilling* [2010], *Bader* [2013] and *Dits* [2013] (Table 2).The K-S test compares two distributions of data, to determine, to a certain level of confidence, the similarity of two datasets based on a p-value. The p-value must be greater than 0.05 to be 95% confident that the two populations are not statistically different [*Gehrels,* 2012]. For this analysis, U/Pb data from sites <25 km apart were combined.

As observed in detrital zircon U/Pb data from previous studies [*Palmer,* 2008; *Schilling,* 2008; *Licht and Palmer,* 2013], sites at the head of the glaciers are statistically similar to each other, whereas sites at the mouth of the glaciers are statistically similar to each other, but dissimilar to the head. Sites at the mouths of these glaciers (KH, CJ, HB) have younger Ross populations (500-550 Ma), in contrast, sites at the heads contain older (550-625 Ma) ages. In West Antarctica, only BIS and KIS are statistically similar, however, BIS exhibits a double peak of 485 and 550 Ma. WIS is most similar to SN, the closest East Antarctic site and CJ, all with a peak at ~520 Ma [*Schilling,* 2010; *Licht and Palmer,* 2013].

4.2 (U-Th)/He

Eighty-four zircon grains from till and Beacon Supergroup sandstones were chosen from the dominant Ross/Pan-African (450-625 Ma) U/Pb age population and analyzed for (U-Th)/He to determine whether double dating would subdivide this

population. The new data was added to existing ZHe data on 27 grains from *Schilling* [2010], which included zircons from KIS, WIS, BG, MH, SN and DN chosen from Grenville, Ross and late Paleozoic U/Pb age populations. Overall, the ZHe ages range from 75-650 Ma (including errors) in till samples (Figure 7-B; Appendix B). The majority of the ZHe ages fall between 115-200 Ma. No overall trend is observed between U/Pb and ZHe ages.

The ZHe ages from the Ross/Pan-African U/Pb population are subdivided into two groups including a 115-200 Ma age population and scatter with 200-650 Ma (Figure 8). Bedrock exposures at all sites containing grains within the 115-200 Ma population are mapped as Beacon Supergroup, except at KH, MR and AG. SN is the only site that does not have any grains within this population and contains an older cluster of ages between 215-380 Ma (including ZHe errors).The oldest ZHe ages were found at sites in the northern central Transantarctic Mountains, at Nimrod and Byrd Glaciers. Sites LW, MR and AG have ages from 300-650 Ma, with no clustering of ages within this range. MR contains the largest range of ZHe ages (67-720) (including errors) and lacks age clusters. The majority of grains from West Antarctica fall within the range from 75-450 Ma with no clusters (Figure 8).

Nine ZHe ages were analyzed from three Beacon sandstones from sites MH, MA and BN (Figure 8-C). The MH and MA sandstones were from the Permian-Triassic Victoria Group, and the BN sandstone is likely from the Devonian Taylor Group. All Beacon sandstone ZHe ages range from 115-200 Ma. Interestingly, the ages from the Taylor Group BN sandstone overlap with the Victoria Group rocks.

All Ross Orogeny grains were subdivided based on ‘old’ (550-625 Ma) versus ‘young’ (450-550 Ma grains) to assess temporal variability of ZHe ages of 115-200 Ma age within Ross/Pan-African Orogeny population. Errors on the ZHe ages were taken into consideration when selecting grains within this population, and the ZHe age pick age was used for calculations. The ‘young’ population had 21 grains, with an average of 165.75 ± 27.61 Ma and the ‘old’ population, with 32 grains, averaged 159.59 ± 21.49 Ma. Both of the datasets had the same median of 160 Ma. Based on the analysis, the dominant 115-200 Ma ZHe population is not different across the spectrum of U/Pb ages (see Appendix D for calculations).

The average age of the ZHe 'pick age' was calculated, and errors of the mean age were calculated based on the maximum and minimum possible age of all of the grains and their errors. The mean age plus error was plotted against the catchment basin size (Figure 14). There is no correlation between ZHe age and size of catchment basin. Byrd Glacier has the largest catchment basin, yet ZHe ages from Nimrod Glacier have a larger range. Although Beardmore has a larger catchment basin than Nimrod, it contains a small distribution of ZHe ages.

Zircons were also compared based on the effective Uranium (eU) concentration in ppm. The eU is used as a proxy for total accumulated radiation damage, which can have an effect on the He diffusivity and ZHe age [*Goldsmith et al.,* 2012]. If there is a correlation (either positive or negative) with eU and ZHe age, this may provide useful information on thermal history. None of the sites exhibit a correlation between eU and ZHe age (Figure 9).

CL images were taken of grains of interest prior to ZHe analysis. The majority of the zircons exhibit zonation and xenocrystic cores (Figure 4), characteristic of crystallization from a magma. When the CL images are used in combination with the Th/U ratio, it may be possible to better determine the crystallization environment of the zircon (metamorphic or magmatic). The majority of the grains used for ZHe analysis had Th/U > 0.1 from ZHe and U/Pb analysis (Figure 10), which is typically interpreted as indicating crystallization from a melt [*Vavra et al.,* 1996; *Hoskin and Black,* 2000]. No correlation was observed between ZHe age and Th/U ratio (Figure 11).

4.3 $^{40}Ar/^{39}Ar$

K-bearing minerals, including hornblendes, biotites and muscovites from WIS, LW, MR and AG were analyzed for $^{40}Ar/^{39}Ar$ values. Sites from LW were added to those from *Palmer* [2008] to increase the number of analyses from the LW sites. Ages from these sites are primarily from 450-570 Ma and are offset from the dominant zircon U/Pb population. WIS ages overlap with Nimrod and Byrd ages but lack grains >520 Ma. The distributions of the $^{40}Ar/^{39}Ar$ ages from this study are similar to $^{40}Ar/^{39}Ar$ data from detrital minerals from Prydz Bay, Dronning Maud Land, and the Weddell Sea [*Roy et al.*, 2007; *Pierce et al*., 2011].

5. Discussion

In the Ross Embayment, the Ross/Pan-African Orogeny age population is ubiquitous among detrital zircons, making it challenging to use U/Pb zircon ages to differentiate source terrains in East and West Antarctica. Double dating has been used in a variety of environments, but this is the first to use U/Pb and ZHe on detrital zircons from glacially eroded till and Beacon Supergroup sandstone in Antarctica. Double dating expands on present provenance studies and can be used to better characterize the geologic and orogenic history of Antarctica.

5.1 East Antarctica

5.1.1 Ross/Pan-African Orogeny

We used grains from multiple detrital zircon U/Pb studies [*Palmer*, 2008; *Schilling*, 2010; *Bader*, 2013; *Dits*, 2013] to compare the spatial distribution of the Ross/Pan-African grains within East Antarctic tills (Figure 12). More than 75% of the ages from the mouth of outlet glaciers in the southern and central Transantarctic Mountains are <550 Ma, and document igneous activity and metamorphism associated with the Ross Orogeny from 480-550 Ma [*Goodge*, 2007]. All of these sites have physical characteristics within the moraine that tills are locally sourced from nearby bedrock exposures [*Schilling*, 2010; *Licht and Palmer*, 2013].

Till at the head of outlet glaciers in the Transantarctic Mountains have a larger proportion of grains >550 Ma, sourced from the Ross and/or Pan-African Orogenies (450-625 Ma) and moraines at most of these sites have physical characteristics indicating a mix of locally and derived and farther traveled, subglacially eroded material [*Schilling*, 2010; *Licht and Palmer*, 2013; *Bader*, 2013; *Dits*, 2013]. There are no known published ages of Granite Harbour Intrusive outcrops in the Transantarctic Mountains older than 545 ± 5 Ma (from a diorite and leucogranite near AG) [*Goodge et al.*, 2012]. Zircon U/Pb ages on one erratic granite cobble from a moraine at AG has a mean age of 589 ± 5 Ma [*Goodge et al.*, 2012]. Across the continent, *Jacobs et al*. [1998] described magmatic growth and/or metamorphic overgrowth on zircons from ~550-600 Ma from bedrock samples collected in Dronning Maud Land. Our data suggest that such materials and/or their erosional products must extend toward the interior of East Antarctica and into the catchments stretching at least from Byrd to Scott Glacier. Sites at the northern end of the

study area (LW, MR and AG) are south of inferred limit of the Ross Orogen affecting the East Antarctic cratonic basement mapped by *Goodge and Finn* [2010] (Figure 3), and likely contain more grains unaffected by the Ross Orogeny.

Preliminary $^{40}Ar/^{39}Ar$ data from LW, MR and AG show an abundance of ages within the Ross/Pan-African Orogeny (Figure 13). The $^{40}Ar/^{39}Ar$ ages overlap the U/Pb Ross/Pan-African population but the largest population is shifted 25-50 Ma younger. A few ZHe grains immediately follow the $^{40}Ar/^{39}Ar$ age population implying that rocks in the Byrd and Nimrod catchments record a continuous cooling event related to igneous and metamorphic activity associated with Ross and/or Pan-African Orogenies.

ZHe ages were compared to the apatite fission track (AFT) ages from the north side of the Miller Range near the head of Nimrod Glacier [*Fitzgerald,* 1994]. AFT ages range from 250-350 Ma, related to cooling of the Granite Harbour Intrusives and/or exhumation of basement rocks to form the Kukri Peneplain [*Fitzgerald,* 1994]. Compared to other sites in the Transantarctic Mountains analyzed with AFT, including some at the middle and mouth of Nimrod Glacier in different geologic units, the Miller Range AFT samples are much older and unaffected by denudation and uplift of the Transantarctic Mountains [*Fitzgerald,* 1994]. In addition, there are no outcrops of Jurassic Ferrar dolerite in the Miller Range; which would have reset the AFT ages to 180 Ma [*Fitzgerald*, 1994]. It is likely that that the ZHe ages >200 Ma reported here from Byrd and Nimrod tills record the same cooling history as the AFT ages.

At the head of Reedy Glacier, SN also contains ZHe ages which span from 200-380 Ma (including errors), similar to ZHe ages from the head of Byrd and Nimrod. These data suggest that bedrock near the head of Reedy Glacier has a similar thermal history to rocks inland of Nimrod and Byrd Glaciers. ZHe ages >200 Ma are absent at sites between Reedy and Nimrod Glaciers.

5.1.2 Break-up of Gondwanaland

All till samples, regardless of adjacent rock type, and Beacon Supergroup sandstones in this study have grains within the dominant ZHe age population, 115-200 Ma, the exception is SN. Various events may have caused a regional resetting of grains during the Jurassic through the Cretaceous as a result of the break-up of Gondwanaland. The abundance of ages in this range suggests that cooling related to a combination of

exhumation, Ferrar magmatism, basin subsidence, and an increased geothermal gradient related to rifting were causes of ZHe age resetting. Interestingly, only MH contains grains with U/Pb ages between 115-200 Ma [*Schilling*, 2010; *Dits*, 2013]. This could represent a localized tectonothermal event followed by rapid cooling.

The thermal impact of Jurassic contact metamorphism on the Beacon Supergroup is well known and variable throughout Victoria Land [*Skinner and Ricker*, 1968]. Less is known about the zone of contact metamorphism in the Transantarctic Mountains, but it is likely the effects were similar. Many studies suggest minor thermal effect on the Beacon from the Ferrar intrusions based on few macroscopic contact metamorphic characteristics [*Gunn and Warren*, 1962; *Skinner and Ricker*, 1968; *Ballance and Watters*, 2002]. In North Victoria Land, arkosic sandstones and siltstones are baked to only a few inches from the dolerite contacts [*Skinner and Ricker*, 1968]. Effects were thought to be minimal because the Beacon was water saturated and thus experienced rapid loss of heat at least in quartz-rich sandstones close to the intrusions [*Turner,* 1981; *Ballance and Watters,* 2002]. Temperatures for calc-silicate hornfels in the Buckley Formation indicate temperatures 300-450°C were reached up to 60 m away from a sill [*Barrett,* 1966]. The presence of prehnite (from alteration of plagioclase) and metamorphic grossularite (ugrandite series garnet) in the Buckley Formation adjacent to Ferrar sills indicate temperatures rose to 300°C [*Jaeger,* 1957; *Barrett et al.*, 1966]. According to *Jaeger* [1957], a diabase sill will increase the temperature at the contact to 665°C and to 580°C at one tenth the width of the sill. Contact metamorphism is evident in a few samples adjacent to the dolerite contact from illite crystallinity [*Gunn and Warren*, 1962; *Ballance and Watters*, 2002; *Bernet and Guapp*, 2005]. Many of the ZHe ages, including errors, reported here are consistent with resetting from intrusion of the Ferrar dolerite. However, many of the ages are <160 Ma, which, if related, would require a long and slow period of cooling.

The Beacon basin has been compared to other continental rifts, such as the East African Rift System (EARS). Estimates on the high geothermal gradient within the East African Rift as a result of upwelling of the lithosphere-asthenosphere boundary below the thin crust [*Wheildon et al*. 1994] are dependent on location. Gradients have been estimated at 30-36°C/km in the Katwe prospect in Western Uganda (a branch of the

EARS), 80°C/km in hot springs in Panyimur in the West Nile region [*Bahati*, 2011] and over 200°C/km, observed in the Kenya Rift (a region of the EARS) [*Wheildon et al*., 1994]. If the Transantarctic Mountain rift experienced similar geothermal gradient temperatures, this would permit burial depths for the Beacon as little as 0.8-1 km (at 200°C/km).

Shallow burial of the Beacon Supergroup prior to intrusion of Ferrar dolerite sills has been constrained to have occurred between 200-230 Ma based on K-feldspar alteration to illite, quartz cementation and minor compaction of Victoria Group sandstone samples [*Bernet and Guapp*, 2005]. *Ballance and Watters* [2002] suggested no more than 500 m of pre-Ferrar burial based on exposed Beacon strata at Allan Hills in Victoria Land. At these depths, temperatures would not have been sufficient to reset the ZHe ages. Although many of the ZHe ages including errors, fall within the period for Beacon burial, digenetic effects indicating a higher temperature, and assumed to be minimal [*Bernet and Guapp*, 2005]. Assuming a geothermal gradient of 25°C/km, the Beacon sediments must have been buried ~6-8 km below sea level to reach temperatures high enough to reset the ZHe clock. An alternative explanation is a higher geothermal gradient, which would allow for burial <6-8 km.

Regional re-setting of ZHe ages would require deeper burial than previously described, and/or an increase in geothermal gradient associated with Jurassic rifting. The Beacon basin was affected by extensional tectonism from rifting between East Antarctica and West Antarctica at approximately 180-175 Ma based on volcanism in the Ellsworth and Transantarctic Mountains [*Schmidt and Rowley*, 1986]. Although little is known about the history and amount of subsidence and the geothermal gradient within the Beacon basin, it must post date Jurassic magmatism. Whether one case, or a combination, the temperatures must have been reached 160-200°C during the mid-Jurassic through the mid-Cretaceous. Because there are no $^{40}Ar/^{39}Ar$ samples less than Ross/Pan-African age, the temperatures must not have exceeded ~300°C to reset the K-bearing minerals.

The majority of grains with a ZHe age of 115-200 Ma from moraines are adjacent to nunataks which are mapped as the Beacon Supergroup, and the moraines contain an abundance of Beacon Supergroup sandstone pebbles [*Licht and Palmer*, 2013; *Bader*, 2013; *Dits*, 2013]. All the ZHe ages of grains from Beacon sandstone erratics measured

to date also fall between 115-200 Ma (Figure 8-C) suggesting that rocks of the Beacon Supergroup in the basin were heated to a temperature of 160-180°C during the mid-Jurassic through the mid-Cretaceous. This interpretation of the Beacon thermal history is supported by three grains with late Triassic-early Permian U/Pb ages that were chosen for ZHe analysis from MH, BG and DN. The three grains have ZHe ages within 115-200 Ma [*Schilling*, 2010].The U/Pb ages are consistent with derivation from the Permo-Triassic magmatic arc [*Elliot and Fanning*, 2008] deposited into the Beacon basin. In addition, few grains from a Proterozoic peak were chosen for ZHe analysis and also have ZHe ages within 115-200 Ma [*Schilling*, 2010]. This implies that regardless of U/Pb age, the ZHe ages from a span of U/Pb ages from glacial till and Beacon sandstones are similar.

Interestingly, several sites where ZHe ages fall between 115-200 Ma are not mapped as Beacon Supergroup, including KH, MR and AG. Sites MR and AG contain a small fraction (15%; 3 grains) within the 115-200 Ma ZHe population, yet Miller Range is mapped as Precambrian Nimrod Group and Granite Harbour Intrusive complex [*Goodge et al.*, 2004; *Goodge*, 2007; *Goodge and Finn*, 2010]. At the mouth of Scott Glacier, site KH exclusively shows ZHe ages of 115-200 Ma and is adjacent to bedrock outcrops mapped as Granite Harbour Intrusives [*Stump et al.*, 2007]. If the zircons from both of these sites were derived from the Granite Harbour Intrusives or the Precambrian Nimrod Group, then the these rock units in these areas must have experienced a similar Jurassic-Cretaceous thermal history as the Beacon Supergroup rocks. Faulting at the head of Nimrod, observed in the Geologists Range, and brought Precambrian Nimrod Group rocks adjacent to the Beacon [*Goodge et al.*, 2012]. However, little is known about the paleotopography of this region following Beacon Supergroup deposition. Whether the Granite Harbour Intrusives and Nimrod Group were higher in elevation from faulting or other tectonic processes, the zircons must have been reset at the same time as those in the Beacon basin.

Another explanation for the 115-200 Ma age population at Nimrod Glacier sites relates to its catchment basin, which is adjacent to the Byrd, Law and Beardmore catchment basins (Figure 1-B). These three catchments have nunataks mapped as Beacon Supergroup, and contain a high percentage of Beacon sandstones and Ferrar dolerite in the moraines (BG, DN, MA, BN and LW, [*Licht and Palmer*, 2013; *Bader*, 2013]). The

extent of the Beacon Supergroup inland from the Transantarctic Mountains is unknown, but based on these observations, and if the ZHe age is recording a Beacon signature then the two sites at Nimrod Glacier (MR and AG) contain a small fraction of Beacon sedimentary rocks within the catchment. The till at KH is dominated by locally derived material; therefore it is unlikely that all of the ZHe ages within the dominant ZHe age population were derived from the Beacon.

5.1.3 Exhumation of the Transantarctic Mountains

The tectonic evolution of the Transantarctic Mountains, including denudation history, is the subject of debate because the extensive ice sheet cover limits access into the sedimentary record and tectonic structure of the mountain range. This includes uncertainty about the timing, amount, and tectonic processes. The wide range in ZHe dates following intrusions of the Ferrar could represent slow denudation and exhumation of 6-10 km of the Transantarctic Mountains [*Fitzgerald,* 1992; *Studinger et al.,* 2004] assuming a standard geothermal gradient of 25°C/km or 1-2 km if the gothermal gradient was steeper. In either cae, this cooling would have occurred over approximately 65 million years spanning from the mid-Jurassic through the mid-Cretaceous. The difficulty in interpreting exhumation from ZHe ages from till is based on the lack of knowledge of grain origin within the stratigraphic column. This is especially true for grains derived from the Beacon, where different stratigraphic levels were exhumed at different times. This spread in ages may also suggest spatial variation in exhumation of the Transantarctic Mountains where the oldest ages originated from the upper part of section and younger ages from the lower part. Additional data are needed to determine if the 65 my range represents cooling in place at shallow depths as geothermal gradient was lower or this is an uplift signal.

Based on the ZHe data in this study, it may be possible to place time constraints on the exhumation of the Transantarctic Mountains. If the zircons at KH are derived from the Granite Harbour Intrusives, and have a ZHe range from 130-200 Ma (including error), KH can act as a constraint to determine cessation of uplift in the mid-Cretaceous. However, the ZHe ages from KH overlap with grains from other locations that may be derived from the Beacon Supergroup. Either the KH grains are locally derived from the Granite Harbour Intrusives, or the grains are from the Beacon. If the grains are from the

Granite Harbour Intrusives, uplift of the granite from lower depths would be needed so to be at a similar elevation to the Beacon, or the elevation of the Granite Harbour Intrusives was higher than the Beacon, and erosion of the granite produced grains within the basin. The ZHe ages from the Granite Harbour Intrusives would be expected to be older than ZHe ages from the Beacon Supergroup being higher in stratigraphic section. However, the paleotopography for this time period is unknown, which, if the Granite Harbour Intrusives or were at a similar elevation as the Beacon, they may also have been reset at a similar time or by different thermal events.

Estimates of the uplift and exhumation of the Transantarctic Mountains to date are based on apatite fission track (AFT) data from vertical wall profiles scattered along the length of the Transantarctic Mountains [*Fitzgerald and Stump*, 1991; *Fitzgerald and Stump*, 1997; *Fitzgerald*, 2001; *Miller et al.*, 2010]. Periods of denudation and uplift are reported at Scott, Beardmore, Shackleton Glaciers, Southern and Northern Victoria Land and Terra Nova Bay although some periods of exhumation are not always present in each area [*Fitzgerald*, 2002]. These sites are typically near the Transantarctic Mountain front.

In order to determine if the ZHe data of this study were related to exhumation events identified by AFT data, synthetic ZHe ages were calculated from AFT. Since AFT has a lower closure temperature than ZHe, one dataset can be recalculated to make it equivalent to the other. In this case, *Fitzgerald* [1991] and *Fitzgerald and Stump* [1997] AFT ages were transformed to ZHe ages. The ZHe ages were projected over a range of cooling temperatures for AFT (90-120°C) [*Laslett et al.*, 1987; *Ketcham et al.*, 1999] and ZHe (160-200°C) [*Reiners et al*., 2004] for early Cretaceous exhumation (see Appendix E for calculations). Because none of the ZHe sites in this study were located near AFT sites, the closest AFT sites were used in comparison (Appendix E). The calculations assumed a geothermal gradient of 25°C/km and constant cooling rate, calculated based on the AFT versus elevation relationship from sites at the Scott Glacier [*Fitzgerald and Stump*, 1997] and Beardmore Glacier [*Fitzgerald*, 1994]. Appendix E shows that the calculated ZHe ages are younger than the ZHe ages of this study. The ZHe ages of this study were not reset from exhumation of the Transantarctic Mountains otherwise would have been contained within the projected ZHe ages. However, if the geothermal gradient

and the cooling rate were different, it is possible that some of the ZHe ages might have been reset. This is especially true for sites at the mouth of the Scott Glacier.

The Mt. Griffith and Fission Wall at the head of Scott Glacier are from the Cambrian Wyatt formation [*Fitzgerald and Stump,* 1997] are closest to the KH site. The KH ZHe ages are older than the calculated ages based on AFT ages. If the cooling rate was slower, the calculated ZHe ages would be older and would include the KH ages. If the grains from KH and the AFT sites were similar, then the KH ages would have been reset from early Cretaceous exhumation of the Transantarctic Mountains. However, the depths of the different rock units are not known, and the amount of uplift during this time is not certain.

5.2 West Antarctica

The West Antarctic rift basin contains sediment eroded from Marie Byrd Land and the Transantarctic Mountains [*Anandakrishnan et al.,* 1998; *Peters et al.,* 2006; *Schilling,* 2010]. An important finding of this study is that most of the West Antarctic tills lack a distinct 'double dating' signature because the ice streams have similar detrital zircon U/Pb, ZHe, and hornblende/mica $^{40}Ar/^{39}Ar$ age distributions as those found in East Antarctica. This was somewhat unexpected given the nature of the topography beneath the West Antarctic ice sheet where the ice streams flow down sediment filled troughs oriented parallel to the Transantarctic Mountains (Figure 1). Based on this, areas such as BIS might be expected to contain a dominant input from Marie Byrd Land and have a different distribution of ages than samples from the Transantarctic Mountains. West Antarctic ice streams contain a large distribution of detrital zircon U/Pb ages spanning from 450-625 Ma, reflecting the diverse provenance of basin fill. More than 75% of the population from these ice streams are <550 Ma and approximately 25% of the population is <500 Ma, sourced from the late Ross Orogeny.

In WIS till, U/Pb and $^{40}Ar/^{39}Ar$ age spectra record a similar early cooling history to the tills from LW and MR+AG (Figure 13). The $^{40}Ar/^{39}Ar$ ages are younger by ~50 Ma from the U/Pb Ross/Pan-African population and the ZHe ages are offset by at least 100 Ma from the youngest $^{40}Ar/^{39}Ar$ population. The ZHe age spectra from WIS ranges from 75-450 Ma including errors, and also exhibit similarity to dominant age populations in East Antarctica. The older ZHe grains are similar to those at the head of Reedy, Nimrod

and Byrd, suggesting basin input from East Antarctic source. Alternatively, the older grains may be sourced from cooling of the Ford Granodiorite in western Marie Byrd Land at 375 Ma and rapid cooling [*Pankhurst et al.,* 1998].

BIS and KIS do not have distinct double dating signatures but they do have distinct young ages, possibly from a Marie Byrd Land source. *Schilling* [2010] identified a <105 Ma U/Pb zircon population in KIS and BIS that can be used to identify West Antarctic ice stream sources in the Ross Sea. Furthermore, three ZHe grains from BIS and WIS are <105 Ma, which may be sourced from granites in Marie Byrd Land. If additional $^{40}Ar/^{39}Ar$ and ZHe ages <105 Ma ages from West Antarctic ice streams have a ~105 Ma signature, this would further identify a West Antarctic signature which can be used to differentiate provenance of Ross Sea till.

5.3. Glacial till as a provenance tool

Provenance studies using glacially eroded till is challenging in East and West Antarctica where the extensive ice sheet cover limits access into the interior and structure of the continent. However, using a variety of provenance tracers on glacial till is useful to derive geological and geochronological information which can be used to better characterize the geology and orogenic history of Antarctica. Till at the heads of outlet glaciers provide the opportunity to study material derived from inaccessible bedrock farther inland of the Transantarctic Mountains. Although the exact stratigraphic neither position nor parent rock of each grain will ever be known, characterizing possible signatures of East Antarctic material provides critical new information to better fingerprint geochronological signatures of inaccessible material. In West Antarctica, distinctive ages <105 Ma that are only found in West Antarctica can be used to possibly identify a West Antarctic signature.

6. Conclusion

Radiogenic isotopes in detrital minerals from glacial moraines are valuable provenance tools that can be used to determine the origin of glacial debris, differentiate signatures of local and otherwise unknown subglacial rock units, and constrain the cooling history of ice-covered terrains. Our extensive new dataset using the combination of detrital zircon U/Pb and (U-Th)/He and detrital hornblende/mica $^{40}Ar/^{39}Ar$ dating on glacial till from across the Transantarctic Mountains provides insight into the effects of heating associated with the Ferrar intrusions and thermal evolution of the Beacon. The Ross/Pan-African Orogeny detrital zircon U/Pb age population (450-625 Ma) is ubiquitous in the Ross Embayment making this population difficult to use to differentiate source terrains. In East Antarctica the distribution of the U/Pb ages varies from the mouth to the heads of outlet glaciers in the Transantarctic Mountains along the length of the central and southern Transantarctic Mountains. Older grains are found at the heads of outlet glaciers where moraines contain more subglacially derived material from the Pan-African Orogeny that was unaffected by later Ross events. Younger grains (450-550 Ma) dominate the ages measured from till collected at the mouths of outlet glaciers. Slow cooling of rocks emplaced near the head of Byrd and Nimrod Glaciers during the Ross/Pan-African Orogeny is indicated by progressively younger ages of the U/Pb, $^{40}Ar/^{39}Ar$ and ZHe age thermochronometers.

An abundance of ZHe ages 115-200 Ma suggests that the region which is the southern and central Transantarctic Mountains today experienced slow, regional cooling or slow uplift during the mid-Jurassic through the mid-Cretaceous. This dominant ZHe age population is represented in Beacon Supergroup sandstones and from till collected adjacent to nunataks mapped as Beacon Supergroup rocks and that have abundant sandstone pebbles in the moraines. Exceptions to the pattern were found at the mouth of the Scott Glacier (KH) and the head of the Nimrod Glacier (MR and AG), which are not mapped as Beacon Supergroup rocks and do not contain sandstone pebbles in the moraines. Although this age population may represent a Beacon-derived signature, it implies that some areas of the Granite Harbour Intrusives and Precambrian Nimrod Group may have been affected by the same thermal event which reset grains within Beacon basin. The regional-scale ZHe ages 115-120 Ma are likely to be the product of a

combination of factors related to the breakup of Gondwana including local heating from intrusion of the Ferrar dolerite, subsidence within the Beacon basin and subsequence exhumation, along with a higher than normal geothermal gradient.

The U/Pb and ZHe age spectra from West Antarctic tills are similar to those found in East Antarctica, though may also include ZHe ages reset from metamorphic events in Marie Byrd Land. Although West Antarctic tills lack a distinctive ‘double dating’ signature, the presence of grains <105 Ma seen in both U/Pb and ZHe ages may be used to identify a possible West Antarctic provenance fingerprint.

Table 1: Sampling information for Ross Embayment samples selected in this study. SAL numbers identify grains used for ZHe analysis. Additional U/Pb analyses are from: ” *Palmer* [2008]; * *Schilling* [2010]; ^ *Bader* [2013]; ~ *Dits* [2013].

Site Name	Site Abbreviation	SAL number	Glacier	Latitude	Longitude	Sampling depth (cm)	Elevation	Local Bedrock
West Antarctic ice streams							(mamsl)	
Bindschadler*	BIS	1776, 1775	NA	-81.07	-140.01	<100	493	NA
Kamb*	KIS	1773, 1772, 1771	NA	-82.43	-135.95	40-50, 140-150, 180-190	527	NA
Whillans*	WIS	1744, 1755	NA	-83.45	-137.76	30-40, 180-190	334	NA
East Antarctica							(m)	
Strickland Nunatak*	SN	1659, 1660	Reedy	-86.49	-124.72	Surface	2086	Unknown metamorphic
Mt. Howe*~	MH	1690, 1691, 1946, 1905, 1906, 1907, 1911, MH6B	Scott	-87.35	-149.93	Surface	2401	Buckley Formation
Karo Hills*	KH	1700	Scott	-86.01	-154.01	Surface	111	Granite Harbour Intrusives
Davis Nunatak*	DN	1694, 1695	Beardmore	-85.63	167.30	Surface	2379	Victoria Group
Beardmore Glacier*	BG	1654	Beardmore	-85.31	164.75	Surface	2247	Victoria Group
Mt. Achernar^	MA	1940, 1942	Law	-84.13	160.98	Surface	1800	Buckley Formation
Argo Glacier	AG	1611	Nimrod	-83.25	156.13	Surface	2347	PreCambrian Nimrod Group & Granite Harbour Intrusives
Milan Ridge	MR	1616	Nimrod	-83.37	157.50	Surface	1958	PreCambrian Nimrod Group & Granite Harbour Intrusives
Turret Nunatak	TN	1607	Nimrod	-82.42	158.00	Surface	1226	Beacon Supergroup
Lone Wolf"	LW	1583	Byrd	-81.34	152.68	Surface	1595	Triassic Group
Bates Nunatak"	BN	BN	Byrd	-80.26	153.65	Surface	1474	Triassic Group

Table 1: Cont. Sampling information for Ross Embayment samples selected in this study. SAL numbers identify grains used for ZHe analysis. Additional U/Pb analyses are from: ” *Palmer* [2008]; * *Schilling* [2010]; ^ *Bader* [2013]; ~ *Dits* (2013].

Site Name	Site Abbreviation	SAL number	Glacier	Latitude	Longitude	Sampling depth (cm)	Elevation	Local Bedrock
Beacon Sandstones								
Mt. Howe~	MHSS	MH106	Scott	-87.35	-149.93	Surface	2401	Beacon Supergroup
Mt. Achernar^	MASS	MA3B1	Law	-84.13	160.98	Surface	1800	Beacon Supergroup
Bates Nunatak”	BNSS	BR	Byrd	-80.26	153.65	Surface	1474	Beacon Supergroup

Table 2: K-S Test p-values using error in the CDF for U/Pb from sites in West and East Antarctica for only the Ross Orogeny (450-625 Ma). Shaded areas indicate p-value > 0.05. [*Palmer*, 2008; *Schilling*, 2010; *Bader*, 2013; *Dits*, 2013]

	BIS															
KIS	**0.17**	KIS														
WIS	0.02	**0.09**	WIS													
SN	0.00	0.00	**0.27**	SN												
MH	0.00	0.00	0.00	0.00	MH											
KH	0.00	0.00	**0.08**	**0.79**	0.00	KH										
DN	0.00	0.00	0.00	0.00	**0.93**	0.00	DN									
BG	0.00	0.00	0.00	0.00	**1.00**	0.00	**0.83**	BG								
CM	0.00	0.00	0.05	0.02	**0.31**	0.00	**0.31**	**0.53**	CM							
MA	0.00	0.00	0.00	0.00	**0.13**	0.00	**0.11**	**0.99**	0.05	MA						
AG+MR	0.00	0.00	0.00	0.00	**0.35**	0.00	**0.18**	**1.00**	**0.23**	**0.99**	AG+MR					
TN	0.00	0.00	0.00	0.00	0.01	0.00	**0.10**	**0.17**	0.00	**0.09**	**0.07**	TN				
BN	0.00	0.00	0.00	0.00	**0.17**	0.00	**0.13**	**0.67**	0.01	**0.72**	**0.44**	**0.99**	BN			
LW	0.00	0.00	0.00	0.00	**0.14**	0.00	**0.08**	**0.89**	0.02	**0.98**	**0.79**	**0.43**	**1.00**	LW		
BR	0.00	0.00	0.04	0.01	**0.97**	0.00	**1.00**	**0.87**	**0.63**	**0.15**	**0.20**	**0.07**	**0.13**	**0.13**	BR	
CJ	0.01	**0.08**	**1.00**	**0.61**	0.00	**0.22**	0.00	0.00	0.02	0.00	0.00	0.00	0.00	0.00	0.01	CJ
HB	0.00	0.00	0.03	**0.70**	0.00	**0.70**	0.00	0.00	0.00	0.00	0.00	0.00	0.00	0.00	0.00	**0.09**

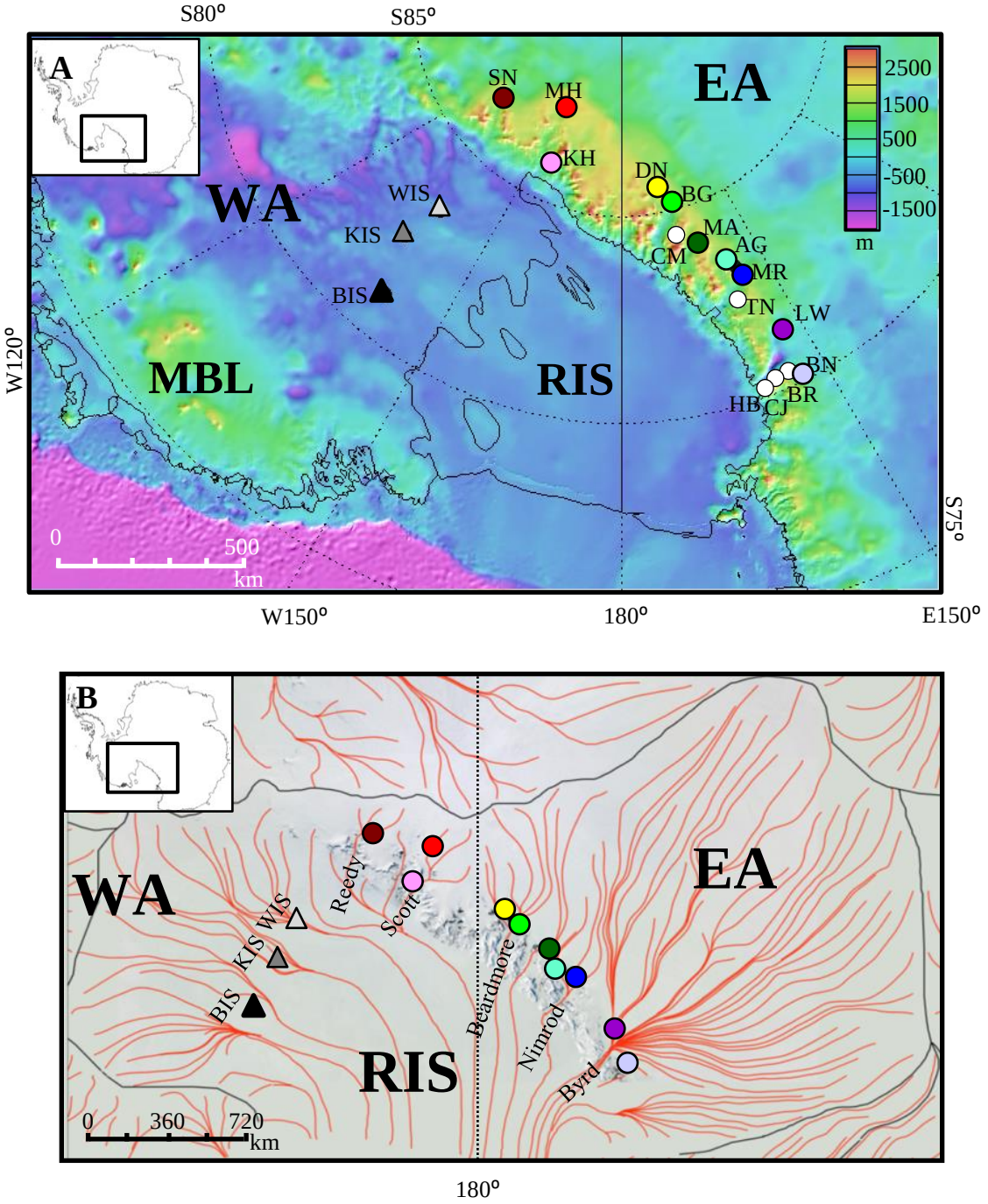

Figure 1-A: Bathymetry and topography map [GeoMapApp] of the Ross Embayment and black lines showing the Ross Ice Shelf perimeter and Antarctic Coastline (SCAR). White dots show sites that only have U/Pb analysis; colored circles and triangles are sites with U/Pb and ZHe analysis. (RIS= Ross Ice shelf; EA=East Antarctica; WA=West Antarctica; MBL=Marie Byrd Land). Sample site abbreviations are the same as those in Table 1.

Figure 1-B: Ice flow lines (red) in the Ross Embayment with labeled glaciers. Black lines show ice divide [*Jezek et al.*, 2011].

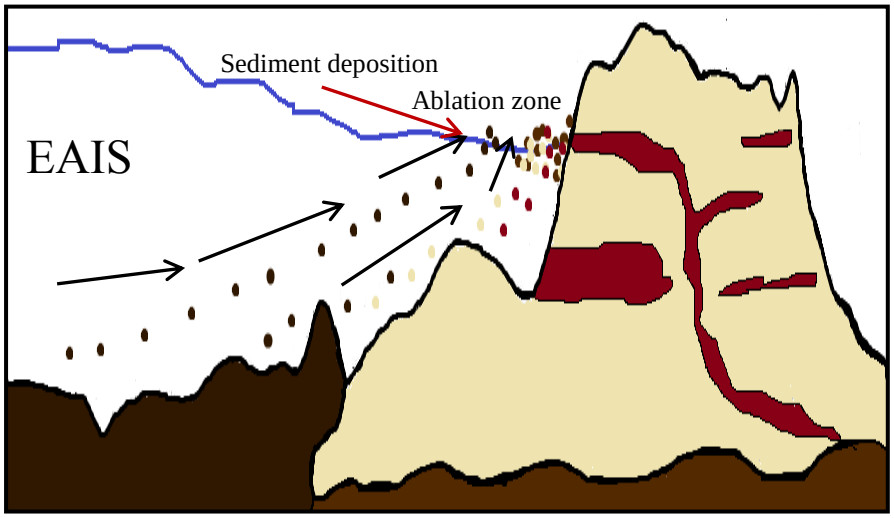

Figure 2: Transport of subglacially eroded sediment to the surface and deposition at moraines adjacent to nunataks in the Transantarctic Mountains (not to scale). Modified from *Whillans and Cassidy* [1983].

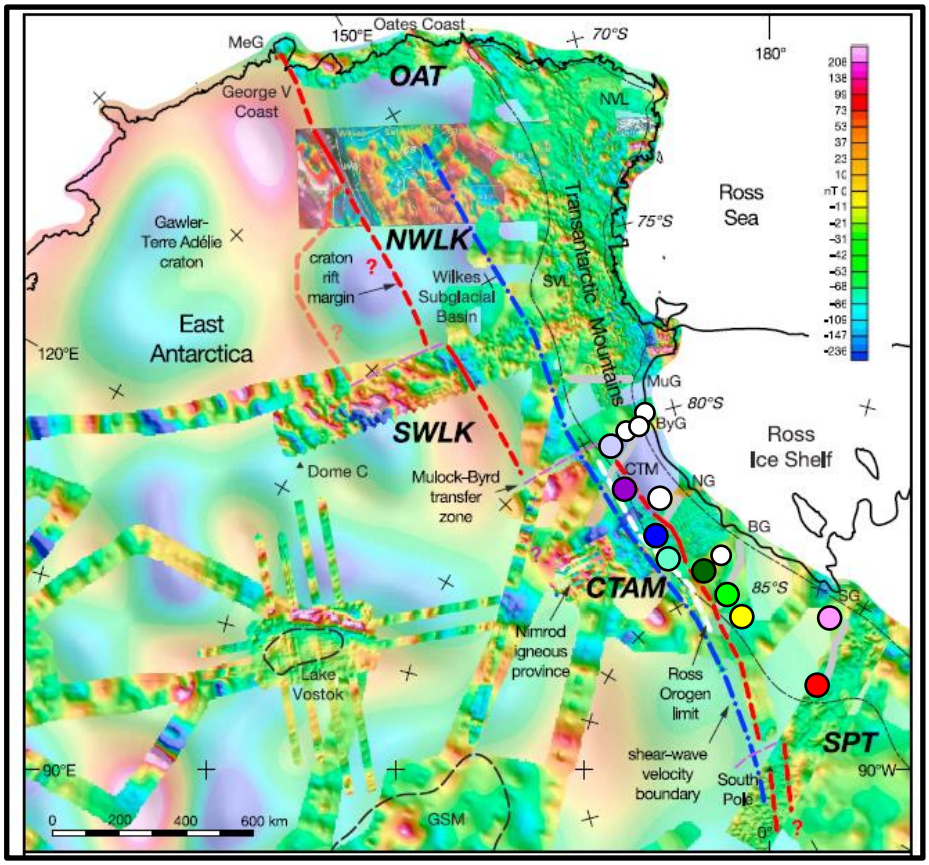

Figure 3: Magnetic map of East Antarctica showing craton rift margin (red line-dashed when uncertain) [*Goodge and Finn*, 2010]. Colored circles are sites with zircon U/Pb and ZHe analysis; white circles are sites with only U/Pb analysis compared in this study.

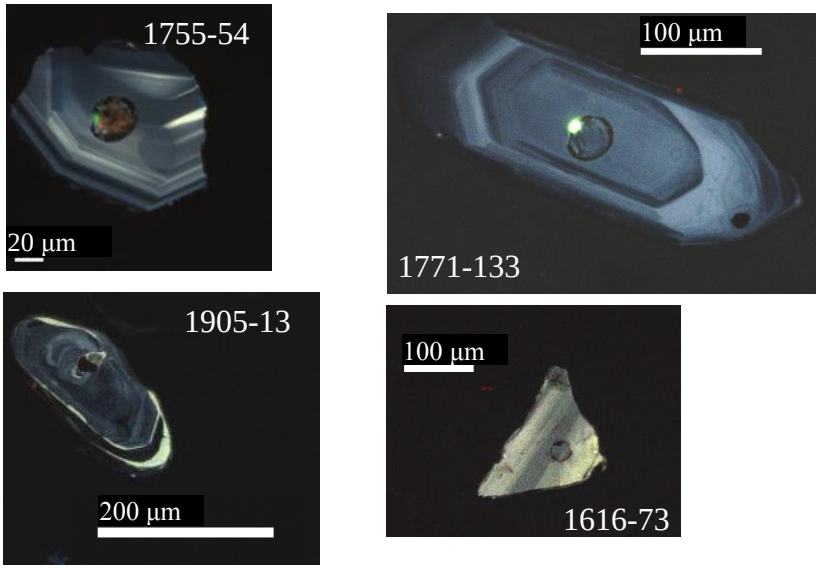

Figure 4: Cl images for grains used for ZHe analysis. Oscillatory zonation is observed in all four grains, typical of grains from a magmatic source.

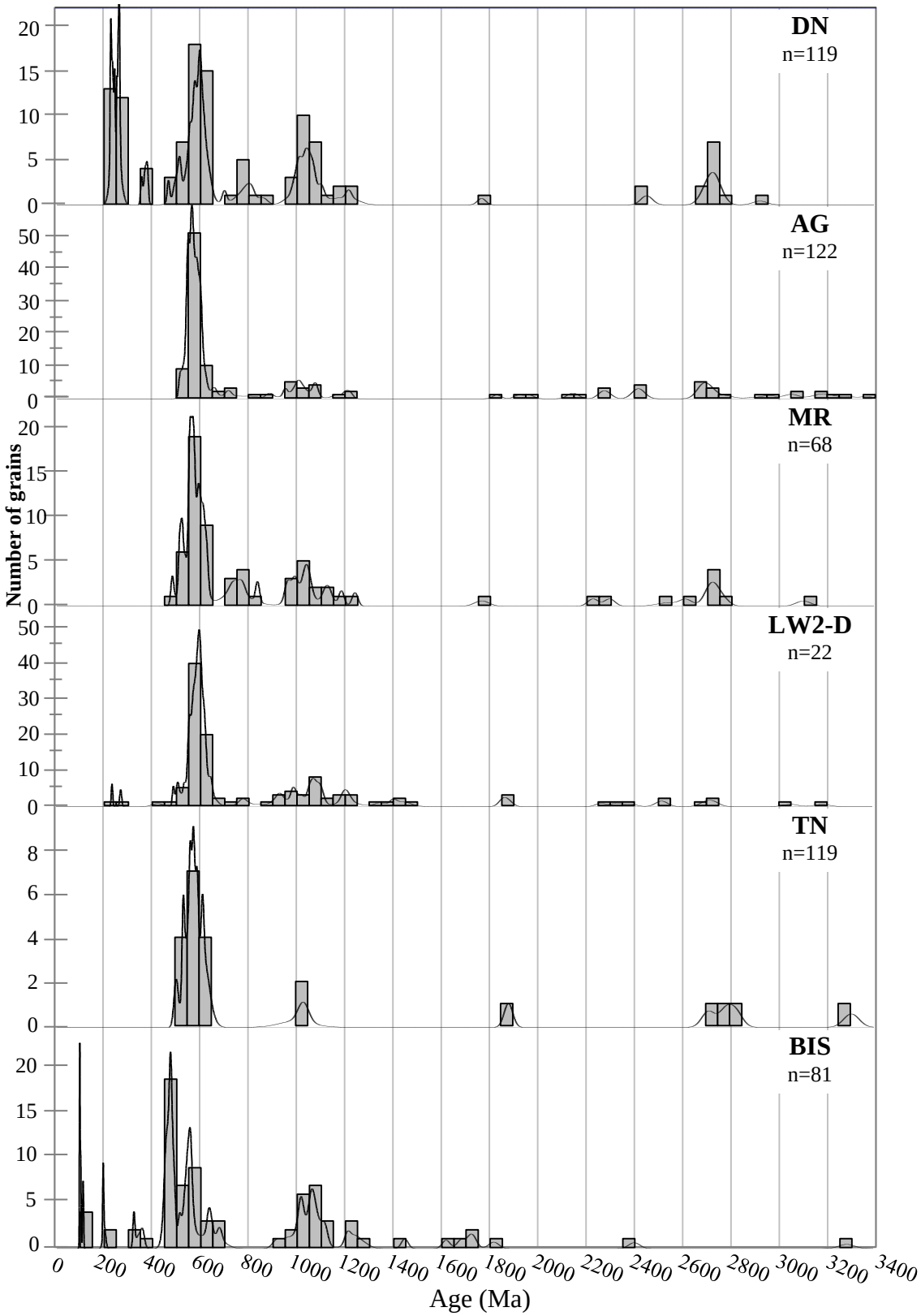

Figure 5: Histograms (bin widths=50 Ma) and normalized probability plots of all detrital zircon U/Pb ages from West and East Antarctica.

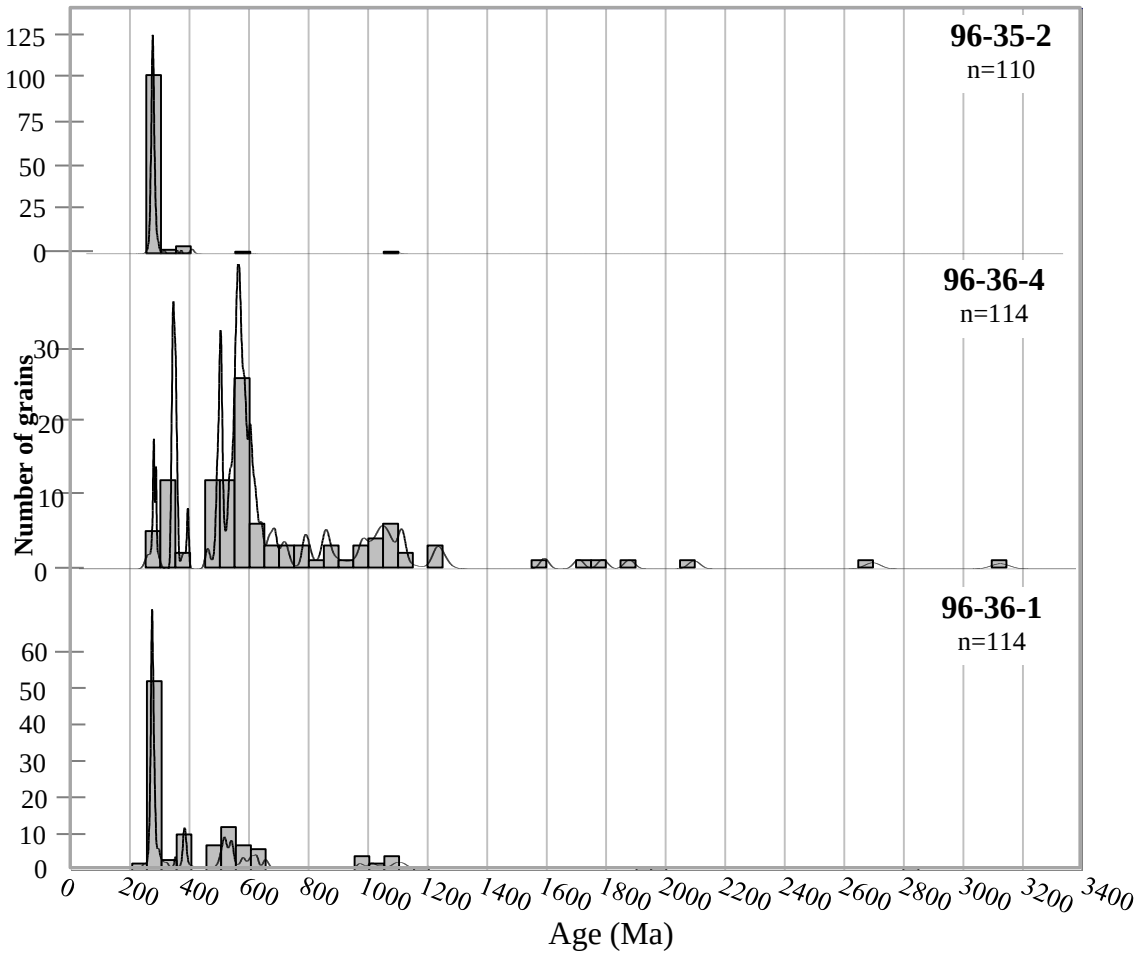

Figure 6: Histograms (bin widths=50 Ma) and normalized probability plots of detrital zircon U/Pb ages previously analyzed by *Elliot and Fanning* [2008].
96-36-4: Fremouw sandstone
96-36-1: Upper Buckley sandstone
96-35-2: Lower Buckley sandstone

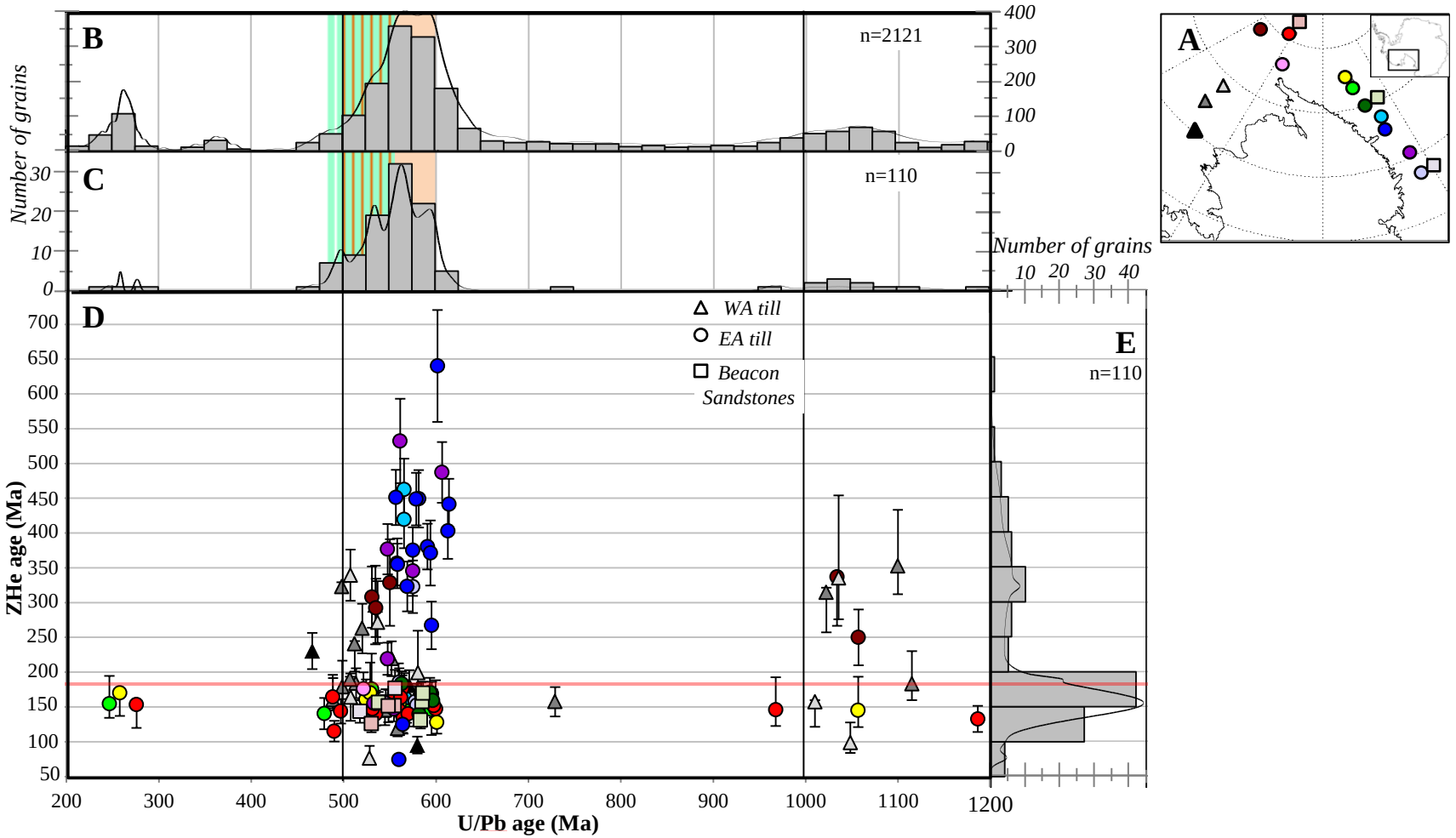

Figure 7: A: Map of Ross Embayment with sites selected for ZHe analysis. (GeoMapApp). Normalized probability plot and histogram for all U/Pb ages from till sites in this study (B); only U/Pb ages measured with ZHe (C). Orange lines: Pan-African Orogeny (650-500 Ma) [*Veevers*, 2003]. Green lines: Ross Orogeny (550-480 Ma) [*Goodge*, 2007]. D: Ages of double-dated grains. E: Normalized probability plot and histogram of ZHe ages. Red line: Ferrar dolerite (184 Ma) [*Encarnación*, 1996].

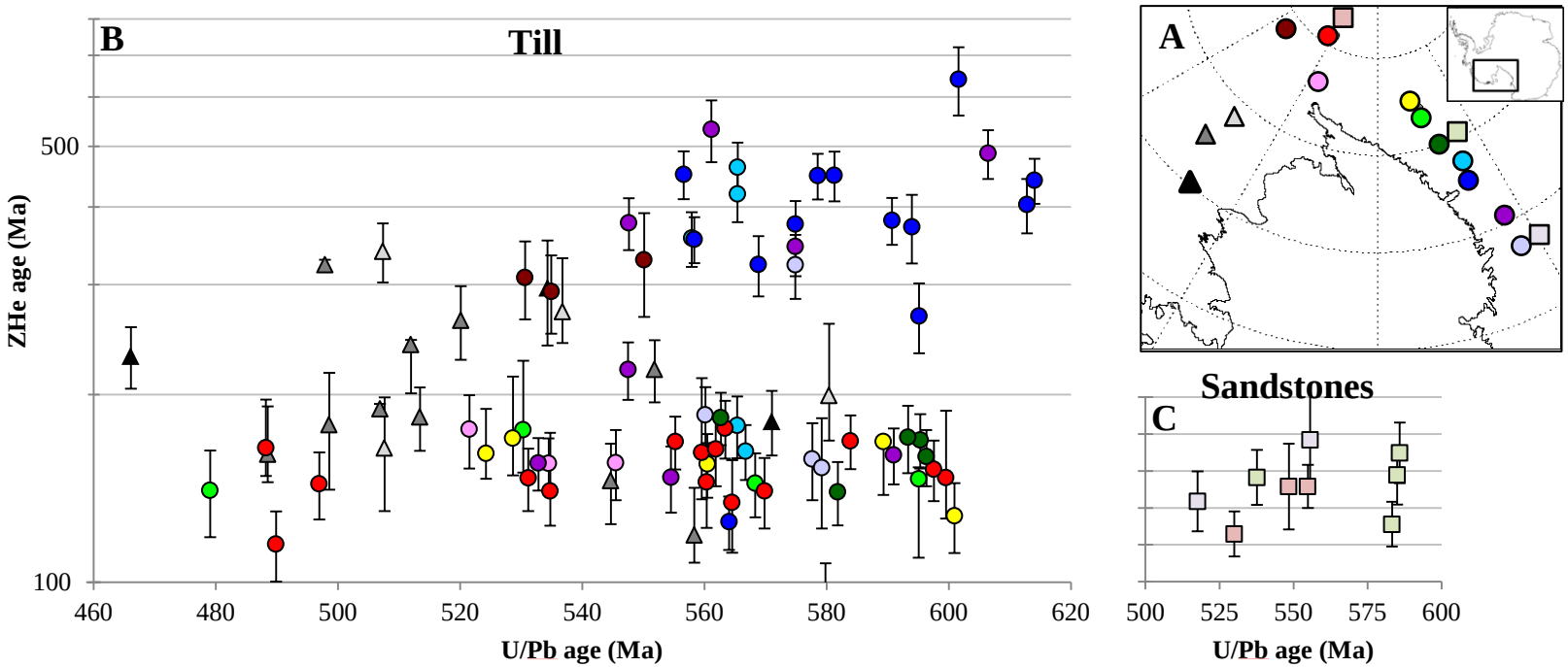

Figure. 8: Comparison of U/Pb ages and ZHe ages on the same grain from the Ross Embayment for only the Ross/Pan-African Orogeny . A: Map of Ross Embayment with sites selected for ZHe analysis. B: U/Pb and ZHe ages on the same grain for only the Ross/Pan-African Orogeny from till. C: U/Pb and ZHe age for Beacon Supergroup sandstones

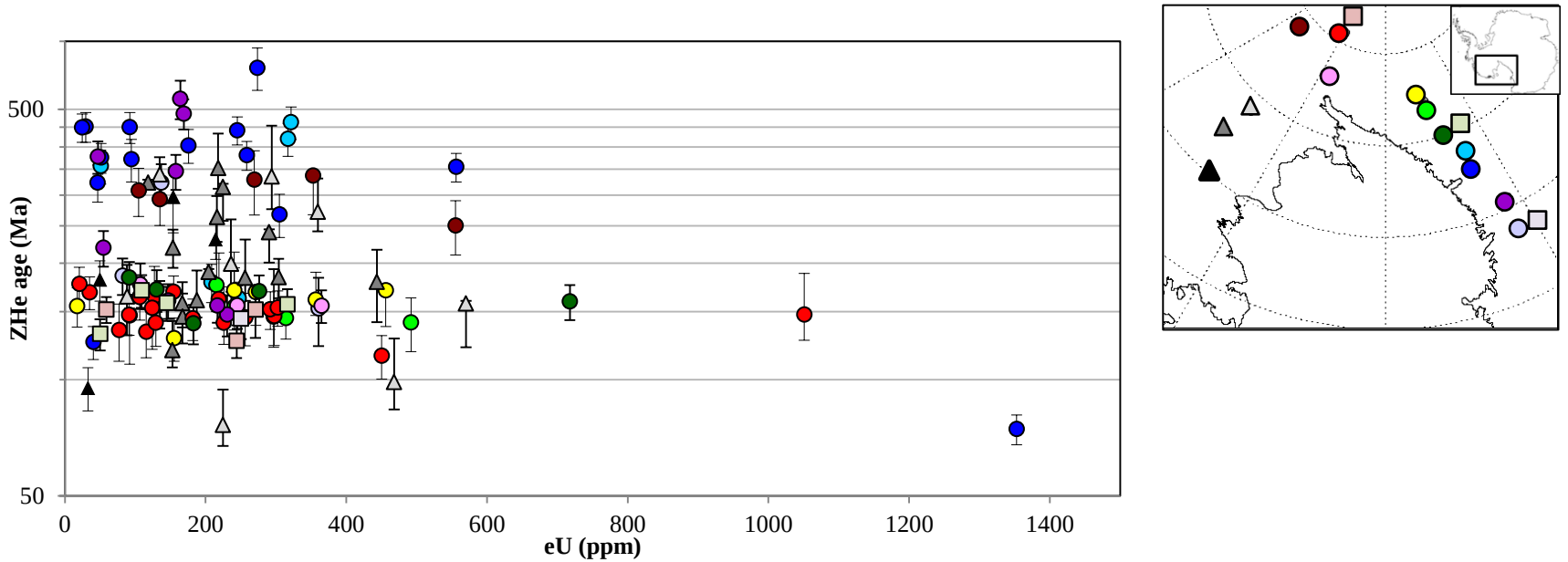

Figure 9: eU versus ZHe age. No correlation is observed between eU and ZHe age.

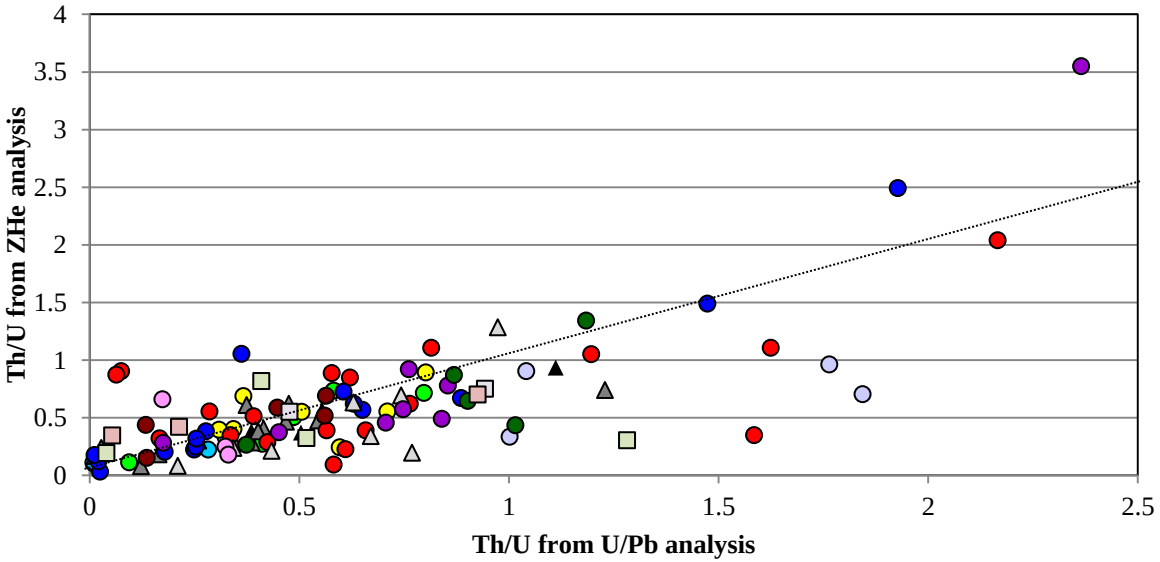

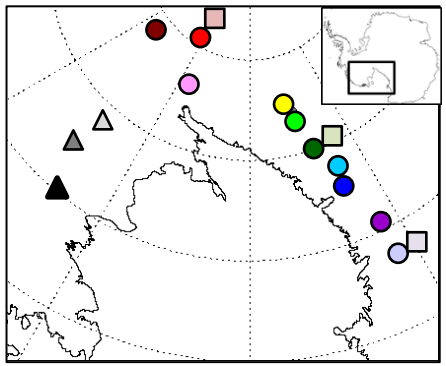

Figure 10: Comparison of Th/U from U/Pb and ZHe analysis. Many of the grains are >0.1 from U/Pb and ZHe analysis indicating derivation from a magmatic source. Dashed line indicates 1:1 correlation line.

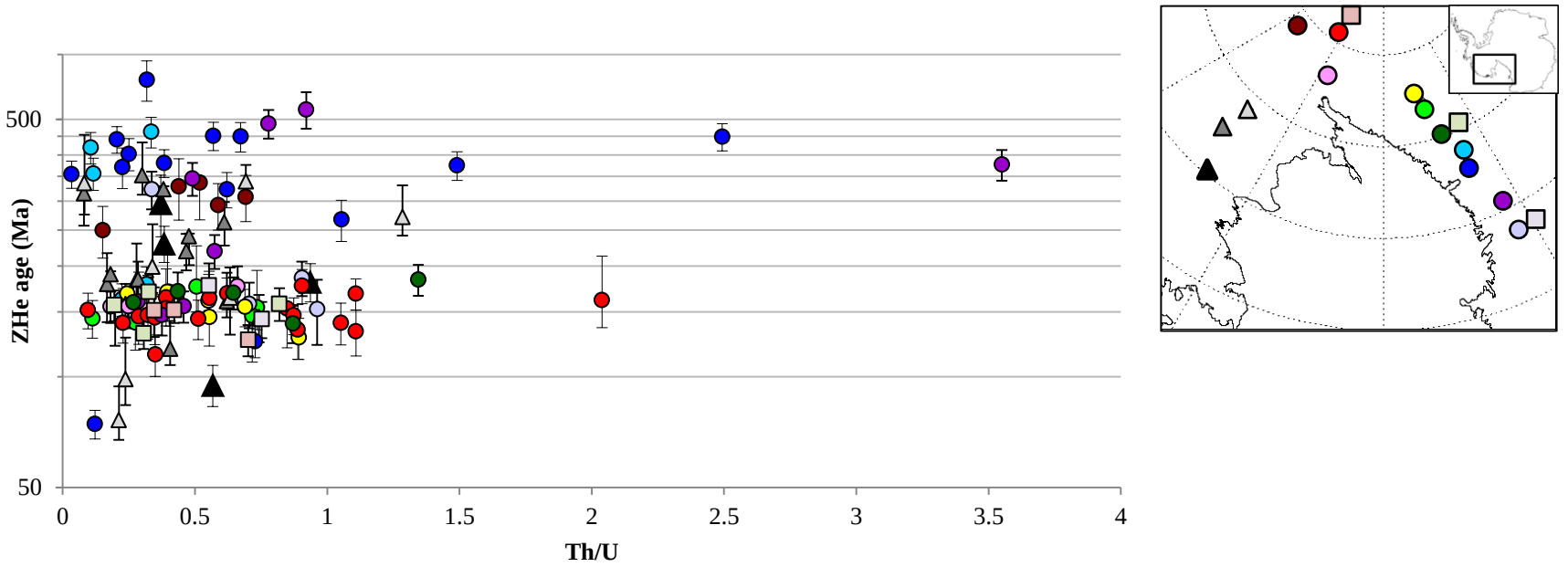

Figure 11: Th/U ratio versus ZHe age. No correlation is observed between Th/U and ZHe age.

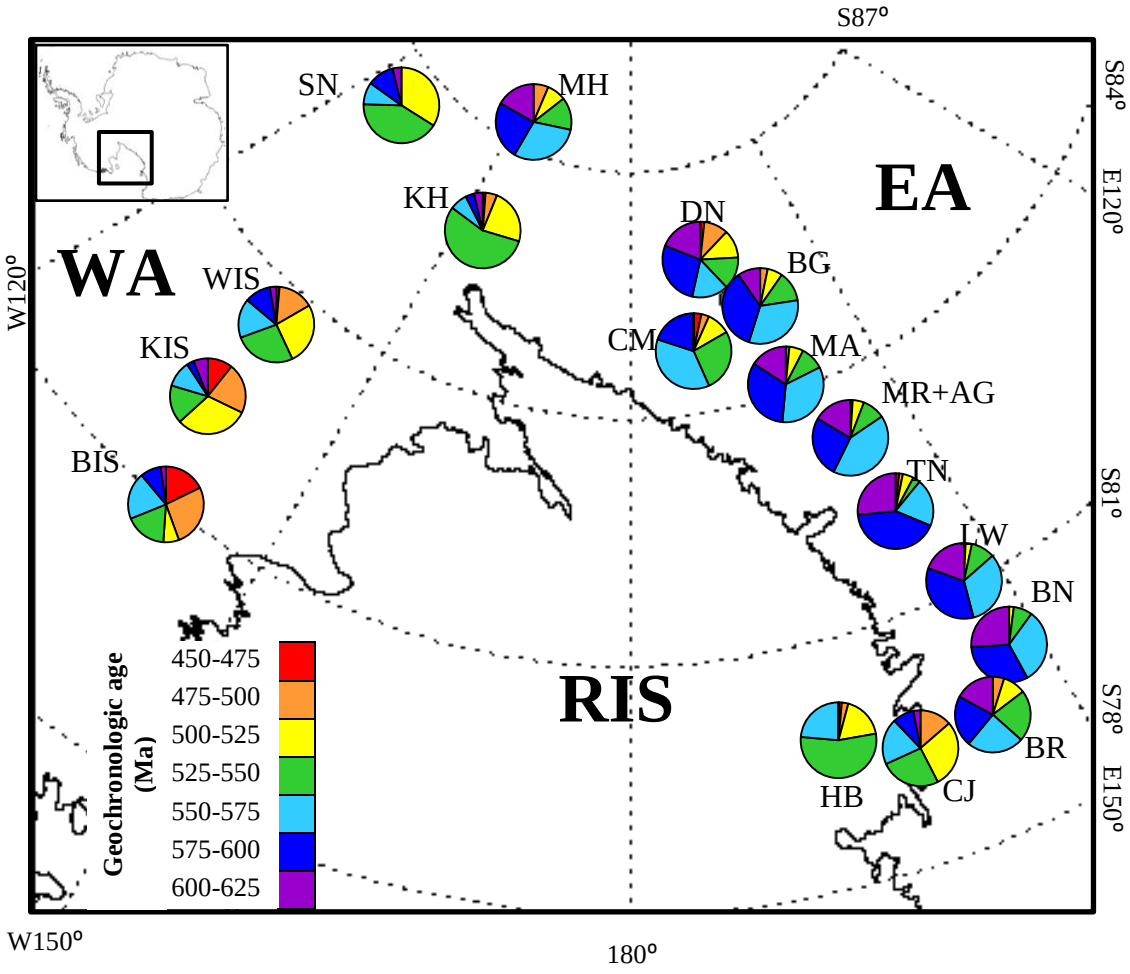

Figure 12: Pie charts showing the distribution of detrital zircon U/Pb Ross/Pan-African ages (450-625 Ma) in the Ross Embayment for all till samples [*Schilling*, 2010; *Licht and Palmer*, 2013; *Bader*, 2013; *Dits*, 2013]. Sites MR and AG were combined and all sites at LW were combined.

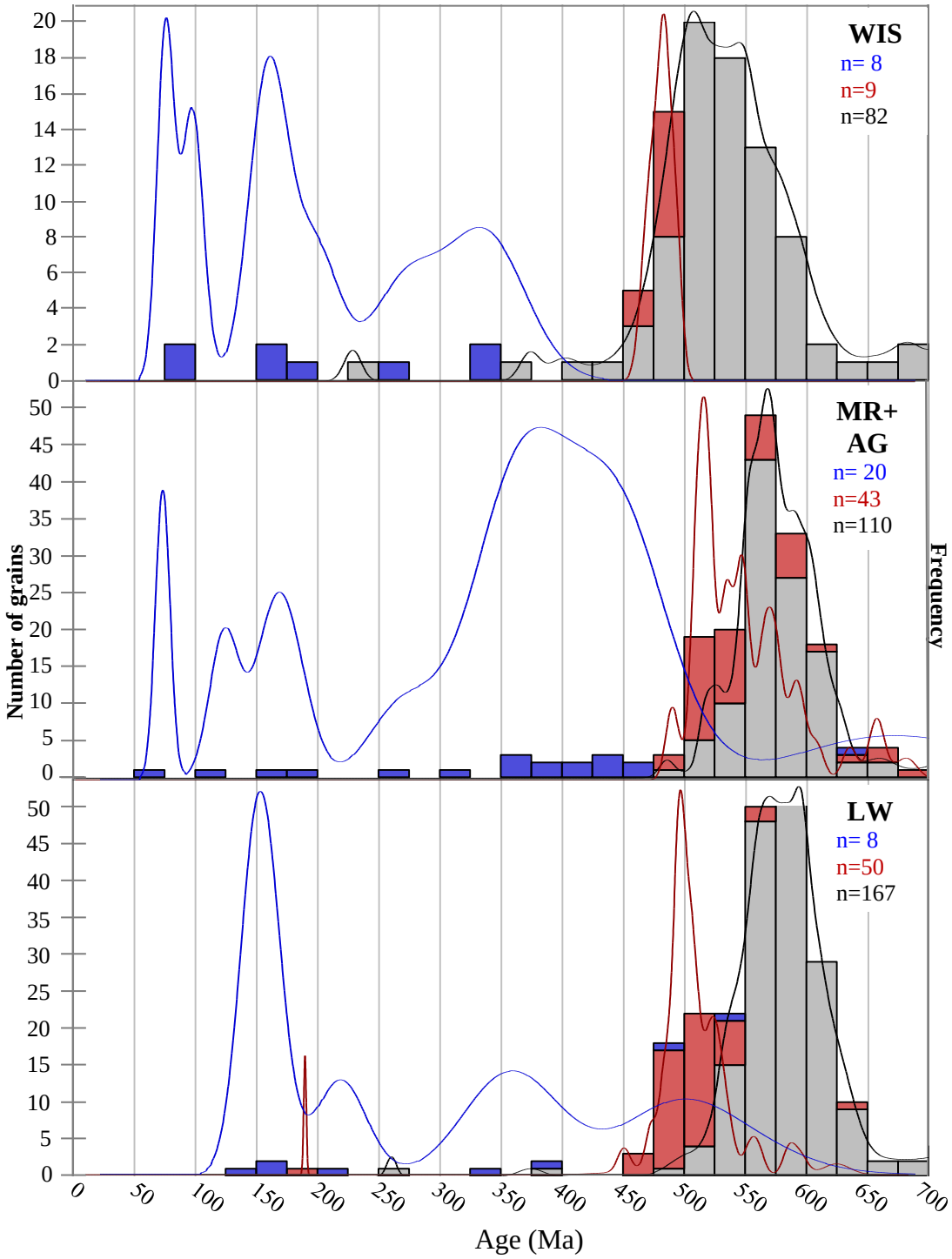

Figure 13: Stacked histograms (bin widths of 25 Ma) and normalized probability plots for all sites with ZHe (blue), $^{40}Ar/^{39}Ar$ (red), and U/Pb (black). The peak height from the normalized probability plots is calculated by the number of grains and error on the ages (2σ). $^{40}Ar/^{39}Ar$ ages were from hornblende for all sites except at LW which include hornblende, biotite and muscovite from *Palmer et al*,. [2012]. Bin widths were based on the error on U/Pb and $^{40}Ar/^{39}Ar$ ages; this may not be ideal for ZHe as some errors exceed 25 Ma.

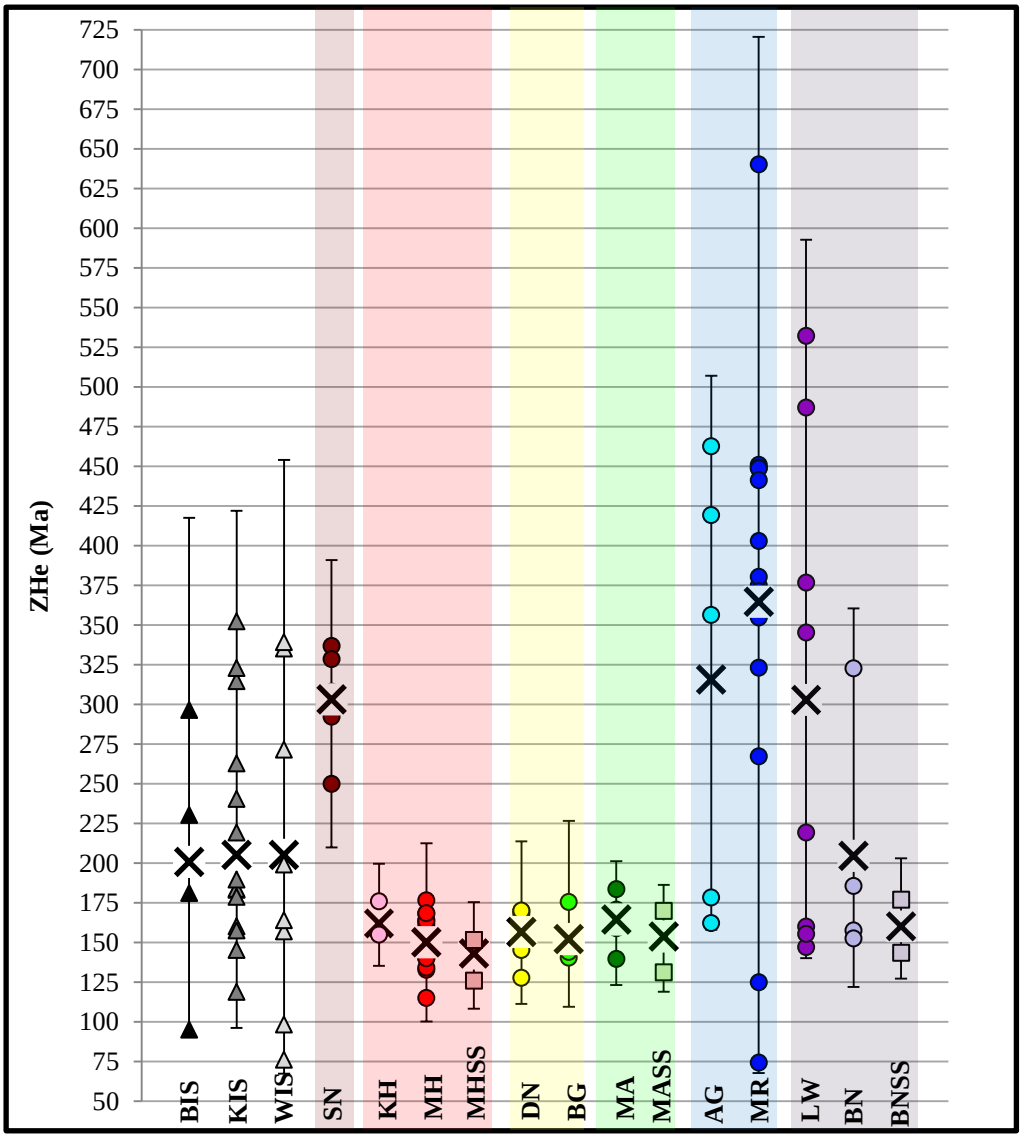

Figure 14: Age range for all ZHe ages from till and Beacon Supergroup sandstones from the Ross Embayment. Black 'X' indicates the average of all ZHe ages from each site based on the ZHe age pick ages. Error bars on the average are based on the maximum and minimum age of each ZHe age including errors. Colored circles are individual ZHe ages from each site. Site abbreviations are the same as in table x. Colored boxes indicate associated glacier (purple=Byrd Glacier; blue=Nimrod Glacier; green=Law Glacier; yellow=Beardmore Glacier; red=Scott Glacier; dark red=Reedy Glacier)

Appendix A: U/Pb detrital zircon geochronologic analyses by Laser-Ablation Multicollector ICP Mass Spectrometry

					Isotope ratios					Apparent ages (Ma)							
U (ppm)	206Pb 204Pb	U/Th	206Pb* 207Pb*	± (%)	207Pb* 235U*	± (%)	206Pb* 238U	± (%)	error corr.	206Pb* 238U*	± (Ma)	207Pb* 235U	± (Ma)	206Pb* 207Pb*	± (Ma)	**Best age (Ma)**	**± (Ma)**
SAL 1695 DN																	
59.0	10463	0.7	19.6	22.0	0.2474	22.3	0.0352	4.0	0.18	222.9	8.7	224.5	45.0	241.3	511.9	222.9	8.7
218.8	33009	1.2	19.9	4.3	0.2504	4.4	0.0361	0.9	0.20	228.3	1.9	226.9	9.0	211.9	100.0	228.3	1.9
82.8	10880	1.2	21.9	7.8	0.2283	8.2	0.0362	2.6	0.31	229.3	5.8	208.8	15.5	-15.9	188.3	229.3	5.8
396.6	67434	1.9	19.5	1.6	0.2568	2.0	0.0364	1.1	0.55	230.2	2.4	232.1	4.1	251.1	37.5	230.2	2.4
136.1	51476	1.4	19.8	2.8	0.2578	3.7	0.0369	2.4	0.65	233.8	5.6	232.9	7.8	223.9	65.7	233.8	5.6
828.8	16863	0.7	19.4	1.2	0.2633	2.2	0.0370	1.8	0.83	233.9	4.1	237.3	4.6	271.1	28.1	233.9	4.1
2961.1	25917	0.5	20.0	0.5	0.2553	2.0	0.0370	1.9	0.96	234.0	4.4	230.9	4.1	199.8	12.5	234.0	4.4
279.8	43260	0.5	19.5	4.3	0.2649	4.6	0.0376	1.4	0.31	237.7	3.3	238.6	9.7	247.8	100.0	237.7	3.3
197.6	16927	0.7	19.8	5.4	0.2630	5.8	0.0378	2.1	0.37	239.0	5.0	237.1	12.2	217.4	123.9	239.0	5.0
164.4	20808	0.9	19.4	5.9	0.2746	6.2	0.0385	1.9	0.31	243.8	4.6	246.4	13.6	271.1	135.2	243.8	4.6
174.6	54444	1.2	20.1	3.7	0.2645	4.5	0.0386	2.7	0.59	244.0	6.4	238.3	9.7	182.0	85.4	244.0	6.4
253.8	25968	1.7	19.8	4.1	0.2710	4.7	0.0388	2.4	0.51	245.6	5.8	243.5	10.2	223.1	94.2	245.6	5.8
676.4	10884	0.8	19.0	4.0	0.2836	4.0	0.0390	0.8	0.19	246.7	1.8	253.5	9.0	317.1	90.0	246.7	1.8
440.6	50264	1.9	19.3	1.8	0.2878	3.4	0.0402	2.9	0.85	254.2	7.1	256.8	7.7	280.6	41.2	254.2	7.1
269.1	34482	1.0	19.4	3.9	0.2867	4.0	0.0403	1.0	0.25	254.6	2.5	255.9	9.0	268.5	88.3	254.6	2.5
186.5	26733	1.5	19.9	7.1	0.2830	7.3	0.0408	1.7	0.23	257.6	4.3	253.0	16.3	210.5	163.8	257.6	4.3
182.2	21950	1.1	19.4	2.7	0.2934	3.1	0.0414	1.6	0.49	261.4	4.0	261.2	7.3	259.6	62.9	261.4	4.0
60.1	8256	1.7	21.4	10.2	0.2669	10.3	0.0414	1.7	0.16	261.5	4.3	240.2	22.1	37.3	244.1	261.5	4.3
298.4	60132	2.2	19.2	2.9	0.2985	3.5	0.0415	2.0	0.57	261.9	5.1	265.3	8.2	294.7	66.1	261.9	5.1
165.6	36758	2.0	20.4	6.1	0.2806	6.3	0.0416	1.4	0.22	262.5	3.5	251.1	14.0	145.9	143.9	262.5	3.5
610.7	106147	3.0	19.5	1.4	0.2984	1.8	0.0421	1.1	0.62	265.8	2.9	265.1	4.1	259.3	31.7	265.8	2.9
184.8	21465	0.7	20.1	5.0	0.2897	5.2	0.0422	1.5	0.29	266.2	4.0	258.3	12.0	187.5	117.0	266.2	4.0
207.3	6727	1.3	18.6	5.1	0.3136	7.9	0.0424	6.0	0.76	267.4	15.8	276.9	19.2	358.3	115.4	267.4	15.8

Appendix A: Cont. U/Pb detrital zircon geochronologic analyses by Laser-Ablation Multicollector ICP Mass Spectrometry

					Isotope ratios					Apparent ages (Ma)							
U (ppm)	206Pb 204Pb	U/Th	206Pb* 207Pb*	± (%)	207Pb* 235U*	± (%)	206Pb* 238U	± (%)	error corr.	206Pb* 238U*	± (Ma)	207Pb* 235U	± (Ma)	206Pb* 207Pb*	± (Ma)	**Best age (Ma)**	**± (Ma)**
SAL 1695 DN Cont.																	
208.4	35491	1.4	20.1	3.6	0.2917	4.2	0.0425	2.2	0.52	268.5	5.7	259.9	9.6	182.8	83.0	268.5	5.7
170.5	31976	1.1	19.1	2.8	0.3146	4.4	0.0435	3.5	0.78	274.6	9.3	277.7	10.8	304.5	63.2	274.6	9.3
1088.0	20372	3.4	18.2	1.7	0.4326	2.2	0.0571	1.4	0.63	357.9	5.0	365.0	6.9	410.4	38.8	357.9	5.0
239.9	38344	3.1	18.3	2.3	0.4476	2.8	0.0594	1.6	0.57	372.0	5.8	375.6	8.9	398.0	52.5	372.0	5.8
290.7	23440	3.0	18.3	2.0	0.4527	2.9	0.0599	2.0	0.70	375.2	7.3	379.2	9.1	403.2	45.7	375.2	7.3
464.4	75515	1.8	18.5	1.2	0.4559	1.7	0.0610	1.1	0.68	381.9	4.2	381.4	5.3	378.3	27.7	381.9	4.2
475.2	68720	2.1	17.8	1.0	0.5834	1.6	0.0754	1.3	0.81	468.8	5.8	466.6	6.0	456.0	21.1	468.8	5.8
914.0	18809	2.5	16.6	1.0	0.6614	5.2	0.0798	5.1	0.98	495.1	24.2	515.5	20.9	606.6	20.9	495.1	24.2
89.3	15368	1.5	17.2	4.1	0.6410	4.5	0.0800	1.8	0.41	496.2	8.8	502.9	17.8	533.7	89.9	496.2	8.8
319.0	33505	1.1	17.2	1.2	0.6599	2.0	0.0825	1.5	0.78	511.2	7.6	514.5	8.0	529.5	27.1	511.2	7.6
225.1	68161	4.5	17.3	1.8	0.6622	3.2	0.0830	2.6	0.82	513.8	12.8	515.9	12.8	525.5	39.9	513.8	12.8
517.8	80311	2.0	17.2	0.6	0.6701	1.4	0.0834	1.3	0.91	516.6	6.5	520.8	5.8	539.3	13.3	516.6	6.5
98.4	39100	2.4	17.3	2.9	0.6925	3.6	0.0870	2.1	0.60	537.9	11.0	534.3	14.9	518.7	63.0	537.9	11.0
241.8	7388	3.2	16.2	3.5	0.7493	7.6	0.0878	6.7	0.89	542.7	35.0	567.8	33.0	669.6	75.2	542.7	35.0
130.5	51365	2.5	17.2	3.8	0.7104	4.2	0.0886	1.7	0.42	547.3	9.2	545.0	17.6	535.6	82.8	547.3	9.2
92.5	32736	1.4	17.2	2.0	0.7145	3.1	0.0890	2.4	0.76	549.6	12.6	547.4	13.3	538.5	44.4	549.6	12.6
295.9	190677	4.0	16.9	1.0	0.7383	1.6	0.0904	1.3	0.78	557.7	6.8	561.4	7.0	576.6	22.1	557.7	6.8
118.8	7656	4.2	16.6	3.4	0.7524	3.7	0.0905	1.3	0.34	558.2	6.7	569.6	16.0	615.4	74.4	558.2	6.7
22.1	10777	2.7	18.3	13.0	0.6858	13.3	0.0908	2.9	0.22	560.5	15.6	530.3	55.2	402.3	292.9	560.5	15.6
472.6	8551	6.4	16.4	0.9	0.7734	2.1	0.0918	1.9	0.90	566.4	10.2	581.7	9.3	642.1	19.5	566.4	10.2
30.6	17930	1.0	17.0	6.3	0.7512	6.7	0.0927	2.3	0.35	571.4	12.6	568.9	29.1	559.1	136.8	571.4	12.6
190.0	77845	1.7	16.8	2.1	0.7610	2.3	0.0928	0.8	0.37	572.0	4.6	574.6	10.1	584.9	46.5	572.0	4.6
121.5	67410	3.1	17.2	2.2	0.7513	2.7	0.0936	1.6	0.60	576.8	9.1	569.0	11.8	537.9	47.4	576.8	9.1

Appendix A: Cont. U/Pb detrital zircon geochronologic analyses by Laser-Ablation Multicollector ICP Mass Spectrometry

					Isotope ratios					Apparent ages (Ma)							
U (ppm)	206Pb 204Pb	U/Th	206Pb* 207Pb*	± (%)	207Pb* 235U*	± (%)	206Pb* 238U	± (%)	error corr.	206Pb* 238U*	± (Ma)	207Pb* 235U	± (Ma)	206Pb* 207Pb*	± (Ma)	**Best age (Ma)**	**± (Ma)**
SAL 1695 DN Cont.																	
99.8	50492	1.2	17.3	2.2	0.7479	2.6	0.0937	1.4	0.55	577.3	7.9	567.0	11.4	526.0	48.1	577.3	7.9
184.4	17256	1.1	16.7	1.4	0.7759	1.7	0.0939	1.1	0.62	578.4	6.0	583.1	7.8	601.6	29.8	578.4	6.0
90.8	37021	1.0	17.1	3.9	0.7613	4.7	0.0943	2.6	0.56	581.2	14.7	574.8	20.8	549.6	86.1	581.2	14.7
297.8	165298	5.0	16.2	1.1	0.8105	3.7	0.0955	3.5	0.95	587.8	19.9	602.7	16.9	659.2	24.1	587.8	19.9
76.2	27285	2.4	16.8	4.6	0.7857	4.9	0.0955	1.8	0.36	588.0	9.9	588.7	21.8	591.5	98.8	588.0	9.9
107.7	51578	0.3	16.9	2.8	0.7791	3.2	0.0957	1.4	0.44	589.0	7.9	584.9	14.0	569.4	61.6	589.0	7.9
49.1	23572	1.4	16.4	4.7	0.8048	5.5	0.0958	2.9	0.53	589.5	16.5	599.5	25.0	637.4	100.7	589.5	16.5
30.5	9405	0.3	17.3	10.1	0.7662	10.3	0.0960	2.1	0.20	590.7	11.6	577.6	45.4	526.5	221.7	590.7	11.6
360.3	104543	2.6	16.8	0.7	0.7908	2.5	0.0962	2.4	0.95	592.1	13.3	591.6	11.1	589.8	16.0	592.1	13.3
534.3	126700	1.5	16.7	0.8	0.7982	1.1	0.0969	0.8	0.69	596.3	4.4	595.8	5.0	594.1	17.5	596.3	4.4
788.2	28103	18.2	16.5	0.8	0.8101	1.8	0.0971	1.6	0.90	597.3	9.2	602.5	8.1	622.3	16.5	597.3	9.2
722.3	96369	2.1	16.5	0.4	0.8151	2.0	0.0976	2.0	0.98	600.2	11.3	605.3	9.2	624.5	7.6	600.2	11.3
211.8	74494	1.2	16.7	1.7	0.8078	2.0	0.0977	1.0	0.52	600.9	5.8	601.2	8.9	602.3	36.3	600.9	5.8
1717.6	1065456	9.9	16.7	0.2	0.8074	1.1	0.0977	1.1	0.98	601.0	6.4	601.0	5.2	600.9	5.1	601.0	6.4
175.5	49370	1.9	16.8	1.8	0.8046	3.2	0.0982	2.7	0.82	603.7	15.3	599.4	14.6	583.2	39.8	603.7	15.3
181.2	76886	1.0	16.8	1.3	0.8124	2.3	0.0987	1.8	0.81	606.8	10.7	603.8	10.3	592.7	28.5	606.8	10.7
597.5	252333	1.6	16.6	0.4	0.8259	2.9	0.0992	2.9	0.99	609.8	16.9	611.4	13.5	617.1	9.6	609.8	16.9
455.4	84869	1.4	16.5	0.7	0.8322	1.7	0.0995	1.6	0.92	611.8	9.2	614.8	7.9	626.1	14.2	611.8	9.2
598.9	158303	2.3	16.7	0.3	0.8253	1.2	0.0999	1.2	0.97	613.6	7.1	611.0	5.7	601.2	7.0	613.6	7.1
199.2	48372	1.4	16.4	1.1	0.8440	2.6	0.1001	2.4	0.90	615.0	13.8	621.4	12.1	644.8	24.3	615.0	13.8
279.1	17653	0.4	16.3	2.4	0.8554	3.1	0.1009	1.9	0.62	619.9	11.3	627.6	14.4	655.6	51.7	619.9	11.3
134.2	53626	1.2	14.6	3.4	0.9661	10.1	0.1024	9.5	0.94	628.2	56.6	686.4	50.2	882.3	70.8	628.2	56.6
109.2	91233	0.6	16.6	2.6	0.8490	3.5	0.1024	2.3	0.66	628.6	13.6	624.1	16.1	607.6	56.2	628.6	13.6

Appendix A: Cont. U/Pb detrital zircon geochronologic analyses by Laser-Ablation Multicollector ICP Mass Spectrometry

					Isotope ratios					Apparent ages (Ma)							
U (ppm)	206Pb 204Pb	U/Th	206Pb* 207Pb*	± (%)	207Pb* 235U*	± (%)	206Pb* 238U	± (%)	error corr.	206Pb* 238U*	± (Ma)	207Pb* 235U	± (Ma)	206Pb* 207Pb*	± (Ma)	**Best age** (Ma)	± (Ma)
SAL 1695 DN Cont.																	
247.4	18283	0.4	16.4	0.9	0.8663	2.3	0.1033	2.1	0.92	633.6	12.7	633.6	10.8	633.7	19.8	633.6	12.7
259.9	189906	3.0	15.5	1.6	0.9225	3.1	0.1034	2.6	0.85	634.2	15.7	663.7	14.9	765.1	34.0	634.2	15.7
242.9	148564	3.9	15.9	1.3	0.9041	3.1	0.1046	2.8	0.91	641.0	17.2	653.9	14.9	698.6	27.2	641.0	17.2
531.2	27777	5.7	14.8	1.1	1.0687	1.9	0.1149	1.5	0.79	700.9	9.8	738.1	9.8	852.7	23.8	700.9	9.8
446.3	185180	2.4	14.6	1.4	1.1828	7.3	0.1250	7.2	0.98	759.6	51.4	792.6	40.3	886.7	29.4	759.6	51.4
119.2	10736	1.0	14.3	1.2	1.2289	4.4	0.1275	4.2	0.96	773.5	30.6	813.9	24.5	925.7	24.9	773.5	30.6
183.3	10303	3.8	14.0	0.8	1.2774	5.0	0.1295	4.9	0.99	785.1	36.4	835.7	28.4	972.6	16.5	785.1	36.4
602.7	20435	1.3	14.4	0.5	1.2481	3.9	0.1303	3.9	0.99	789.4	29.1	822.6	22.2	913.2	10.2	789.4	29.1
426.2	34420	1.0	14.2	0.6	1.2761	2.6	0.1313	2.5	0.97	795.0	18.8	835.1	14.7	943.3	13.2	795.0	18.8
157.7	72229	4.1	14.5	0.9	1.2773	2.1	0.1344	1.9	0.91	812.9	14.5	835.6	12.0	896.5	18.3	812.9	14.5
241.4	81221	3.8	14.5	0.5	1.3536	2.3	0.1428	2.3	0.98	860.3	18.3	869.1	13.6	891.6	9.8	860.3	18.3
246.0	226258	2.1	14.0	1.1	1.4293	8.5	0.1456	8.4	0.99	876.5	68.7	901.3	50.6	962.6	21.9	962.6	21.9
413.8	183988	14.8	13.9	0.6	1.4442	1.4	0.1454	1.2	0.89	875.4	10.0	907.5	8.2	986.4	12.8	986.4	12.8
293.4	226258	1.3	13.8	0.7	1.6541	1.5	0.1655	1.4	0.90	987.5	12.7	991.1	9.8	999.2	13.5	999.2	13.5
160.2	242344	1.1	13.7	0.9	1.7219	1.5	0.1717	1.2	0.79	1021.6	11.2	1016.7	9.6	1006.4	18.6	1006.4	18.6
524.0	38854	1.9	13.7	0.6	1.4927	1.9	0.1488	1.8	0.95	894.0	14.9	927.4	11.4	1007.8	11.7	1007.8	11.7
228.0	145838	4.1	13.7	0.6	1.6075	3.2	0.1601	3.2	0.98	957.1	28.1	973.2	20.2	1009.5	12.9	1009.5	12.9
39.0	26657	3.5	13.7	3.5	1.6656	3.8	0.1657	1.3	0.34	988.3	11.9	995.5	24.0	1011.4	71.9	1011.4	71.9
400.5	183325	10.8	13.7	0.4	1.6270	1.0	0.1615	0.9	0.91	965.3	8.2	980.7	6.4	1015.2	8.6	1015.2	8.6
335.4	121805	1.3	13.6	0.5	1.6399	3.3	0.1616	3.3	0.99	965.4	29.5	985.7	21.0	1031.0	10.0	1031.0	10.0
1467.1	41604	6.6	13.6	0.1	1.7002	0.8	0.1672	0.7	0.98	996.7	6.8	1008.6	4.8	1034.6	2.8	1034.6	2.8
270.7	169182	2.8	13.5	0.5	1.7460	5.2	0.1711	5.1	0.99	1018.0	48.5	1025.7	33.4	1042.1	10.8	1042.1	10.8
146.5	76789	3.1	13.5	1.0	1.7412	3.1	0.1705	2.9	0.95	1015.1	27.3	1023.9	19.8	1042.8	19.9	1042.8	19.9

Appendix A: Cont. U/Pb detrital zircon geochronologic analyses by Laser-Ablation Multicollector ICP Mass Spectrometry

					Isotope ratios					Apparent ages (Ma)							
U (ppm)	206Pb 204Pb	U/Th	206Pb* 207Pb*	± (%)	207Pb* 235U*	± (%)	206Pb* 238U	± (%)	error corr.	206Pb* 238U*	± (Ma)	207Pb* 235U	± (Ma)	206Pb* 207Pb*	± (Ma)	**Best age (Ma)**	**± (Ma)**
SAL 1695 DN Cont.																	
257.6	126856	1.0	13.5	0.7	1.6746	2.3	0.1637	2.2	0.96	977.1	19.6	998.9	14.4	1047.2	13.3	1047.2	13.3
155.3	131713	2.2	13.5	0.8	1.7244	1.3	0.1682	1.0	0.77	1002.4	9.6	1017.7	8.6	1050.8	17.0	1050.8	17.0
377.5	32491	3.6	13.4	0.5	1.6569	4.1	0.1614	4.1	0.99	964.7	36.7	992.2	26.1	1053.6	10.2	1053.6	10.2
251.8	210316	2.2	13.4	0.4	1.8051	1.8	0.1748	1.7	0.97	1038.6	16.3	1047.3	11.5	1065.6	9.0	1065.6	9.0
125.4	48022	3.6	13.3	1.8	1.8115	2.5	0.1753	1.7	0.69	1041.2	16.4	1049.6	16.2	1067.2	36.1	1067.2	36.1
291.1	209533	0.6	13.3	0.5	1.7336	1.7	0.1674	1.6	0.95	997.8	14.7	1021.1	10.8	1071.3	10.8	1071.3	10.8
350.5	2490	2.7	13.1	1.9	1.8390	3.0	0.1753	2.3	0.78	1041.3	22.3	1059.5	19.6	1097.2	37.4	1097.2	37.4
154.4	34178	2.6	13.1	1.2	1.8683	3.6	0.1781	3.3	0.94	1056.4	32.5	1069.9	23.5	1097.6	24.5	1097.6	24.5
144.5	177402	1.4	13.1	0.5	1.9013	1.1	0.1809	1.0	0.90	1072.0	9.8	1081.5	7.3	1100.9	9.4	1100.9	9.4
104.0	85763	0.7	12.6	1.3	2.1555	1.8	0.1977	1.2	0.65	1163.1	12.4	1166.8	12.3	1173.8	26.7	1173.8	26.7
392.7	219971	6.1	12.5	2.6	1.5946	4.7	0.1445	3.8	0.82	870.1	31.2	968.1	29.1	1197.8	52.1	1197.8	52.1
285.0	277379	1.0	12.4	0.3	2.2813	1.6	0.2050	1.6	0.98	1202.2	17.4	1206.5	11.4	1214.3	6.1	1214.3	6.1
526.4	93029	1.8	12.2	1.6	1.6675	2.0	0.1481	1.2	0.63	890.2	10.4	996.2	12.6	1237.6	30.4	1237.6	30.4
80.4	36004	1.3	9.3	1.0	4.3517	2.0	0.2925	1.8	0.88	1654.0	25.9	1703.2	16.6	1764.3	17.5	1764.3	17.5
355.0	334528	4.4	6.3	0.3	9.6722	3.1	0.4411	3.1	0.99	2355.4	60.4	2404.1	28.3	2445.5	5.8	2445.5	5.8
90.4	416006	2.0	6.3	0.5	9.7108	6.1	0.4417	6.0	1.00	2358.4	119.3	2407.7	55.9	2449.7	9.2	2449.7	9.2
387.6	854999	3.0	5.5	0.2	11.8485	2.3	0.4688	2.2	1.00	2478.4	46.2	2592.5	21.1	2682.9	3.1	2682.9	3.1
624.3	8640	3.3	5.4	0.1	11.6495	0.8	0.4599	0.8	0.99	2439.1	17.0	2576.7	7.9	2686.7	1.6	2686.7	1.6
101.1	148353	1.4	5.4	0.5	12.7723	1.6	0.4958	1.5	0.95	2595.9	33.1	2663.0	15.4	2714.4	8.6	2714.4	8.6
212.0	370573	1.6	5.3	0.1	12.8849	1.0	0.4998	1.0	0.99	2612.9	22.3	2671.3	9.9	2715.7	2.4	2715.7	2.4
75.0	36167	2.9	5.3	1.4	11.3077	3.6	0.4369	3.4	0.92	2336.9	65.8	2548.8	33.9	2722.1	22.9	2722.1	22.9
95.5	145233	1.6	5.3	0.2	13.2599	3.2	0.5123	3.2	1.00	2666.4	70.5	2698.3	30.5	2722.3	3.8	2722.3	3.8
743.5	1188424	1.1	5.3	0.0	13.6015	1.0	0.5252	1.0	1.00	2721.3	22.8	2722.4	9.7	2723.1	0.8	2723.1	0.8

Appendix A: Cont. U/Pb detrital zircon geochronologic analyses by Laser-Ablation Multicollector ICP Mass Spectrometry

					Isotope ratios					Apparent ages (Ma)							
U (ppm)	206Pb 204Pb	U/Th	206Pb* 207Pb*	± (%)	207Pb* 235U*	± (%)	206Pb* 238U	± (%)	error corr.	206Pb* 238U*	± (Ma)	207Pb* 235U	± (Ma)	206Pb* 207Pb*	± (Ma)	**Best age (Ma)**	**±** (Ma)
SAL 1695 DN Cont.																	
140.6	300165	1.8	5.3	0.2	12.8049	3.1	0.4926	3.1	1.00	2581.9	66.8	2665.4	29.6	2729.4	2.7	2729.4	2.7
109.4	112740	2.4	5.3	0.6	12.8196	4.0	0.4916	4.0	0.99	2577.4	84.6	2666.5	37.9	2734.7	9.8	2734.7	9.8
158.8	56918	2.5	5.2	0.3	12.1843	3.4	0.4612	3.4	1.00	2444.9	69.3	2618.7	32.1	2755.9	4.3	2755.9	4.3
215.1	346978	0.5	4.7	0.1	16.1390	1.4	0.5537	1.4	1.00	2840.4	32.4	2885.1	13.6	2916.4	2.3	2916.4	2.3
SAL 1607 TN																	
222.1	22432	2.4	20.0	2.0	0.2592	2.5	0.0376	1.4	0.57	237.7	3.3	234.0	5.2	197.1	47.2	237.7	3.3
3084.0	223810	0.4	20.1	0.3	0.2970	1.9	0.0433	1.8	0.99	273.4	4.9	264.0	4.3	181.6	6.3	273.4	4.9
363.1	2838	1.0	16.7	2.4	0.5639	6.1	0.0684	5.5	0.91	426.2	22.8	454.0	22.2	597.5	52.9	426.2	22.8
1019.0	256454	2.9	17.6	0.4	0.6215	0.8	0.0793	0.7	0.85	491.8	3.3	490.8	3.2	486.0	9.7	491.8	3.3
187.2	88549	1.6	17.6	1.1	0.6357	2.2	0.0812	2.0	0.87	503.0	9.5	499.6	8.8	484.1	24.1	503.0	9.5
262.5	86852	1.0	17.3	2.0	0.6563	2.2	0.0823	0.8	0.37	509.8	3.9	512.3	8.7	523.7	44.0	509.8	3.9
338.5	202641	1.5	17.2	1.4	0.6725	2.2	0.0841	1.7	0.78	520.7	8.7	522.2	9.0	529.0	30.0	520.7	8.7
651.3	239381	11.8	17.1	0.5	0.6989	1.2	0.0867	1.0	0.88	536.1	5.4	538.1	4.9	546.6	12.0	536.1	5.4
140.6	52896	1.5	17.0	2.6	0.7037	5.3	0.0868	4.6	0.87	536.4	23.9	541.0	22.2	560.4	56.1	536.4	23.9
247.9	43130	2.4	15.9	2.6	0.7732	3.8	0.0893	2.8	0.74	551.6	14.9	581.6	16.9	700.6	54.9	551.6	14.9
251.6	72554	1.5	17.0	2.4	0.7299	2.7	0.0899	1.3	0.49	555.2	7.1	556.5	11.7	561.9	52.0	555.2	7.1
1092.3	457421	3.5	17.0	0.5	0.7301	1.1	0.0902	1.0	0.90	556.6	5.1	556.6	4.5	556.7	10.0	556.6	5.1
796.7	101821	4.9	17.0	0.5	0.7312	1.7	0.0902	1.6	0.95	556.6	8.7	557.3	7.3	559.9	11.8	556.6	8.7
159.4	41518	4.0	17.1	1.8	0.7289	2.3	0.0906	1.4	0.63	559.3	7.6	555.9	9.7	542.0	38.4	559.3	7.6
236.3	63806	3.4	17.2	1.7	0.7299	2.0	0.0908	1.2	0.58	560.3	6.4	556.5	8.7	540.8	36.2	560.3	6.4
471.2	191964	1.9	16.9	0.6	0.7424	1.8	0.0908	1.6	0.94	560.5	8.8	563.8	7.6	577.2	13.0	560.5	8.8
256.2	110717	2.9	17.0	0.9	0.7406	2.9	0.0913	2.8	0.95	563.2	14.9	562.8	12.5	561.1	19.8	563.2	14.9
57.4	27138	0.5	17.2	4.7	0.7353	5.0	0.0917	1.8	0.35	565.3	9.6	559.7	21.7	536.7	103.1	565.3	9.6

Appendix A: Cont. U/Pb detrital zircon geochronologic analyses by Laser-Ablation Multicollector ICP Mass Spectrometry

					Isotope ratios					Apparent ages (Ma)							
U (ppm)	206Pb 204Pb	U/Th	206Pb* 207Pb*	± (%)	207Pb* 235U*	± (%)	206Pb* 238U	± (%)	error corr.	206Pb* 238U*	± (Ma)	207Pb* 235U	± (Ma)	206Pb* 207Pb*	± (Ma)	**Best age (Ma)**	**± (Ma)**
SAL 1607 TN Cont.																	
28.5	11815	0.6	18.1	12.3	0.7006	12.5	0.0919	2.4	0.19	566.8	12.8	539.1	52.3	423.9	274.5	566.8	12.8
27.4	16250	0.9	17.0	5.7	0.7511	7.8	0.0926	5.3	0.69	570.8	29.1	568.8	33.8	561.2	123.3	570.8	29.1
124.8	22178	0.4	16.4	2.2	0.7793	2.4	0.0927	1.1	0.44	571.6	5.9	585.1	10.8	637.6	46.9	571.6	5.9
619.6	122674	1.2	16.9	0.6	0.7619	0.8	0.0931	0.6	0.73	574.0	3.4	575.1	3.7	579.5	12.5	574.0	3.4
310.6	10705	3.4	16.5	1.1	0.7810	1.8	0.0935	1.4	0.78	576.2	7.6	586.1	7.9	624.4	24.2	576.2	7.6
275.0	120279	1.5	16.6	1.0	0.7795	2.0	0.0938	1.7	0.88	577.8	9.6	585.2	8.8	614.2	20.6	577.8	9.6
222.8	88690	1.2	17.0	1.9	0.7634	2.3	0.0940	1.2	0.55	579.0	6.9	576.0	10.0	564.1	41.3	579.0	6.9
135.1	44894	0.6	16.9	2.4	0.7681	3.5	0.0943	2.6	0.73	581.1	14.3	578.7	15.6	569.0	52.7	581.1	14.3
391.6	160635	1.2	16.9	0.8	0.7720	2.2	0.0946	2.1	0.93	582.7	11.6	580.9	9.8	574.0	17.2	582.7	11.6
356.9	43875	1.8	16.9	0.5	0.7733	1.9	0.0949	1.8	0.96	584.6	9.9	581.7	8.2	570.4	11.8	584.6	9.9
566.3	367006	10.6	16.9	0.6	0.7785	2.6	0.0952	2.5	0.97	586.1	13.9	584.6	11.3	578.9	13.8	586.1	13.9
989.2	466827	4.7	16.8	0.4	0.7802	1.8	0.0952	1.7	0.98	586.4	9.6	585.6	7.8	582.5	7.8	586.4	9.6
533.6	337697	2.4	16.8	0.7	0.7840	1.6	0.0952	1.4	0.90	586.5	7.8	587.8	6.9	592.7	14.7	586.5	7.8
44.5	16601	0.5	16.3	8.7	0.8083	9.7	0.0954	4.4	0.45	587.2	24.4	601.5	44.1	655.9	186.6	587.2	24.4
230.7	86893	1.0	16.7	0.7	0.7911	1.6	0.0956	1.4	0.89	588.3	7.8	591.8	7.0	605.1	15.7	588.3	7.8
154.6	34640	3.3	16.5	2.0	0.8027	3.2	0.0958	2.5	0.78	589.6	14.2	598.3	14.6	631.5	43.4	589.6	14.2
79.8	27211	0.5	16.8	2.2	0.7865	3.8	0.0958	3.1	0.82	589.7	17.3	589.2	16.8	587.3	46.8	589.7	17.3
64.0	19071	0.4	16.8	3.9	0.7860	4.2	0.0959	1.6	0.38	590.2	9.1	588.9	18.8	584.0	84.4	590.2	9.1
150.4	43375	0.6	16.8	2.2	0.7859	3.1	0.0959	2.3	0.72	590.3	12.7	588.9	14.1	583.3	47.8	590.3	12.7
110.7	56336	0.9	17.0	2.7	0.7772	5.0	0.0960	4.2	0.84	591.2	23.5	583.9	22.1	555.7	59.8	591.2	23.5
194.0	22134	0.7	16.7	2.6	0.7935	3.1	0.0962	1.7	0.56	592.3	9.9	593.2	14.0	596.6	55.8	592.3	9.9
416.8	54269	1.4	16.6	0.8	0.8003	1.4	0.0964	1.2	0.82	593.2	6.6	597.0	6.4	611.6	17.6	593.2	6.6
144.6	63333	0.6	16.9	1.4	0.7904	4.4	0.0967	4.2	0.95	595.0	23.7	591.4	19.7	577.8	30.8	595.0	23.7

Appendix A: Cont. U/Pb detrital zircon geochronologic analyses by Laser-Ablation Multicollector ICP Mass Spectrometry

					Isotope ratios					Apparent ages (Ma)							
U (ppm)	206Pb 204Pb	U/Th	206Pb* 207Pb*	± (%)	207Pb* 235U*	± (%)	206Pb* 238U	± (%)	error corr.	206Pb* 238U*	± (Ma)	207Pb* 235U	± (Ma)	206Pb* 207Pb*	± (Ma)	**Best age** (Ma)	± (Ma)
SAL 1607 TN Cont.																	
134.6	49902	1.0	17.0	2.2	0.7826	2.9	0.0967	1.9	0.65	595.0	10.5	587.0	12.8	555.9	47.6	595.0	10.5
186.6	67887	0.9	16.9	0.9	0.7917	2.2	0.0970	2.0	0.91	596.6	11.3	592.1	9.8	575.0	19.4	596.6	11.3
172.8	36174	0.8	16.6	1.6	0.8061	1.8	0.0971	0.9	0.47	597.2	4.9	600.3	8.2	612.1	34.3	597.2	4.9
331.3	58537	1.4	16.7	1.0	0.8027	2.1	0.0972	1.8	0.87	597.8	10.2	598.3	9.4	600.3	22.4	597.8	10.2
603.6	130834	1.8	16.7	0.7	0.8023	4.5	0.0972	4.5	0.99	598.1	25.6	598.1	20.5	598.2	15.4	598.1	25.6
98.0	38147	1.9	16.7	3.4	0.8058	3.7	0.0974	1.4	0.39	599.2	8.2	600.1	16.7	603.3	73.6	599.2	8.2
517.3	122625	2.4	16.8	0.6	0.8004	1.3	0.0975	1.1	0.88	599.7	6.5	597.0	5.8	587.1	13.0	599.7	6.5
199.5	66776	4.8	14.7	3.6	0.9125	4.1	0.0975	1.9	0.47	599.8	11.1	658.4	19.8	864.6	74.8	599.8	11.1
314.3	40086	1.8	16.4	0.7	0.8181	2.2	0.0976	2.1	0.94	600.1	11.8	607.0	10.0	632.8	15.8	600.1	11.8
153.0	59928	0.4	16.6	3.1	0.8136	3.3	0.0978	1.2	0.35	601.4	6.7	604.5	15.0	616.0	66.6	601.4	6.7
192.4	57293	1.3	16.7	1.2	0.8096	1.4	0.0979	0.7	0.49	602.1	3.9	602.3	6.3	602.7	26.0	602.1	3.9
221.5	86590	1.6	16.6	1.6	0.8167	2.1	0.0984	1.2	0.60	604.8	7.1	606.2	9.4	611.6	35.6	604.8	7.1
746.0	77886	16.4	16.4	0.5	0.8274	1.5	0.0985	1.4	0.94	605.7	8.0	612.2	6.8	636.3	11.1	605.7	8.0
1163.3	246829	4.9	16.6	0.3	0.8183	0.9	0.0987	0.8	0.95	606.9	4.8	607.1	4.0	607.9	5.8	606.9	4.8
526.2	79153	1.7	16.6	0.6	0.8198	1.2	0.0988	1.1	0.89	607.1	6.4	608.0	5.7	611.0	12.3	607.1	6.4
310.2	101148	3.3	16.8	1.6	0.8200	2.8	0.0998	2.3	0.82	613.3	13.2	608.1	12.6	588.6	34.4	613.3	13.2
102.5	27342	1.8	16.7	2.6	0.8248	2.8	0.1001	1.1	0.40	615.2	6.6	610.7	13.0	594.1	56.3	615.2	6.6
235.2	92250	4.0	14.9	3.3	0.9243	5.0	0.1002	3.7	0.75	615.7	22.0	664.6	24.3	834.4	68.3	615.7	22.0
261.8	88907	1.7	16.6	0.8	0.8317	1.3	0.1003	1.0	0.77	616.2	5.7	614.6	5.8	608.5	17.5	616.2	5.7
213.1	19319	1.8	15.7	1.1	0.8882	4.5	0.1009	4.3	0.97	619.5	25.7	645.4	21.4	737.2	23.7	619.5	25.7
374.7	156616	2.1	16.5	0.8	0.8462	1.0	0.1010	0.6	0.62	620.1	3.8	622.6	4.8	631.5	17.4	620.1	3.8
74.5	21723	2.3	16.4	2.9	0.8471	3.3	0.1010	1.5	0.48	620.1	9.2	623.1	15.1	633.7	61.6	620.1	9.2
495.0	227553	5.6	16.7	0.7	0.8367	1.6	0.1011	1.4	0.90	620.7	8.5	617.3	7.4	605.0	14.7	620.7	8.5

Appendix A: Cont. U/Pb detrital zircon geochronologic analyses by Laser-Ablation Multicollector ICP Mass Spectrometry

					Isotope ratios					Apparent ages (Ma)							
U (ppm)	206Pb 204Pb	U/Th	206Pb* 207Pb*	± (%)	207Pb* 235U*	± (%)	206Pb* 238U	± (%)	error corr.	206Pb* 238U*	± (Ma)	207Pb* 235U	± (Ma)	206Pb* 207Pb*	± (Ma)	**Best age (Ma)**	± (Ma)
SAL 1607 TN Cont.																	
580.4	293983	6.2	16.5	0.5	0.8430	1.8	0.1011	1.7	0.96	621.1	10.4	620.8	8.5	619.6	11.7	621.1	10.4
176.5	75045	2.7	16.3	1.7	0.8538	2.0	0.1012	1.1	0.56	621.3	6.6	626.7	9.4	646.4	36.1	621.3	6.6
263.3	98646	1.8	16.6	0.9	0.8525	1.6	0.1025	1.3	0.82	628.8	7.7	626.0	7.3	616.0	19.5	628.8	7.7
192.1	55607	1.9	16.4	1.4	0.8778	1.8	0.1047	1.2	0.65	641.7	7.2	639.8	8.6	633.0	29.4	641.7	7.2
676.8	94061	4.7	16.3	1.2	0.8982	1.5	0.1059	1.0	0.63	648.9	5.9	650.7	7.3	657.2	25.3	648.9	5.9
74.4	29896	1.5	16.2	3.3	0.9077	5.0	0.1069	3.7	0.75	654.9	23.0	655.8	23.9	659.1	70.8	654.9	23.0
300.9	58006	4.3	15.0	1.1	0.9854	2.6	0.1073	2.3	0.90	657.1	14.6	696.4	13.0	825.4	22.9	657.1	14.6
184.1	60955	1.3	15.0	2.1	1.1088	8.4	0.1203	8.1	0.97	732.1	56.3	757.6	44.9	833.6	43.9	732.1	56.3
1034.1	50548	12.2	14.9	0.9	1.1861	2.3	0.1283	2.1	0.92	778.2	15.3	794.1	12.4	839.1	18.3	778.2	15.3
192.0	46891	3.6	14.9	1.3	1.2145	3.5	0.1308	3.3	0.93	792.5	24.5	807.3	19.7	848.2	26.6	792.5	24.5
494.9	339532	2.0	14.4	1.2	1.3704	4.0	0.1433	3.8	0.95	863.4	30.6	876.3	23.3	909.1	25.2	863.4	30.6
209.3	115379	2.8	14.4	0.8	1.4370	2.7	0.1503	2.6	0.96	902.8	22.0	904.5	16.3	908.7	15.8	908.7	15.8
345.9	215227	2.7	14.3	0.6	1.4599	1.1	0.1515	0.9	0.85	909.2	7.7	914.0	6.5	925.6	11.7	925.6	11.7
1047.7	249465	10.9	14.2	0.5	1.4093	3.4	0.1453	3.4	0.99	874.4	27.5	892.9	20.3	938.8	11.1	938.8	11.1
350.8	28518	3.5	14.1	0.9	1.5484	1.2	0.1580	0.8	0.69	945.7	7.3	949.9	7.5	959.4	18.0	959.4	18.0
95.6	52166	1.0	13.9	1.3	1.6130	2.2	0.1630	1.7	0.81	973.4	15.7	975.3	13.5	979.3	25.6	979.3	25.6
581.2	488045	2.6	13.9	0.3	1.6711	1.0	0.1683	0.9	0.95	1002.5	8.5	997.6	6.1	986.9	6.3	986.9	6.3
419.8	472317	3.0	13.9	0.6	1.6753	1.2	0.1683	1.1	0.89	1002.8	10.1	999.2	7.8	991.3	11.6	991.3	11.6
302.9	141365	2.2	13.7	0.7	1.5614	2.5	0.1557	2.4	0.96	932.8	21.0	955.0	15.6	1006.6	14.1	1006.6	14.1
429.3	307773	2.0	13.6	0.6	1.7475	1.6	0.1729	1.5	0.93	1028.2	14.5	1026.2	10.5	1022.1	11.9	1022.1	11.9
122.8	100810	1.0	13.5	1.1	1.8870	1.4	0.1842	0.9	0.61	1089.8	8.6	1076.5	9.3	1049.8	22.3	1049.8	22.3
372.4	496253	3.2	13.4	0.4	1.7500	1.6	0.1705	1.6	0.96	1014.9	14.6	1027.2	10.4	1053.4	8.7	1053.4	8.7
267.8	175294	2.2	13.4	0.6	1.8566	3.0	0.1804	2.9	0.98	1069.3	28.6	1065.8	19.5	1058.6	11.3	1058.6	11.3

Appendix A: Cont. U/Pb detrital zircon geochronologic analyses by Laser-Ablation Multicollector ICP Mass Spectrometry

					Isotope ratios					Apparent ages (Ma)							
U (ppm)	206Pb 204Pb	U/Th	206Pb* 207Pb*	± (%)	207Pb* 235U*	± (%)	206Pb* 238U	± (%)	error corr.	206Pb* 238U*	± (Ma)	207Pb* 235U	± (Ma)	206Pb* 207Pb*	± (Ma)	**Best age (Ma)**	± (Ma)
SAL 1607 TN Cont.																	
70.1	38717	1.5	13.4	2.3	1.8313	3.7	0.1779	2.9	0.79	1055.7	28.7	1056.8	24.5	1059.1	46.0	1059.1	46.0
224.7	178694	2.2	13.3	0.5	1.8694	1.4	0.1806	1.3	0.93	1070.4	12.5	1070.3	9.0	1070.2	10.4	1070.2	10.4
216.5	145401	2.1	13.3	0.6	1.8941	1.2	0.1825	1.1	0.88	1080.8	10.6	1079.0	8.1	1075.4	11.8	1075.4	11.8
211.9	175520	1.0	13.3	0.9	1.9220	2.5	0.1847	2.3	0.94	1092.8	23.2	1088.8	16.5	1080.8	17.3	1080.8	17.3
230.9	373805	1.2	13.2	0.7	1.9721	1.7	0.1892	1.5	0.92	1117.3	15.6	1106.0	11.1	1084.0	13.2	1084.0	13.2
351.7	106013	2.5	13.1	0.5	1.9572	1.9	0.1866	1.8	0.96	1103.0	18.0	1100.9	12.5	1096.8	10.9	1096.8	10.9
279.7	94848	2.1	13.1	0.9	1.9947	1.2	0.1896	0.8	0.66	1119.3	8.0	1113.7	8.0	1102.8	17.8	1102.8	17.8
314.0	128899	2.1	13.1	0.6	1.8255	1.1	0.1732	1.0	0.86	1029.5	9.4	1054.7	7.5	1107.1	11.5	1107.1	11.5
33.7	24490	1.1	12.5	3.3	2.3183	3.5	0.2110	1.2	0.33	1234.2	13.2	1217.9	24.9	1189.2	65.4	1189.2	65.4
153.0	77731	0.4	12.5	0.8	2.3353	1.1	0.2115	0.8	0.70	1236.8	8.6	1223.1	7.7	1198.9	15.2	1198.9	15.2
201.3	152841	2.3	12.5	0.7	2.2371	2.0	0.2025	1.8	0.93	1189.0	19.9	1192.7	13.7	1199.6	13.8	1199.6	13.8
89.9	142873	1.4	12.4	2.2	2.3923	6.6	0.2158	6.2	0.94	1259.9	70.7	1240.3	47.0	1206.5	43.1	1206.5	43.1
111.7	39076	1.6	12.4	0.7	2.3113	1.6	0.2074	1.4	0.88	1214.9	15.5	1215.8	11.2	1217.3	14.5	1217.3	14.5
43.6	35249	0.8	12.4	1.7	2.2694	2.2	0.2034	1.3	0.60	1193.6	14.1	1202.8	15.2	1219.4	33.9	1219.4	33.9
63.3	73159	1.7	11.6	1.2	2.7062	1.5	0.2273	1.0	0.66	1320.1	12.1	1330.2	11.4	1346.4	22.4	1346.4	22.4
22.3	29894	1.1	11.5	6.6	2.5256	6.8	0.2106	1.7	0.25	1232.1	19.1	1279.4	49.5	1359.8	126.8	1359.8	126.8
237.5	230811	1.4	11.3	0.3	2.9914	1.5	0.2442	1.5	0.97	1408.7	18.4	1405.4	11.4	1400.5	6.5	1400.5	6.5
90.9	50026	1.4	11.1	1.2	2.3712	4.6	0.1914	4.5	0.96	1128.8	46.1	1234.0	33.0	1422.7	23.9	1422.7	23.9
194.2	90833	2.0	10.9	1.3	3.1710	2.3	0.2509	1.9	0.83	1443.1	24.4	1450.1	17.6	1460.4	24.4	1460.4	24.4
412.1	487811	1.7	8.8	0.2	5.2233	1.2	0.3340	1.2	0.99	1857.8	19.6	1856.4	10.5	1854.9	3.0	1854.9	3.0
76.4	87157	0.9	8.8	0.6	5.2370	3.2	0.3337	3.1	0.98	1856.4	49.9	1858.6	26.9	1861.1	11.3	1861.1	11.3
573.0	696335	2.0	8.7	0.3	5.2531	1.8	0.3307	1.8	0.99	1841.6	28.9	1861.3	15.6	1883.3	5.0	1883.3	5.0
287.4	267634	8.3	7.0	0.2	8.1813	0.9	0.4153	0.9	0.99	2238.9	17.7	2251.3	8.6	2262.5	2.8	2262.5	2.8

Appendix A: Cont. U/Pb detrital zircon geochronologic analyses by Laser-Ablation Multicollector ICP Mass Spectrometry

					Isotope ratios					Apparent ages (Ma)							
U (ppm)	206Pb 204Pb	U/Th	206Pb* 207Pb*	± (%)	207Pb* 235U*	± (%)	206Pb* 238U	± (%)	error corr.	206Pb* 238U*	± (Ma)	207Pb* 235U	± (Ma)	206Pb* 207Pb*	± (Ma)	**Best age (Ma)**	± (Ma)
SAL 1607 TN Cont.																	
603.5	41626	3.5	6.8	1.3	8.6599	4.5	0.4243	4.3	0.95	2280.1	81.7	2302.9	40.6	2323.1	22.9	2323.1	22.9
321.5	11139	1.5	6.5	1.6	6.4963	4.8	0.3077	4.5	0.94	1729.2	67.8	2045.4	41.9	2381.3	28.0	2381.3	28.0
88.7	153782	0.4	6.0	0.4	10.8865	0.9	0.4771	0.8	0.87	2514.7	16.6	2513.5	8.5	2512.4	7.4	2512.4	7.4
196.9	469182	2.1	6.0	0.2	10.4802	1.3	0.4589	1.3	0.99	2434.7	25.6	2478.2	11.8	2514.0	2.6	2514.0	2.6
267.8	13740	1.9	5.4	0.3	12.0822	1.8	0.4768	1.8	0.98	2513.1	36.6	2610.8	16.8	2687.5	5.5	2687.5	5.5
166.7	376109	1.4	5.3	0.1	13.5712	0.8	0.5248	0.8	0.98	2719.4	18.3	2720.3	7.9	2720.9	2.5	2720.9	2.5
61.4	69624	1.4	5.3	0.4	13.5295	1.8	0.5218	1.8	0.97	2706.9	38.9	2717.4	17.1	2725.1	7.0	2725.1	7.0
272.7	53404	1.3	4.4	0.4	17.6398	2.8	0.5579	2.7	0.99	2858.0	62.7	2970.3	26.4	3047.2	6.8	3047.2	6.8
191.0	257328	1.9	4.0	0.1	21.7612	0.9	0.6342	0.9	1.00	3166.0	22.2	3173.1	8.6	3177.6	1.4	3177.6	1.4
SAL 1616 MR																	
339.5	62232	0.6	17.8	0.9	0.6062	1.6	0.0782	1.3	0.81	485.3	6.0	481.2	6.1	461.5	20.9	485.3	6.0
349.5	12772	1.0	17.0	1.6	0.6672	3.8	0.0822	3.5	0.90	509.3	17.0	519.0	15.6	562.2	35.7	509.3	17.0
236.9	70678	4.3	17.5	1.5	0.6590	1.8	0.0835	1.0	0.55	516.7	4.9	514.0	7.3	502.1	33.4	516.7	4.9
1339.0	476891	43.8	17.4	0.2	0.6633	1.2	0.0837	1.2	0.98	518.0	6.1	516.6	5.0	510.8	5.1	518.0	6.1
363.2	99785	4.4	17.1	1.3	0.6851	1.5	0.0851	0.8	0.51	526.8	4.0	529.8	6.3	543.1	28.8	526.8	4.0
157.2	72864	1.3	17.2	1.9	0.6825	2.1	0.0854	0.9	0.43	528.0	4.7	528.3	8.8	529.6	42.2	528.0	4.7
290.4	55557	85.0	16.9	1.1	0.7090	1.3	0.0871	0.7	0.55	538.5	3.8	544.2	5.6	568.1	23.9	538.5	3.8
605.8	149012	361.2	17.1	0.6	0.7266	2.3	0.0899	2.2	0.96	554.7	11.5	554.5	9.6	554.0	14.0	554.7	11.5
360.7	9773	0.8	16.8	0.8	0.7395	1.4	0.0900	1.2	0.81	555.3	6.1	562.1	6.1	589.6	18.0	555.3	6.1
74.8	53497	1.5	17.5	4.8	0.7111	4.8	0.0902	0.9	0.18	556.6	4.7	545.4	20.4	498.9	105.0	556.6	4.7
382.9	74470	39.9	16.9	0.5	0.7389	2.4	0.0905	2.4	0.98	558.3	12.6	561.8	10.4	575.6	10.1	558.3	12.6
2228.6	962345	46.7	17.0	0.2	0.7363	0.6	0.0908	0.6	0.96	560.0	3.2	560.2	2.6	561.3	3.6	560.0	3.2
994.5	43949	78.5	16.9	0.8	0.7426	1.4	0.0910	1.2	0.84	561.4	6.5	563.9	6.2	574.2	17.0	561.4	6.5

Appendix A: Cont. U/Pb detrital zircon geochronologic analyses by Laser-Ablation Multicollector ICP Mass Spectrometry

					Isotope ratios					Apparent ages (Ma)							
U (ppm)	206Pb 204Pb	U/Th	206Pb* 207Pb*	± (%)	207Pb* 235U*	± (%)	206Pb* 238U	± (%)	error corr.	206Pb* 238U*	± (Ma)	207Pb* 235U	± (Ma)	206Pb* 207Pb*	± (Ma)	**Best age (Ma)**	**± (Ma)**
SAL 1616 MR Cont.																	
46.3	15961	1.7	18.0	4.5	0.7009	5.1	0.0914	2.4	0.47	564.0	12.9	539.3	21.2	436.3	99.8	564.0	12.9
78.2	33505	1.6	16.6	3.2	0.7665	3.3	0.0923	1.0	0.29	568.8	5.3	577.8	14.5	613.0	68.1	568.8	5.3
293.2	154814	3.5	16.9	1.4	0.7569	2.2	0.0928	1.7	0.78	572.1	9.4	572.2	9.7	573.0	30.1	572.1	9.4
232.1	46686	90.1	16.8	1.1	0.7645	2.0	0.0929	1.7	0.83	572.9	9.2	576.6	8.9	591.2	24.5	572.9	9.2
194.1	51903	0.9	16.9	0.5	0.7609	1.3	0.0930	1.2	0.90	573.3	6.3	574.5	5.6	579.5	11.9	573.3	6.3
18.7	6977	0.8	18.4	16.6	0.6961	17.0	0.0930	3.8	0.22	573.4	20.7	536.5	71.1	382.4	375.8	573.4	20.7
62.0	65639	0.7	16.5	3.8	0.7774	4.4	0.0933	2.3	0.52	574.9	12.5	584.0	19.6	619.6	81.6	574.9	12.5
89.6	36445	0.8	16.9	2.3	0.7644	2.6	0.0935	1.2	0.45	576.3	6.4	576.6	11.5	577.6	50.9	576.3	6.4
28.0	10604	0.5	18.1	22.2	0.7168	22.3	0.0939	2.2	0.10	578.6	12.3	548.7	94.8	426.8	500.2	578.6	12.3
81.6	30011	1.1	17.0	1.8	0.7635	2.6	0.0944	1.8	0.71	581.3	10.0	576.0	11.2	555.3	39.5	581.3	10.0
288.0	95416	3.6	16.8	0.4	0.7892	1.1	0.0960	1.0	0.93	590.7	5.6	590.7	4.8	590.7	8.5	590.7	5.6
224.5	102580	4.0	16.3	1.3	0.8155	3.9	0.0965	3.6	0.94	594.0	20.7	605.5	17.7	649.2	27.8	594.0	20.7
256.1	69337	2.8	16.8	1.4	0.7954	1.7	0.0967	0.9	0.56	595.1	5.3	594.3	7.5	590.9	29.8	595.1	5.3
504.0	177345	3.9	16.7	0.6	0.8085	0.8	0.0978	0.5	0.66	601.6	3.0	601.6	3.7	601.5	13.2	601.6	3.0
247.6	125465	2.1	16.5	1.1	0.8188	1.9	0.0982	1.5	0.79	603.9	8.4	607.4	8.5	620.5	24.5	603.9	8.4
382.2	124403	1.3	16.7	0.8	0.8161	1.7	0.0989	1.5	0.88	608.0	8.9	605.9	7.9	597.9	17.8	608.0	8.9
117.5	44739	3.9	16.5	3.2	0.8355	10.6	0.0997	10.1	0.95	612.8	59.1	616.7	49.0	631.0	68.4	612.8	59.1
448.4	228811	5.6	16.6	0.7	0.8287	1.2	0.0999	1.0	0.81	614.0	5.7	612.9	5.5	608.6	15.2	614.0	5.7
56.0	30121	0.9	16.4	5.5	0.8439	6.1	0.1003	2.6	0.43	616.2	15.3	621.3	28.4	640.0	118.8	616.2	15.3
132.0	72294	7.7	16.4	1.3	0.8468	1.9	0.1008	1.4	0.73	619.0	8.2	622.9	8.8	636.9	27.8	619.0	8.2
189.6	8510	1.7	16.1	3.5	0.8700	4.3	0.1014	2.4	0.57	622.7	14.4	635.6	20.1	681.6	74.8	622.7	14.4
633.2	279870	145.3	16.6	0.6	0.8511	1.2	0.1024	1.1	0.88	628.3	6.4	625.2	5.7	614.2	12.5	628.3	6.4
367.1	39065	5.1	15.0	1.5	1.0687	6.4	0.1164	6.2	0.97	709.7	41.9	738.1	33.6	825.2	31.5	709.7	41.9

Appendix A: Cont. U/Pb detrital zircon geochronologic analyses by Laser-Ablation Multicollector ICP Mass Spectrometry

					Isotope ratios					Apparent ages (Ma)							
U (ppm)	206Pb 204Pb	U/Th	206Pb* 207Pb*	± (%)	207Pb* 235U*	± (%)	206Pb* 238U	± (%)	error corr.	206Pb* 238U*	± (Ma)	207Pb* 235U	± (Ma)	206Pb* 207Pb*	± (Ma)	**Best age** (Ma)	± (Ma)
SAL 1616 MR Cont.																	
208.2	119206	3.2	14.9	1.1	1.1248	2.9	0.1216	2.7	0.92	739.5	18.5	765.3	15.5	841.3	23.9	739.5	18.5
228.3	105213	4.1	14.4	2.0	1.1736	4.4	0.1225	4.0	0.89	744.7	27.8	788.3	24.3	913.9	41.0	744.7	27.8
283.9	116339	4.0	14.2	3.5	1.2058	10.0	0.1243	9.3	0.94	755.4	66.6	803.3	55.4	938.4	71.6	755.4	66.6
293.2	91749	2.7	14.8	1.0	1.1899	2.2	0.1276	1.9	0.90	774.4	14.2	795.9	11.9	856.6	19.7	774.4	14.2
738.1	5426	3.9	14.0	3.9	1.2613	8.3	0.1284	7.3	0.88	778.8	53.6	828.5	47.0	964.1	80.3	778.8	53.6
334.4	22533	5.0	14.3	1.8	1.2489	7.4	0.1297	7.2	0.97	786.1	53.3	822.9	41.9	923.8	37.5	786.1	53.3
340.3	54679	6.4	14.2	0.9	1.3466	1.4	0.1389	1.0	0.76	838.4	8.1	866.1	7.9	937.8	17.9	838.4	8.1
459.2	22422	2.7	14.1	0.5	1.4679	1.6	0.1497	1.5	0.94	899.1	12.8	917.3	9.8	961.1	11.0	961.1	11.0
535.2	35383	3.9	13.9	1.0	1.5075	5.1	0.1524	5.0	0.98	914.7	42.3	933.4	30.9	978.0	20.4	978.0	20.4
122.4	126787	3.2	13.8	0.6	1.6823	1.6	0.1688	1.5	0.92	1005.7	13.5	1001.8	10.1	993.5	12.8	993.5	12.8
99.1	167881	2.2	13.7	1.5	1.5612	4.9	0.1549	4.6	0.95	928.3	40.1	955.0	30.2	1016.9	30.6	1016.9	30.6
101.9	43452	6.6	13.7	2.0	1.7156	4.9	0.1699	4.5	0.91	1011.6	41.7	1014.4	31.4	1020.4	40.9	1020.4	40.9
491.7	142394	3.6	13.6	0.7	1.8208	3.6	0.1793	3.5	0.98	1062.9	34.2	1053.0	23.3	1032.4	13.4	1032.4	13.4
193.3	133950	4.1	13.5	0.6	1.7698	4.7	0.1733	4.6	0.99	1030.3	43.9	1034.5	30.2	1043.3	12.6	1043.3	12.6
42.2	25586	0.9	13.5	3.3	1.6779	5.8	0.1639	4.8	0.83	978.3	43.7	1000.2	37.1	1048.6	66.2	1048.6	66.2
109.3	32252	3.1	13.4	0.7	1.6711	1.7	0.1628	1.6	0.90	972.1	14.0	997.6	10.9	1054.1	14.9	1054.1	14.9
33.1	22549	2.2	13.4	4.6	1.8404	5.1	0.1792	2.2	0.43	1062.6	21.6	1060.0	33.4	1054.6	92.0	1054.6	92.0
322.8	270594	1.6	12.9	0.9	1.8163	1.6	0.1705	1.4	0.84	1014.9	12.8	1051.4	10.6	1128.0	17.4	1128.0	17.4
239.9	132897	1.9	12.9	0.9	2.0025	3.6	0.1879	3.5	0.97	1110.2	36.0	1116.4	24.7	1128.4	18.2	1128.4	18.2
569.3	987321	2.2	12.6	0.3	2.0487	2.5	0.1868	2.5	0.99	1103.8	24.9	1131.9	16.9	1186.2	6.2	1186.2	6.2
330.7	236790	2.1	12.2	0.4	2.3656	0.9	0.2096	0.8	0.88	1226.5	9.0	1232.3	6.5	1242.4	8.3	1242.4	8.3
28.1	36125	1.1	9.3	1.7	4.8747	3.2	0.3271	2.8	0.86	1824.1	44.1	1797.9	27.3	1767.6	30.3	1767.6	30.3
352.4	286251	1.6	7.1	0.2	7.2780	1.2	0.3768	1.2	0.99	2061.2	21.0	2146.1	10.8	2228.4	3.5	2228.4	3.5

Appendix A: Cont. U/Pb detrital zircon geochronologic analyses by Laser-Ablation Multicollector ICP Mass Spectrometry

					Isotope ratios					Apparent ages (Ma)							
U (ppm)	206Pb 204Pb	U/Th	206Pb* 207Pb*	± (%)	207Pb* 235U*	± (%)	206Pb* 238U	± (%)	error corr.	206Pb* 238U*	± (Ma)	207Pb* 235U	± (Ma)	206Pb* 207Pb*	± (Ma)	**Best age (Ma)**	**± (Ma)**
SAL 1616 MR Cont.																	
193.3	358310	2.1	6.9	0.2	8.7199	2.1	0.4338	2.1	0.99	2322.6	40.8	2309.2	19.2	2297.3	3.9	2297.3	3.9
242.2	60544	2.4	5.9	2.9	7.9978	5.4	0.3451	4.6	0.85	1911.2	75.6	2230.8	48.8	2538.6	48.1	2538.6	48.1
127.9	273142	2.6	5.7	0.6	8.9169	4.4	0.3677	4.3	0.99	2018.7	74.7	2329.5	39.8	2614.2	10.2	2614.2	10.2
67.2	43136	2.3	5.4	0.5	13.0162	1.8	0.5068	1.7	0.96	2643.2	37.7	2680.8	17.0	2709.4	8.0	2709.4	8.0
38.4	101956	2.3	5.3	0.6	13.5451	1.6	0.5252	1.5	0.94	2721.2	34.3	2718.4	15.6	2716.4	9.6	2716.4	9.6
195.3	401236	2.0	5.3	0.2	13.8049	4.2	0.5313	4.2	1.00	2746.8	93.0	2736.4	39.4	2728.8	2.5	2728.8	2.5
153.8	388935	1.8	5.3	0.2	13.3864	1.4	0.5146	1.4	0.99	2676.2	30.5	2707.3	13.3	2730.6	3.4	2730.6	3.4
139.7	588377	3.0	5.2	0.4	14.3443	1.7	0.5388	1.7	0.97	2778.6	37.8	2772.8	16.3	2768.5	6.3	2768.5	6.3
152.5	34985	2.1	4.2	1.0	15.3964	4.7	0.4709	4.6	0.98	2487.4	95.2	2840.1	45.1	3100.9	16.1	3100.9	16.1
SAL 1611 AG																	
240.6	68824	3.1	17.6	1.6	0.6550	2.0	0.0835	1.2	0.58	516.8	5.7	511.6	8.0	488.2	35.7	516.8	5.7
181.4	40649	2.2	17.3	2.2	0.6732	2.5	0.0845	1.1	0.46	522.8	5.7	522.6	10.2	522.1	48.5	522.8	5.7
246.0	7409	38.8	16.9	2.2	0.7028	2.4	0.0859	0.8	0.33	531.4	4.0	540.4	9.9	578.7	48.4	531.4	4.0
415.0	124700	2.4	16.8	1.5	0.7155	2.6	0.0870	2.1	0.82	537.8	10.9	548.0	10.9	590.4	31.8	537.8	10.9
85.7	27239	1.5	17.3	4.3	0.7031	4.6	0.0884	1.8	0.39	546.3	9.3	540.7	19.3	516.9	93.5	546.3	9.3
72.3	19180	1.8	17.8	4.6	0.6860	5.1	0.0885	2.4	0.46	546.4	12.4	530.4	21.2	462.1	101.1	546.4	12.4
539.1	47379	85.3	17.0	0.6	0.7188	0.9	0.0886	0.8	0.81	547.3	4.0	550.0	4.0	560.9	12.1	547.3	4.0
47.7	13932	0.9	18.4	8.1	0.6658	8.3	0.0888	1.5	0.18	548.6	7.9	518.2	33.6	386.1	182.8	548.6	7.9
151.6	62107	2.3	17.2	2.5	0.7134	2.8	0.0889	1.2	0.42	549.3	6.2	546.8	11.8	536.4	55.4	549.3	6.2
473.9	243284	702.8	17.0	0.6	0.7247	2.1	0.0892	2.0	0.96	550.5	10.8	553.5	9.1	565.5	13.2	550.5	10.8
395.0	213717	2.1	16.9	0.9	0.7287	1.1	0.0893	0.6	0.54	551.2	3.0	555.8	4.5	574.9	19.4	551.2	3.0
77.3	21798	1.3	17.1	4.8	0.7196	5.0	0.0893	1.2	0.23	551.3	6.1	550.4	21.1	546.9	105.4	551.3	6.1
77.0	26337	0.9	17.3	3.9	0.7138	4.1	0.0893	1.3	0.31	551.6	6.7	547.0	17.5	527.6	86.4	551.6	6.7

Appendix A: Cont. U/Pb detrital zircon geochronologic analyses by Laser-Ablation Multicollector ICP Mass Spectrometry

					Isotope ratios					Apparent ages (Ma)							
U (ppm)	206Pb 204Pb	U/Th	206Pb* 207Pb*	± (%)	207Pb* 235U*	± (%)	206Pb* 238U	± (%)	error corr.	206Pb* 238U*	± (Ma)	207Pb* 235U	± (Ma)	206Pb* 207Pb*	± (Ma)	**Best age (Ma)**	**± (Ma)**
SAL 1611 AG Cont.																	
294.1	139519	24.2	17.0	1.0	0.7233	1.2	0.0894	0.7	0.61	551.8	3.9	552.6	5.2	556.0	21.2	551.8	3.9
223.6	99468	1.0	16.8	2.2	0.7366	2.3	0.0898	0.5	0.23	554.5	2.8	560.4	9.7	584.4	47.6	554.5	2.8
78.3	20969	0.9	17.1	4.3	0.7273	6.2	0.0900	4.4	0.71	555.3	23.5	555.0	26.5	553.6	94.5	555.3	23.5
20.0	5185	105.1	16.5	13.2	0.7571	13.5	0.0904	2.9	0.22	557.9	15.6	572.3	59.0	629.9	284.6	557.9	15.6
26.6	9015	2.0	17.9	12.0	0.7002	12.5	0.0907	3.5	0.28	559.5	18.6	538.9	52.2	452.7	267.1	559.5	18.6
526.1	154243	4.7	17.0	0.4	0.7355	1.4	0.0907	1.3	0.96	559.6	7.1	559.8	5.9	560.4	8.7	559.6	7.1
50.2	5203	0.5	17.3	4.1	0.7245	4.6	0.0909	2.1	0.46	561.0	11.3	553.3	19.6	521.8	89.4	561.0	11.3
50.2	19959	1.6	17.4	4.0	0.7216	4.5	0.0910	2.2	0.49	561.7	11.9	551.6	19.3	510.2	87.2	561.7	11.9
38.2	16127	0.2	17.3	11.5	0.7242	11.6	0.0911	1.3	0.11	562.1	6.9	553.2	49.6	516.4	254.1	562.1	6.9
202.8	92700	5.9	16.6	1.9	0.7578	3.1	0.0912	2.4	0.79	562.9	13.1	572.7	13.5	612.0	41.3	562.9	13.1
624.3	254196	18.9	17.0	0.4	0.7403	1.5	0.0913	1.5	0.96	563.4	7.8	562.6	6.5	559.4	8.8	563.4	7.8
381.5	242418	2.4	16.9	1.1	0.7462	1.3	0.0917	0.8	0.61	565.4	4.4	566.0	5.8	568.6	23.3	565.4	4.4
336.6	75858	100.0	17.0	0.9	0.7429	2.2	0.0917	2.0	0.92	565.4	10.7	564.1	9.3	558.7	18.6	565.4	10.7
404.5	155466	3.1	17.0	0.8	0.7452	1.2	0.0917	0.9	0.75	565.4	5.0	565.4	5.3	565.4	17.7	565.4	5.0
1205.9	195392	2.7	16.9	0.4	0.7482	1.0	0.0918	0.9	0.92	566.5	4.9	567.2	4.3	570.0	8.5	566.5	4.9
441.2	168999	3.5	16.8	0.9	0.7547	4.8	0.0919	4.8	0.98	566.7	25.8	571.0	21.1	587.8	19.5	566.7	25.8
47.3	50007	7.1	16.8	5.9	0.7557	6.3	0.0919	2.2	0.34	566.9	11.8	571.5	27.6	589.7	128.8	566.9	11.8
337.8	108675	4.6	16.9	0.8	0.7515	1.7	0.0921	1.5	0.89	568.2	8.4	569.1	7.6	572.8	17.3	568.2	8.4
27.3	13107	1.5	16.7	8.4	0.7605	8.9	0.0922	2.9	0.32	568.6	15.7	574.3	39.2	597.1	183.1	568.6	15.7
136.6	54843	0.8	16.6	2.5	0.7664	2.5	0.0924	0.5	0.22	569.6	3.0	577.7	11.2	609.5	53.5	569.6	3.0
129.5	56706	1.3	16.9	2.8	0.7533	3.0	0.0924	0.8	0.28	569.8	4.5	570.1	12.9	571.5	61.9	569.8	4.5
841.8	21367	4.5	16.6	0.5	0.7669	2.5	0.0925	2.4	0.98	570.0	13.1	578.0	10.8	609.4	11.3	570.0	13.1
83.3	39779	2.1	16.8	2.4	0.7625	3.7	0.0927	2.8	0.76	571.3	15.5	575.4	16.4	591.7	52.8	571.3	15.5

Appendix A: Cont. U/Pb detrital zircon geochronologic analyses by Laser-Ablation Multicollector ICP Mass Spectrometry

					Isotope ratios					Apparent ages (Ma)							
U (ppm)	206Pb 204Pb	U/Th	206Pb* 207Pb*	± (%)	207Pb* 235U*	± (%)	206Pb* 238U	± (%)	error corr.	206Pb* 238U*	± (Ma)	207Pb* 235U	± (Ma)	206Pb* 207Pb*	± (Ma)	**Best age (Ma)**	**± (Ma)**
SAL 1611 AG Cont.																	
158.2	45209	1.1	16.9	1.2	0.7564	2.0	0.0930	1.6	0.78	573.1	8.6	571.9	8.8	567.2	27.2	573.1	8.6
755.3	183927	12.6	16.9	0.4	0.7599	1.4	0.0932	1.4	0.95	574.3	7.6	573.9	6.3	572.5	9.6	574.3	7.6
132.5	117525	2.4	16.4	3.8	0.7835	4.0	0.0932	1.3	0.32	574.6	7.2	587.5	18.0	637.9	82.4	574.6	7.2
1445.4	56202	19.6	16.7	0.7	0.7718	1.6	0.0933	1.5	0.91	575.2	8.0	580.8	7.1	602.7	14.2	575.2	8.0
108.5	47723	0.5	16.7	3.4	0.7730	3.6	0.0934	1.1	0.29	575.9	5.8	581.5	15.9	603.5	74.2	575.9	5.8
140.7	32320	2.7	16.8	2.8	0.7672	3.2	0.0938	1.5	0.47	577.7	8.3	578.2	14.0	580.1	61.1	577.7	8.3
49.8	14087	2.4	17.5	5.3	0.7396	6.0	0.0939	2.8	0.46	578.6	15.4	562.2	25.9	496.0	116.9	578.6	15.4
80.0	34207	1.1	17.4	4.3	0.7462	4.6	0.0941	1.7	0.37	580.0	9.6	566.0	20.1	510.3	94.7	580.0	9.6
264.2	8180	30.5	16.3	1.3	0.7972	2.8	0.0944	2.5	0.89	581.3	13.9	595.2	12.6	648.6	27.0	581.3	13.9
96.3	20424	0.9	17.1	4.7	0.7625	4.8	0.0948	1.0	0.22	583.7	5.8	575.4	21.1	542.8	102.5	583.7	5.8
215.3	84425	1.1	16.6	1.7	0.7919	2.2	0.0954	1.4	0.62	587.5	7.7	592.2	10.0	610.6	37.6	587.5	7.7
67.1	36583	0.6	17.1	4.2	0.7692	4.4	0.0955	1.4	0.30	588.0	7.6	579.3	19.6	545.4	92.3	588.0	7.6
554.1	151133	8.9	16.8	0.6	0.7836	1.1	0.0956	0.8	0.79	588.6	4.7	587.5	4.7	583.2	14.0	588.6	4.7
302.9	87802	1.4	16.8	0.8	0.7879	1.8	0.0958	1.6	0.89	590.0	9.1	590.0	8.1	590.0	17.9	590.0	9.1
265.0	256661	2.6	16.6	1.4	0.7949	1.7	0.0959	0.9	0.56	590.2	5.3	594.0	7.6	608.3	30.5	590.2	5.3
350.8	132882	7.7	16.6	0.8	0.8006	2.3	0.0966	2.2	0.93	594.3	12.3	597.2	10.5	608.0	17.8	594.3	12.3
95.7	39236	0.8	16.9	1.6	0.7897	2.7	0.0966	2.2	0.81	594.6	12.5	591.0	12.2	577.0	35.1	594.6	12.5
65.3	26826	0.4	17.2	2.9	0.7753	3.7	0.0967	2.2	0.60	595.1	12.5	582.8	16.2	535.1	64.0	595.1	12.5
47.8	14740	0.7	17.7	5.4	0.7520	5.6	0.0968	1.5	0.26	595.3	8.5	569.4	24.6	467.1	120.5	595.3	8.5
156.2	76797	2.9	16.3	1.4	0.8202	5.4	0.0968	5.2	0.97	595.4	29.8	608.2	24.8	656.0	29.4	595.4	29.8
115.7	38149	2.0	16.8	3.2	0.7975	3.5	0.0970	1.4	0.40	597.1	8.0	595.4	15.9	589.1	70.2	597.1	8.0
37.3	11316	2.4	16.7	8.6	0.8017	9.0	0.0971	2.7	0.30	597.4	15.3	597.8	40.8	599.4	187.1	597.4	15.3
226.6	119561	1.3	16.7	1.4	0.8025	2.3	0.0974	1.8	0.80	599.0	10.5	598.2	10.4	595.4	30.0	599.0	10.5

Appendix A: Cont. U/Pb detrital zircon geochronologic analyses by Laser-Ablation Multicollector ICP Mass Spectrometry

					Isotope ratios					Apparent ages (Ma)							
U (ppm)	206Pb 204Pb	U/Th	206Pb* 207Pb*	± (%)	207Pb* 235U*	± (%)	206Pb* 238U	± (%)	error corr.	206Pb* 238U*	± (Ma)	207Pb* 235U	± (Ma)	206Pb* 207Pb*	± (Ma)	**Best age (Ma)**	**± (Ma)**
SAL 1611 AG Cont.																	
62.9	27555	0.7	16.6	4.2	0.8092	4.4	0.0975	1.3	0.30	599.5	7.5	602.0	19.9	611.4	90.4	599.5	7.5
338.1	140349	1.6	16.7	1.0	0.8090	1.9	0.0980	1.6	0.85	603.0	9.5	601.9	8.7	597.9	21.6	603.0	9.5
293.8	172558	2.4	16.5	0.9	0.8185	1.5	0.0981	1.2	0.78	603.1	6.6	607.2	6.8	622.4	20.2	603.1	6.6
110.0	36283	1.6	16.7	3.1	0.8120	3.3	0.0981	1.0	0.31	603.4	5.9	603.5	14.8	604.2	67.1	603.4	5.9
360.8	102137	1.6	16.7	0.9	0.8149	1.8	0.0984	1.5	0.86	605.1	8.8	605.2	8.2	605.3	20.0	605.1	8.8
136.9	215431	1.1	16.9	2.5	0.8046	2.9	0.0985	1.4	0.49	605.6	8.3	599.4	13.2	576.2	55.1	605.6	8.3
271.7	125962	6.1	16.7	1.0	0.8122	2.3	0.0986	2.1	0.91	606.4	12.2	603.7	10.5	593.7	20.8	606.4	12.2
280.1	92424	123.2	16.4	1.0	0.8348	1.8	0.0995	1.5	0.82	611.7	8.6	616.3	8.3	633.0	22.2	611.7	8.6
149.9	53544	0.6	16.8	1.9	0.8175	5.4	0.0998	5.0	0.94	613.5	29.3	606.7	24.5	581.3	41.1	613.5	29.3
144.9	33876	2.2	16.4	2.0	0.8528	2.8	0.1013	1.9	0.69	621.8	11.2	626.2	12.9	642.0	43.0	621.8	11.2
334.3	95171	4.8	16.7	1.1	0.8410	1.8	0.1019	1.5	0.81	625.7	8.8	619.7	8.4	598.0	22.7	625.7	8.8
257.8	204388	2.6	15.4	1.4	0.9570	3.8	0.1068	3.6	0.93	654.3	22.1	681.7	18.9	773.4	29.2	654.3	22.1
417.8	59839	4.0	16.0	1.0	0.9289	1.9	0.1079	1.6	0.85	660.8	10.1	667.1	9.3	688.2	21.6	660.8	10.1
451.0	225367	7.6	14.5	3.4	1.0946	7.3	0.1148	6.5	0.88	700.7	42.9	750.8	38.8	903.0	70.4	700.7	42.9
191.0	34553	4.3	15.0	1.2	1.0875	2.2	0.1181	1.9	0.85	719.7	12.8	747.3	11.7	830.8	24.6	719.7	12.8
122.9	52239	1.2	15.3	1.6	1.1057	5.6	0.1229	5.4	0.96	747.5	38.1	756.1	30.0	781.6	33.2	747.5	38.1
1121.0	331725	5.8	14.2	0.5	1.3148	4.4	0.1350	4.4	0.99	816.3	33.6	852.2	25.4	947.1	10.2	816.3	33.6
188.5	85402	3.9	14.5	0.9	1.4090	2.0	0.1480	1.8	0.88	890.0	14.8	892.7	12.0	899.5	19.5	890.0	14.8
767.1	39936	1.4	14.1	0.3	1.4768	1.7	0.1510	1.7	0.99	906.4	14.1	920.9	10.2	955.9	5.9	955.9	5.9
72.4	21801	3.6	14.0	3.0	1.3929	3.6	0.1415	2.1	0.57	853.4	16.4	885.9	21.5	968.1	61.2	968.1	61.2
292.1	153170	5.4	13.8	0.7	1.6651	2.6	0.1670	2.5	0.96	995.4	23.2	995.3	16.6	995.0	14.6	995.0	14.6
113.5	13429	1.5	13.8	2.7	1.5156	6.6	0.1516	6.0	0.91	910.1	50.9	936.7	40.3	999.7	55.8	999.7	55.8
179.9	48474	3.1	13.8	1.3	1.5602	2.5	0.1561	2.1	0.85	935.0	18.4	954.6	15.4	999.8	26.8	999.8	26.8

Appendix A: Cont. U/Pb detrital zircon geochronologic analyses by Laser-Ablation Multicollector ICP Mass Spectrometry

					Isotope ratios					Apparent ages (Ma)							
U (ppm)	206Pb 204Pb	U/Th	206Pb* 207Pb*	± (%)	207Pb* 235U*	± (%)	206Pb* 238U	± (%)	error corr.	206Pb* 238U*	± (Ma)	207Pb* 235U	± (Ma)	206Pb* 207Pb*	± (Ma)	**Best age (Ma)**	**± (Ma)**
SAL 1611 AG Cont.																	
456.7	42055	15.4	13.7	0.5	1.6114	2.2	0.1604	2.2	0.97	959.2	19.4	974.7	14.0	1009.7	10.4	1009.7	10.4
201.5	290641	3.6	13.6	0.7	1.7999	3.0	0.1779	2.9	0.97	1055.6	28.1	1045.4	19.4	1024.2	13.9	1024.2	13.9
133.4	132434	5.0	13.6	1.0	1.7314	2.7	0.1704	2.5	0.93	1014.5	23.9	1020.3	17.5	1032.7	19.6	1032.7	19.6
29.1	14946	0.2	13.4	5.5	1.6023	6.2	0.1557	2.9	0.46	932.9	24.9	971.1	38.6	1058.7	110.0	1058.7	110.0
137.6	88813	1.4	13.3	1.1	1.8667	1.3	0.1806	0.8	0.57	1070.0	7.5	1069.4	8.9	1068.1	22.1	1068.1	22.1
263.3	175489	6.8	13.3	0.6	1.8608	5.4	0.1790	5.3	0.99	1061.3	52.3	1067.3	35.5	1079.5	12.5	1079.5	12.5
221.1	150424	1.0	13.3	0.5	1.9437	1.2	0.1869	1.1	0.91	1104.4	11.1	1096.3	8.1	1080.2	10.1	1080.2	10.1
181.2	143952	1.6	12.7	1.0	1.9658	2.9	0.1807	2.7	0.93	1070.9	26.5	1103.9	19.3	1169.4	20.4	1169.4	20.4
341.8	414698	1.4	12.4	0.2	2.2923	0.9	0.2070	0.9	0.96	1212.6	9.9	1209.9	6.6	1205.2	4.8	1205.2	4.8
281.8	272767	1.3	12.3	0.5	2.2784	2.5	0.2037	2.5	0.98	1195.0	27.1	1205.6	17.9	1224.6	10.5	1224.6	10.5
219.4	281106	2.3	8.9	0.3	4.8368	1.2	0.3130	1.2	0.98	1755.5	18.7	1791.3	10.5	1833.3	4.5	1833.3	4.5
497.6	103553	4.2	8.5	0.8	4.7521	1.9	0.2925	1.7	0.91	1654.1	25.2	1776.5	15.9	1923.4	13.9	1923.4	13.9
452.4	725336	7.9	8.3	0.2	5.4665	1.9	0.3280	1.9	0.99	1828.7	30.3	1895.4	16.5	1969.1	3.9	1969.1	3.9
184.2	216263	1.8	7.5	0.4	6.3679	2.7	0.3469	2.7	0.99	1919.9	44.3	2027.9	23.7	2139.6	7.2	2139.6	7.2
133.7	101932	1.0	7.4	0.3	7.2784	1.9	0.3921	1.9	0.99	2132.3	34.5	2146.2	17.1	2159.4	5.0	2159.4	5.0
330.0	154486	7.8	7.0	0.1	7.3494	1.3	0.3711	1.2	0.99	2034.6	21.7	2154.8	11.2	2271.4	2.5	2271.4	2.5
587.6	163186	0.5	6.9	0.1	7.8172	1.4	0.3939	1.4	1.00	2140.9	25.3	2210.2	12.5	2275.1	1.6	2275.1	1.6
286.7	698413	0.7	6.9	0.1	8.5550	1.3	0.4257	1.3	0.99	2286.2	24.7	2291.8	11.7	2296.7	2.4	2296.7	2.4
65.2	102792	1.3	6.4	0.7	8.6405	2.1	0.4022	2.0	0.94	2179.4	36.2	2300.8	19.0	2410.5	12.1	2410.5	12.1
188.6	250038	8.2	6.4	1.0	8.0764	3.1	0.3758	2.9	0.94	2056.4	51.5	2239.6	28.0	2411.5	17.3	2411.5	17.3
90.6	131931	1.0	6.4	0.3	8.8439	3.6	0.4073	3.6	1.00	2202.7	66.3	2322.0	32.5	2428.7	5.3	2428.7	5.3
88.9	108135	1.1	6.3	0.4	9.4024	3.2	0.4315	3.2	0.99	2312.3	62.4	2378.1	29.7	2434.9	6.9	2434.9	6.9
146.4	158923	2.2	5.5	0.7	11.6659	1.8	0.4629	1.7	0.93	2452.4	35.1	2578.0	17.3	2678.2	11.2	2678.2	11.2

Appendix A: Cont. U/Pb detrital zircon geochronologic analyses by Laser-Ablation Multicollector ICP Mass Spectrometry

					Isotope ratios					Apparent ages (Ma)							
U (ppm)	206Pb 204Pb	U/Th	206Pb* 207Pb*	± (%)	207Pb* 235U*	± (%)	206Pb* 238U	± (%)	error corr.	206Pb* 238U*	± (Ma)	207Pb* 235U	± (Ma)	206Pb* 207Pb*	± (Ma)	**Best age** (Ma)	± (Ma)
SAL 1611 AG Cont.																	
352.6	474023	1.1	5.5	0.2	10.9504	2.6	0.4333	2.6	1.00	2320.7	50.5	2518.9	24.1	2682.7	2.7	2682.7	2.7
30.0	23878	2.0	5.4	0.9	12.1033	2.5	0.4761	2.4	0.93	2510.4	49.0	2612.4	23.7	2692.5	15.0	2692.5	15.0
129.7	119372	1.5	5.4	0.3	12.5820	1.4	0.4945	1.4	0.98	2590.2	29.8	2648.9	13.4	2694.0	4.4	2694.0	4.4
104.5	217370	2.4	5.4	0.3	12.1421	2.2	0.4768	2.2	0.99	2513.3	45.1	2615.4	20.6	2695.5	5.6	2695.5	5.6
514.5	104051	8.7	5.4	0.2	12.4630	1.8	0.4841	1.8	1.00	2544.9	37.6	2639.9	16.9	2713.6	2.6	2713.6	2.6
168.3	195487	3.6	5.3	0.5	10.8407	1.8	0.4165	1.8	0.96	2244.5	33.5	2509.6	17.1	2731.6	8.4	2731.6	8.4
221.6	491329	1.7	5.3	0.2	13.5391	1.6	0.5201	1.6	0.99	2699.6	35.6	2718.0	15.4	2731.7	3.5	2731.7	3.5
170.0	204578	1.4	5.1	0.1	14.0351	0.9	0.5205	0.9	0.99	2701.3	19.3	2752.1	8.4	2789.5	1.8	2789.5	1.8
536.8	12090	6.4	4.7	3.4	15.9005	7.8	0.5471	7.1	0.90	2813.0	161.7	2870.8	75.1	2911.7	54.3	2911.7	54.3
149.3	78031	2.2	4.6	0.3	17.5093	1.7	0.5823	1.7	0.98	2958.1	39.6	2963.2	16.4	2966.6	5.4	2966.6	5.4
169.2	289856	2.5	4.3	0.1	18.4648	0.9	0.5822	0.9	0.99	2957.9	21.2	3014.3	8.7	3052.1	1.8	3052.1	1.8
218.1	326254	1.8	4.3	0.1	18.4609	0.7	0.5789	0.7	0.98	2944.5	15.9	3014.1	6.6	3060.8	2.0	3060.8	2.0
58.0	139163	1.0	4.1	0.6	20.3302	2.0	0.6012	1.9	0.95	3034.5	46.6	3107.2	19.6	3154.5	10.1	3154.5	10.1
172.0	656093	1.2	4.0	0.1	20.4184	1.7	0.5900	1.7	1.00	2989.5	40.4	3111.4	16.4	3191.0	2.2	3191.0	2.2
335.3	611121	1.3	3.9	0.1	20.8473	2.0	0.5947	2.0	1.00	3008.6	48.4	3131.5	19.6	3211.3	2.2	3211.3	2.2
382.6	63799	4.1	3.8	0.5	16.0467	7.9	0.4371	7.9	1.00	2337.5	155.2	2879.6	76.0	3284.2	8.6	3284.2	8.6
111.8	140666	1.6	3.6	0.4	23.4700	6.0	0.6043	6.0	1.00	3047.2	144.8	3246.6	58.3	3372.3	6.9	3372.3	6.9
SAL 1776 BIS																	
258.9	12689	0.7	20.6	10.3	0.1082	10.5	0.0162	1.9	0.18	103.6	2.0	104.3	10.4	120.9	243.5	103.6	2.0
631.1	34698	1.1	20.8	5.0	0.1086	5.5	0.0164	2.3	0.41	105.0	2.3	104.7	5.5	98.2	118.7	105.0	2.3
376.4	14075	1.0	21.8	8.9	0.1059	9.3	0.0168	2.5	0.26	107.2	2.6	102.2	9.0	-10.9	216.1	107.2	2.6
397.2	26645	2.1	21.1	5.8	0.1206	6.1	0.0184	1.8	0.29	117.7	2.0	115.6	6.6	74.0	138.5	117.7	2.0
785.4	1889	0.9	18.8	2.1	0.2322	2.4	0.0317	1.3	0.53	200.9	2.5	212.0	4.7	337.5	47.0	200.9	2.5

Appendix A: Cont. U/Pb detrital zircon geochronologic analyses by Laser-Ablation Multicollector ICP Mass Spectrometry

					Isotope ratios					Apparent ages (Ma)							
U (ppm)	206Pb 204Pb	U/Th	206Pb* 207Pb*	± (%)	207Pb* 235U*	± (%)	206Pb* 238U	± (%)	error corr.	206Pb* 238U*	± (Ma)	207Pb* 235U	± (Ma)	206Pb* 207Pb*	± (Ma)	**Best age (Ma)**	**± (Ma)**
SAL 1776 BIS Cont.																	
240.0	36316	1.1	19.9	6.5	0.2229	7.3	0.0322	3.4	0.47	204.3	6.9	204.3	13.6	204.3	150.6	204.3	6.9
415.1	89736	2.0	19.0	1.5	0.3783	2.0	0.0521	1.3	0.63	327.5	4.0	325.8	5.5	313.5	35.0	327.5	4.0
403.1	77345	2.4	19.0	3.1	0.3994	4.6	0.0550	3.4	0.74	345.1	11.4	341.2	13.3	314.7	69.7	345.1	11.4
365.1	52886	1.8	18.6	1.8	0.4293	2.9	0.0580	2.3	0.79	363.4	8.2	362.7	9.0	357.9	41.1	363.4	8.2
87.0	36889	2.1	17.4	6.5	0.5756	7.0	0.0726	2.5	0.36	451.9	11.0	461.6	25.9	510.3	143.5	451.9	11.0
768.0	233037	1.7	17.8	1.0	0.5701	1.9	0.0736	1.6	0.86	457.8	7.1	458.1	6.9	459.7	21.3	457.8	7.1
211.6	54870	3.3	17.9	1.7	0.5665	2.6	0.0737	1.9	0.75	458.4	8.6	455.7	9.5	442.2	38.4	458.4	8.6
283.3	96337	1.8	17.6	1.7	0.5802	4.1	0.0743	3.8	0.91	461.7	16.8	464.6	15.4	478.6	38.1	461.7	16.8
106.8	24264	1.2	18.0	3.0	0.5704	3.4	0.0743	1.5	0.45	462.1	6.9	458.3	12.5	439.0	67.4	462.1	6.9
335.2	95617	2.7	17.6	2.1	0.5858	3.2	0.0746	2.4	0.74	463.9	10.7	468.2	12.0	489.4	47.4	463.9	10.7
99.0	59985	1.8	17.6	6.1	0.5901	6.4	0.0755	2.1	0.32	469.2	9.4	470.9	24.1	479.6	133.8	469.2	9.4
219.4	23420	2.3	17.3	2.2	0.6066	2.5	0.0760	1.1	0.46	472.5	5.2	481.4	9.5	524.3	48.0	472.5	5.2
193.4	48757	2.0	17.8	2.7	0.5935	3.8	0.0764	2.7	0.72	474.8	12.5	473.1	14.4	464.6	58.9	474.8	12.5
393.4	76775	2.0	17.6	2.1	0.6019	3.1	0.0767	2.3	0.75	476.6	10.6	478.4	11.8	487.2	45.6	476.6	10.6
368.5	132003	2.0	17.8	1.9	0.5965	2.2	0.0770	1.1	0.49	478.3	4.9	475.0	8.2	459.2	41.9	478.3	4.9
240.2	196482	2.7	17.7	2.3	0.6019	2.6	0.0772	1.1	0.43	479.1	5.1	478.4	9.9	475.1	51.7	479.1	5.1
232.3	44418	2.2	17.9	1.8	0.5965	3.0	0.0774	2.4	0.80	480.6	11.1	475.0	11.4	448.1	40.2	480.6	11.1
853.5	8104	3.3	17.2	2.6	0.6226	3.1	0.0775	1.7	0.54	481.0	7.8	491.4	12.1	540.6	57.0	481.0	7.8
178.3	32320	2.3	17.9	2.9	0.6000	3.7	0.0779	2.3	0.62	483.4	10.6	477.2	13.9	447.7	63.6	483.4	10.6
232.7	37167	1.8	17.3	2.0	0.6229	2.3	0.0780	1.1	0.49	483.9	5.3	491.6	8.9	527.8	43.7	483.9	5.3
171.5	24889	2.0	17.4	3.0	0.6201	3.7	0.0784	2.2	0.59	486.4	10.2	489.9	14.3	506.3	65.0	486.4	10.2
918.1	181646	4.1	17.5	0.6	0.6225	2.4	0.0791	2.3	0.97	490.5	10.9	491.4	9.2	495.6	12.5	490.5	10.9
338.1	71100	2.3	17.2	1.8	0.6411	2.1	0.0798	1.2	0.55	494.9	5.6	503.0	8.5	540.0	39.1	494.9	5.6

Appendix A: Cont. U/Pb detrital zircon geochronologic analyses by Laser-Ablation Multicollector ICP Mass Spectrometry

					Isotope ratios					Apparent ages (Ma)							
U (ppm)	206Pb 204Pb	U/Th	206Pb* 207Pb*	± (%)	207Pb* 235U*	± (%)	206Pb* 238U	± (%)	error corr.	206Pb* 238U*	± (Ma)	207Pb* 235U	± (Ma)	206Pb* 207Pb*	± (Ma)	**Best age (Ma)**	**± (Ma)**
SAL 1776 BIS Cont.																	
591.7	47774	3.2	16.8	2.5	0.6699	6.8	0.0817	6.3	0.93	506.4	30.7	520.6	27.6	583.5	53.3	506.4	30.7
192.0	55368	1.3	17.4	1.6	0.6616	2.1	0.0835	1.3	0.63	516.8	6.5	515.6	8.3	510.1	35.0	516.8	6.5
411.8	140825	2.8	17.1	0.8	0.6978	3.0	0.0868	2.9	0.97	536.4	14.9	537.5	12.5	542.2	16.7	536.4	14.9
110.4	33062	3.1	17.3	4.1	0.6965	4.7	0.0874	2.2	0.46	540.3	11.2	536.7	19.5	521.4	90.8	540.3	11.2
82.6	15183	5.9	16.9	5.3	0.7147	5.5	0.0875	1.8	0.32	540.5	9.2	547.6	23.5	576.9	114.4	540.5	9.2
201.1	120601	0.9	17.2	2.9	0.7034	5.7	0.0877	4.9	0.86	541.8	25.4	540.8	23.9	536.8	64.2	541.8	25.4
150.2	50194	0.9	17.6	3.0	0.6965	3.6	0.0888	1.9	0.52	548.3	9.8	536.7	14.8	487.7	67.0	548.3	9.8
513.5	279840	7.3	17.2	1.2	0.7219	1.8	0.0899	1.3	0.75	554.7	7.1	551.8	7.5	539.7	25.4	554.7	7.1
109.6	29010	1.9	16.1	4.2	0.7737	4.6	0.0901	1.7	0.37	556.1	9.1	581.9	20.2	683.9	90.6	556.1	9.1
422.8	206744	7.1	17.3	1.5	0.7243	2.8	0.0908	2.4	0.85	560.0	12.9	553.2	12.0	525.3	32.6	560.0	12.9
248.1	51592	32.7	17.1	1.1	0.7348	2.2	0.0911	1.9	0.86	561.8	10.1	559.3	9.4	549.4	24.5	561.8	10.1
35.1	12295	0.9	17.1	9.1	0.7360	9.5	0.0911	2.6	0.28	562.2	14.2	560.1	40.9	551.5	199.6	562.2	14.2
562.4	381880	9.5	17.0	1.3	0.7399	1.7	0.0912	1.1	0.65	562.5	6.0	562.4	7.3	561.8	27.9	562.5	6.0
79.2	37859	3.6	18.0	7.5	0.7004	7.7	0.0914	1.9	0.25	563.9	10.5	539.0	32.2	434.8	166.3	563.9	10.5
409.4	68242	2.0	16.6	1.1	0.7943	3.5	0.0958	3.3	0.95	589.7	18.7	593.6	15.6	608.4	23.0	589.7	18.7
14.5	3807	124.8	18.2	22.6	0.7383	23.5	0.0973	6.4	0.27	598.9	36.6	561.4	101.6	412.5	510.9	598.9	36.6
118.1	39173	1.2	16.3	2.9	0.8684	4.2	0.1026	3.1	0.73	629.3	18.4	634.7	19.8	653.8	61.7	629.3	18.4
428.4	81979	4.3	16.3	1.0	0.8812	1.7	0.1040	1.4	0.81	637.9	8.6	641.6	8.3	654.9	21.8	637.9	8.6
349.3	25605	2.5	16.3	1.2	0.8925	2.2	0.1054	1.8	0.83	645.8	11.0	647.7	10.3	654.3	25.8	645.8	11.0
652.8	199478	9.5	16.0	1.4	0.9205	4.4	0.1068	4.2	0.95	654.4	26.2	662.6	21.6	690.7	29.9	654.4	26.2
357.8	132721	3.1	15.6	0.7	0.9883	1.7	0.1115	1.6	0.92	681.7	10.1	697.9	8.6	750.4	14.5	681.7	10.1
462.2	279286	17.6	15.6	1.0	1.0064	4.3	0.1139	4.1	0.97	695.6	27.3	707.0	21.7	743.6	20.9	695.6	27.3
260.7	200176	4.0	14.4	0.9	1.4213	3.1	0.1480	2.9	0.96	890.0	24.4	897.9	18.3	917.4	18.5	917.4	18.5

Appendix A: Cont. U/Pb detrital zircon geochronologic analyses by Laser-Ablation Multicollector ICP Mass Spectrometry

					Isotope ratios					Apparent ages (Ma)							
U (ppm)	206Pb 204Pb	U/Th	206Pb* 207Pb*	± (%)	207Pb* 235U*	± (%)	206Pb* 238U	± (%)	error corr.	206Pb* 238U*	± (Ma)	207Pb* 235U	± (Ma)	206Pb* 207Pb*	± (Ma)	**Best age** (Ma)	± (Ma)
SAL 1776 BIS Cont.																	
210.1	145689	0.8	14.1	1.3	1.4714	3.2	0.1504	2.9	0.91	903.1	24.3	918.7	19.1	956.3	26.7	956.3	26.7
149.8	94336	1.9	14.0	1.2	1.4057	2.9	0.1426	2.7	0.92	859.2	21.4	891.3	17.2	971.9	23.8	971.9	23.8
318.8	155736	2.9	13.7	0.8	1.7256	2.7	0.1718	2.5	0.96	1022.1	24.0	1018.1	17.0	1009.6	15.6	1009.6	15.6
360.2	287959	2.8	13.7	0.9	1.5011	2.1	0.1493	1.9	0.90	896.9	15.5	930.8	12.6	1012.0	18.5	1012.0	18.5
320.4	236644	2.6	13.7	0.4	1.7689	2.7	0.1754	2.6	0.99	1041.7	25.4	1034.1	17.3	1018.0	8.7	1018.0	8.7
967.0	30352	4.0	13.7	0.5	1.6284	2.4	0.1613	2.4	0.98	963.9	21.2	981.2	15.3	1020.3	10.4	1020.3	10.4
765.0	9865	4.1	13.5	1.0	1.6676	4.7	0.1634	4.6	0.97	975.9	41.4	996.3	29.7	1041.3	21.2	1041.3	21.2
346.4	148524	2.6	13.5	0.9	1.7256	2.4	0.1689	2.2	0.93	1006.1	20.8	1018.1	15.5	1044.1	17.8	1044.1	17.8
432.8	113687	3.3	13.4	0.5	1.8354	1.8	0.1784	1.7	0.97	1058.2	16.8	1058.2	11.7	1058.2	9.1	1058.2	9.1
199.1	104722	1.1	13.4	0.9	1.8253	2.5	0.1773	2.3	0.93	1052.1	22.0	1054.6	16.1	1059.8	18.7	1059.8	18.7
309.6	340266	2.5	13.4	0.5	1.8549	1.1	0.1799	1.0	0.89	1066.2	9.8	1065.2	7.5	1063.0	10.5	1063.0	10.5
100.2	65149	1.5	13.4	2.4	1.9073	2.6	0.1849	1.0	0.37	1093.5	9.8	1083.6	17.4	1063.8	48.6	1063.8	48.6
62.8	67253	1.3	13.3	2.0	1.9494	2.8	0.1886	2.0	0.71	1113.6	20.3	1098.2	18.8	1067.9	39.9	1067.9	39.9
466.7	190477	1.8	13.3	0.3	1.8579	1.3	0.1791	1.3	0.97	1062.1	12.8	1066.3	8.9	1074.8	6.7	1074.8	6.7
211.2	121174	2.5	13.2	0.8	1.7591	3.1	0.1686	3.0	0.97	1004.3	28.2	1030.5	20.3	1086.6	15.8	1086.6	15.8
129.5	65844	1.2	13.1	1.1	1.9773	1.8	0.1882	1.4	0.80	1111.7	14.7	1107.8	12.1	1100.2	21.4	1100.2	21.4
115.6	90625	3.6	13.1	1.0	1.9950	1.7	0.1899	1.3	0.80	1120.8	13.9	1113.8	11.4	1100.3	20.2	1100.3	20.2
569.1	83183	2.7	13.0	0.3	2.0125	2.1	0.1898	2.0	0.99	1120.5	20.9	1119.8	14.0	1118.3	6.8	1118.3	6.8
198.6	319968	1.7	12.4	0.4	2.3382	2.5	0.2106	2.5	0.99	1231.8	27.9	1224.0	18.0	1210.1	8.3	1210.1	8.3
344.1	319798	2.4	12.3	1.8	1.9691	6.5	0.1757	6.3	0.96	1043.4	60.4	1105.0	44.0	1228.3	35.6	1228.3	35.6
219.0	260414	2.5	12.2	1.0	2.3858	1.7	0.2117	1.4	0.82	1238.0	15.8	1238.3	12.3	1238.8	19.4	1238.8	19.4
145.1	135068	1.0	12.0	1.4	2.5617	2.0	0.2233	1.4	0.69	1299.3	16.1	1289.8	14.4	1273.9	27.7	1273.9	27.7
152.7	136130	5.9	11.0	0.6	3.1181	2.0	0.2484	1.9	0.95	1430.3	24.2	1437.2	15.3	1447.3	11.9	1447.3	11.9

Appendix A: Cont. U/Pb detrital zircon geochronologic analyses by Laser-Ablation Multicollector ICP Mass Spectrometry

					Isotope ratios					Apparent ages (Ma)							
U (ppm)	206Pb 204Pb	U/Th	206Pb* 207Pb*	± (%)	207Pb* 235U*	± (%)	206Pb* 238U	± (%)	error corr.	206Pb* 238U*	± (Ma)	207Pb* 235U	± (Ma)	206Pb* 207Pb*	± (Ma)	**Best age (Ma)**	± (Ma)
SAL 1776 BIS Cont.																	
916.0	339861	1.1	10.0	0.5	3.8421	1.4	0.2795	1.4	0.95	1588.7	19.1	1601.6	11.5	1618.6	8.6	1618.6	8.6
323.9	272931	6.4	9.7	0.6	4.0099	1.5	0.2823	1.4	0.93	1602.7	20.1	1636.2	12.4	1679.5	10.4	1679.5	10.4
247.7	425502	2.7	9.5	0.4	4.5099	1.7	0.3111	1.6	0.97	1746.2	25.2	1732.8	14.1	1716.6	7.6	1716.6	7.6
251.5	352869	2.0	9.4	0.3	4.5174	1.6	0.3091	1.6	0.98	1736.2	23.8	1734.2	13.3	1731.7	6.4	1731.7	6.4
69.9	112475	1.0	9.0	1.2	4.7387	1.8	0.3096	1.4	0.75	1738.9	20.6	1774.1	15.1	1815.8	21.6	1815.8	21.6
280.8	57582	3.6	6.5	1.2	8.3686	5.1	0.3929	5.0	0.97	2136.2	90.2	2271.8	46.4	2396.1	20.8	2396.1	20.8
149.3	166493	2.1	3.8	1.5	21.6567	3.6	0.5933	3.3	0.91	3002.9	79.9	3168.5	35.4	3275.0	23.5	3275.0	23.5
SAL 1583 LW2-D																	
34.9	19446	0.4	16.2	10.0	0.6921	10.2	0.0812	2.0	0.20	503.3	9.7	534.1	42.5	667.9	215.1	503.3	9.7
622.0	20624	1.4	17.0	0.4	0.7004	0.7	0.0862	0.6	0.82	532.8	2.9	539.1	2.9	565.6	8.7	532.8	2.9
86.5	22907	1.3	17.5	4.1	0.6966	5.0	0.0886	3.0	0.59	547.5	15.8	536.8	21.0	491.4	89.4	547.5	15.8
100.3	32275	0.4	17.2	3.6	0.7105	4.4	0.0887	2.6	0.59	547.6	13.9	545.0	18.8	534.3	78.4	547.6	13.9
319.2	136477	2.2	15.4	1.8	0.8053	4.0	0.0898	3.6	0.90	554.5	19.0	599.8	18.0	774.9	37.0	554.5	19.0
268.0	94907	1.3	17.1	1.0	0.7346	1.5	0.0909	1.1	0.72	561.1	5.8	559.2	6.4	551.5	22.6	561.1	5.8
150.3	42652	1.2	17.1	2.3	0.7535	2.6	0.0933	1.1	0.42	574.9	6.0	570.2	11.2	551.7	51.0	574.9	6.0
82.3	23489	3.0	17.3	5.4	0.7463	5.9	0.0934	2.5	0.42	575.5	13.5	566.1	25.6	528.4	117.6	575.5	13.5
39.5	17742	1.9	16.2	6.3	0.8022	6.6	0.0940	2.2	0.33	579.4	12.0	598.1	30.0	669.5	134.2	579.4	12.0
265.4	37809	3.6	15.2	4.9	0.8723	5.9	0.0959	3.2	0.55	590.2	18.2	636.8	27.9	805.8	103.2	590.2	18.2
120.1	60674	5.7	17.1	3.1	0.7759	3.3	0.0960	1.1	0.32	591.0	6.0	583.2	14.7	552.9	68.3	591.0	6.0
148.0	45790	1.2	16.5	1.5	0.8232	4.1	0.0986	3.8	0.93	606.4	22.2	609.8	18.9	622.4	32.9	606.4	22.2
182.7	153927	2.7	16.5	1.8	0.8341	2.1	0.0997	1.1	0.52	612.9	6.4	615.9	9.7	626.7	38.5	612.9	6.4
178.7	71514	1.1	16.6	1.8	0.8461	3.2	0.1017	2.6	0.82	624.6	15.6	622.5	14.8	614.9	38.9	624.6	15.6
109.0	49396	1.8	16.1	2.9	0.8915	4.8	0.1040	3.8	0.79	637.6	22.9	647.2	22.9	680.8	62.9	637.6	22.9

Appendix A: Cont. U/Pb detrital zircon geochronologic analyses by Laser-Ablation Multicollector ICP Mass Spectrometry

					Isotope ratios					Apparent ages (Ma)							
U (ppm)	206Pb 204Pb	U/Th	206Pb* 207Pb*	± (%)	207Pb* 235U*	± (%)	206Pb* 238U	± (%)	error corr.	206Pb* 238U*	± (Ma)	207Pb* 235U	± (Ma)	206Pb* 207Pb*	± (Ma)	**Best age (Ma)**	**± (Ma)**
SAL 1583 LW2-D Cont.																	
180.0	190847	1.4	13.8	3.3	1.5765	7.9	0.1577	7.2	0.91	944.0	62.9	961.0	49.1	1000.1	67.3	1000.1	67.3
215.3	96015	1.9	13.6	1.1	1.6492	3.6	0.1626	3.4	0.95	971.1	30.6	989.3	22.5	1029.8	22.4	1029.8	22.4
58.7	127344	0.8	8.7	1.0	5.2291	2.4	0.3300	2.2	0.91	1838.4	35.7	1857.4	20.9	1878.6	18.2	1878.6	18.2
153.7	40939	2.7	5.4	0.8	11.8008	5.3	0.4605	5.3	0.99	2441.6	107.4	2588.7	50.0	2706.0	12.5	2706.0	12.5
257.9	54576	1.9	5.2	0.6	12.9075	3.2	0.4829	3.1	0.98	2539.8	65.4	2672.9	29.9	2775.2	10.2	2775.2	10.2
102.2	230846	1.5	5.0	0.2	14.9831	5.7	0.5459	5.7	1.00	2807.9	129.9	2814.2	54.4	2818.6	2.7	2818.6	2.7
14.1	36277	1.0	3.7	0.6	24.9153	4.1	0.6727	4.0	0.99	3316.3	103.9	3304.9	39.6	3298.0	9.9	3298.0	9.9
SAL 1964 96-35-2																	
149.8	5894	1.1	19.5	7.0	0.2802	9.7	0.0397	6.8	0.70	251.1	16.6	250.8	21.6	248.7	160.7	251.1	16.6
98.7	2310	0.7	17.1	14.1	0.3213	14.3	0.0399	2.4	0.17	252.2	5.9	282.9	35.4	544.5	310.0	252.2	5.9
216.6	2280	1.2	18.0	8.0	0.3064	8.0	0.0401	0.7	0.08	253.5	1.6	271.4	19.1	428.8	178.3	253.5	1.6
82.6	6756	1.5	19.6	17.1	0.2827	17.6	0.0403	4.3	0.24	254.5	10.6	252.8	39.5	237.0	397.5	254.5	10.6
423.1	93872	1.6	19.5	2.1	0.2851	2.3	0.0403	1.1	0.47	254.5	2.7	254.7	5.3	255.9	47.6	254.5	2.7
84.0	2030	1.7	18.4	15.0	0.3034	15.3	0.0404	3.0	0.20	255.4	7.5	269.0	36.1	389.2	337.9	255.4	7.5
137.5	2932	1.7	18.5	7.5	0.3009	8.2	0.0405	3.3	0.40	255.6	8.2	267.1	19.3	368.7	170.0	255.6	8.2
166.1	28046	0.6	18.9	4.7	0.2964	4.8	0.0405	0.9	0.18	256.2	2.2	263.5	11.2	329.7	107.5	256.2	2.2
460.5	47285	0.7	16.8	15.1	0.3331	15.3	0.0406	2.1	0.14	256.3	5.4	291.9	38.8	587.5	330.4	256.3	5.4
108.8	23059	1.1	19.5	13.6	0.2880	13.7	0.0406	1.5	0.11	256.7	3.9	257.0	31.2	259.4	314.5	256.7	3.9
171.9	2610	1.3	18.2	6.3	0.3087	6.8	0.0407	2.4	0.35	257.2	6.0	273.2	16.2	412.7	142.1	257.2	6.0
227.3	94626	1.3	19.8	3.1	0.2837	3.5	0.0407	1.7	0.49	257.2	4.3	253.6	7.9	220.7	71.1	257.2	4.3
177.8	34235	1.2	18.7	5.9	0.3002	6.1	0.0407	1.5	0.25	257.3	3.8	266.6	14.2	349.0	133.1	257.3	3.8
194.9	15112	1.7	19.6	3.8	0.2868	4.0	0.0407	1.3	0.33	257.4	3.4	256.0	9.1	243.2	87.6	257.4	3.4
48.6	6634	0.9	18.8	18.3	0.2995	18.5	0.0408	2.9	0.15	257.5	7.2	266.0	43.4	342.0	417.3	257.5	7.2

Appendix A: Cont. U/Pb detrital zircon geochronologic analyses by Laser-Ablation Multicollector ICP Mass Spectrometry

					Isotope ratios					Apparent ages (Ma)							
U (ppm)	206Pb 204Pb	U/Th	206Pb* 207Pb*	± (%)	207Pb* 235U*	± (%)	206Pb* 238U	± (%)	error corr.	206Pb* 238U*	± (Ma)	207Pb* 235U	± (Ma)	206Pb* 207Pb*	± (Ma)	**Best age (Ma)**	± (Ma)
SAL 1964 96-35-2 Cont.																	
147.7	27582	0.9	20.0	5.4	0.2809	5.6	0.0408	1.4	0.25	257.6	3.5	251.4	12.4	193.8	125.3	257.6	3.5
214.3	23557	0.7	19.4	4.4	0.2909	5.1	0.0408	2.7	0.52	258.1	6.7	259.2	11.7	269.8	100.2	258.1	6.7
343.7	1689	1.3	18.3	3.8	0.3081	4.0	0.0408	1.2	0.30	258.1	3.1	272.7	9.7	400.2	86.3	258.1	3.1
401.3	7759	1.3	18.8	3.7	0.2990	3.7	0.0409	0.7	0.19	258.3	1.8	265.6	8.7	331.1	83.4	258.3	1.8
104.0	16137	1.3	21.1	6.9	0.2676	7.6	0.0409	3.1	0.41	258.4	7.8	240.8	16.2	71.7	164.1	258.4	7.8
166.7	10674	0.7	18.7	5.3	0.3020	5.4	0.0410	1.3	0.24	258.9	3.4	268.0	12.8	348.6	119.2	258.9	3.4
117.5	7486	1.0	17.2	12.4	0.3279	12.6	0.0410	2.4	0.19	258.9	6.1	287.9	31.7	531.0	272.9	258.9	6.1
99.1	19615	1.0	19.6	4.8	0.2877	5.2	0.0410	2.0	0.39	258.9	5.1	256.7	11.8	236.8	110.8	258.9	5.1
143.7	24606	0.9	18.8	4.2	0.3010	4.7	0.0410	2.2	0.46	258.9	5.5	267.2	11.1	340.2	94.9	258.9	5.5
321.4	36841	1.4	19.3	3.6	0.2923	4.0	0.0410	1.6	0.41	259.0	4.1	260.4	9.2	272.6	83.6	259.0	4.1
194.5	22534	1.2	19.3	5.0	0.2939	5.3	0.0411	1.6	0.30	259.6	4.0	261.6	12.1	280.4	115.1	259.6	4.0
239.3	61527	1.2	19.8	3.5	0.2860	4.0	0.0411	2.1	0.51	259.6	5.2	255.4	9.1	216.7	80.5	259.6	5.2
106.4	11994	1.0	19.7	8.4	0.2885	8.4	0.0411	1.2	0.15	259.8	3.1	257.4	19.2	235.3	193.2	259.8	3.1
92.2	18238	0.8	20.1	12.1	0.2821	12.2	0.0412	1.5	0.13	260.0	3.9	252.4	27.3	181.8	282.8	260.0	3.9
236.9	71596	1.3	19.6	5.5	0.2895	5.8	0.0412	1.8	0.31	260.1	4.6	258.1	13.1	240.7	126.2	260.1	4.6
212.9	19609	1.2	19.7	3.4	0.2879	3.8	0.0412	1.6	0.42	260.1	4.1	256.9	8.6	227.5	79.5	260.1	4.1
490.4	45161	0.8	19.4	2.2	0.2934	2.9	0.0412	2.0	0.67	260.4	5.0	261.2	6.8	268.9	50.4	260.4	5.0
205.9	23893	1.4	19.6	5.0	0.2894	5.0	0.0412	0.8	0.17	260.4	2.2	258.1	11.5	237.4	114.4	260.4	2.2
143.7	27130	0.7	20.0	7.4	0.2839	7.8	0.0412	2.5	0.32	260.4	6.4	253.8	17.5	192.6	171.4	260.4	6.4
288.7	17654	1.6	18.9	3.9	0.3007	4.1	0.0412	1.0	0.25	260.5	2.6	267.0	9.6	324.0	89.7	260.5	2.6
253.6	81512	1.3	19.2	5.8	0.2961	5.9	0.0413	0.9	0.16	260.6	2.4	263.3	13.7	287.6	132.9	260.6	2.4
32.7	4655	0.2	16.8	14.8	0.3382	15.6	0.0413	4.7	0.30	260.7	11.9	295.8	39.9	582.9	323.8	260.7	11.9
122.3	13581	1.1	20.0	7.2	0.2845	7.3	0.0413	1.4	0.19	260.9	3.6	254.2	16.5	192.6	167.5	260.9	3.6

Appendix A: Cont. U/Pb detrital zircon geochronologic analyses by Laser-Ablation Multicollector ICP Mass Spectrometry

					Isotope ratios					Apparent ages (Ma)							
U (ppm)	206Pb 204Pb	U/Th	206Pb* 207Pb*	± (%)	207Pb* 235U*	± (%)	206Pb* 238U	± (%)	error corr.	206Pb* 238U*	± (Ma)	207Pb* 235U	± (Ma)	206Pb* 207Pb*	± (Ma)	**Best age** (Ma)	± (Ma)
SAL 1964 96-35-2 Cont.																	
109.1	11170	1.8	18.3	11.6	0.3112	13.0	0.0413	5.8	0.45	260.9	14.8	275.1	31.3	397.3	261.2	260.9	14.8
220.8	24513	1.0	19.5	4.0	0.2927	4.5	0.0413	2.1	0.46	261.1	5.3	260.7	10.3	257.4	91.7	261.1	5.3
229.4	7760	0.7	18.9	6.5	0.3018	6.5	0.0413	0.7	0.11	261.2	1.8	267.8	15.3	325.8	147.2	261.2	1.8
327.4	108926	1.2	19.0	1.9	0.3002	2.2	0.0414	1.1	0.52	261.2	2.9	266.6	5.2	313.9	43.2	261.2	2.9
226.0	19453	1.4	19.4	3.9	0.2944	4.1	0.0414	1.3	0.31	261.4	3.3	262.0	9.5	267.2	89.3	261.4	3.3
243.2	29963	1.2	19.9	5.1	0.2868	5.4	0.0414	1.8	0.33	261.5	4.6	256.0	12.3	206.2	118.8	261.5	4.6
108.0	25413	1.4	19.7	7.6	0.2901	8.2	0.0414	3.0	0.37	261.5	7.8	258.6	18.7	232.8	175.7	261.5	7.8
188.3	28267	1.2	19.6	5.0	0.2907	5.2	0.0414	1.6	0.31	261.5	4.2	259.1	12.0	236.9	115.1	261.5	4.2
345.8	18017	1.6	19.4	3.7	0.2947	4.3	0.0414	2.2	0.51	261.5	5.6	262.2	10.0	268.4	85.9	261.5	5.6
145.6	21070	1.6	19.5	5.4	0.2931	5.7	0.0414	1.9	0.33	261.6	4.9	261.0	13.2	256.0	124.4	261.6	4.9
195.8	20068	0.9	19.3	3.8	0.2951	4.0	0.0414	1.3	0.32	261.6	3.3	262.6	9.3	271.3	87.7	261.6	3.3
221.3	26676	1.2	19.6	3.2	0.2908	3.5	0.0414	1.4	0.41	261.6	3.6	259.2	7.9	237.2	72.8	261.6	3.6
261.5	17975	1.2	19.4	3.5	0.2944	3.6	0.0414	1.1	0.31	261.6	2.9	262.0	8.4	265.7	79.5	261.6	2.9
176.9	12006	1.3	18.8	3.3	0.3046	4.3	0.0414	2.7	0.62	261.7	6.8	270.0	10.1	342.5	75.6	261.7	6.8
224.2	37785	0.9	18.9	4.2	0.3032	4.6	0.0415	1.7	0.37	262.1	4.4	268.9	10.8	328.3	96.1	262.1	4.4
242.0	38423	1.6	19.2	4.3	0.2976	4.7	0.0415	1.9	0.40	262.1	4.8	264.5	10.9	285.9	98.6	262.1	4.8
410.0	13093	1.1	19.2	3.6	0.2983	3.6	0.0415	0.7	0.19	262.2	1.8	265.0	8.4	290.0	81.1	262.2	1.8
296.2	132015	1.1	19.1	3.4	0.2999	4.3	0.0415	2.7	0.62	262.3	6.9	266.3	10.1	301.7	77.3	262.3	6.9
219.3	65595	1.1	19.5	3.5	0.2932	3.8	0.0415	1.6	0.41	262.3	4.1	261.1	8.9	249.9	80.7	262.3	4.1
178.3	31759	0.8	19.0	4.9	0.3021	5.1	0.0415	1.4	0.27	262.4	3.6	268.1	12.1	318.2	112.3	262.4	3.6
199.2	16166	1.9	19.2	5.0	0.2991	5.1	0.0416	1.4	0.26	262.4	3.5	265.7	12.0	294.2	113.4	262.4	3.5
87.1	6536	0.8	17.4	13.6	0.3291	13.9	0.0416	2.9	0.21	262.5	7.5	288.9	34.9	508.5	299.9	262.5	7.5
492.0	68803	1.0	19.5	2.1	0.2944	2.2	0.0416	0.7	0.30	262.8	1.7	262.0	5.1	254.5	48.1	262.8	1.7

Appendix A: Cont. U/Pb detrital zircon geochronologic analyses by Laser-Ablation Multicollector ICP Mass Spectrometry

					Isotope ratios					Apparent ages (Ma)							
U (ppm)	206Pb 204Pb	U/Th	206Pb* 207Pb*	± (%)	207Pb* 235U*	± (%)	206Pb* 238U	± (%)	error corr.	206Pb* 238U*	± (Ma)	207Pb* 235U	± (Ma)	206Pb* 207Pb*	± (Ma)	**Best age (Ma)**	± (Ma)
SAL 1964 96-35-2 Cont.																	
225.6	19893	0.9	18.9	4.1	0.3036	4.2	0.0416	1.1	0.25	263.0	2.7	269.2	10.0	323.6	93.5	263.0	2.7
297.1	23477	1.3	19.4	2.3	0.2959	2.7	0.0416	1.4	0.54	263.0	3.7	263.2	6.2	264.8	51.9	263.0	3.7
116.9	14821	1.1	19.5	10.8	0.2946	10.9	0.0417	1.7	0.16	263.3	4.4	262.2	25.2	252.4	248.1	263.3	4.4
154.8	21585	0.9	19.1	4.4	0.3011	5.0	0.0417	2.3	0.45	263.3	5.8	267.3	11.7	302.4	101.5	263.3	5.8
243.9	50981	1.0	19.2	4.6	0.2998	4.7	0.0417	1.2	0.26	263.4	3.2	266.3	11.1	291.8	104.6	263.4	3.2
467.6	89413	1.1	19.3	1.7	0.2976	2.2	0.0417	1.5	0.65	263.6	3.8	264.5	5.2	273.1	38.7	263.6	3.8
256.7	37434	1.1	19.6	2.7	0.2929	3.3	0.0417	1.8	0.56	263.6	4.7	260.9	7.5	236.7	62.7	263.6	4.7
185.8	50075	1.3	19.0	6.5	0.3027	6.8	0.0417	2.3	0.33	263.6	5.9	268.5	16.2	311.7	147.0	263.6	5.9
85.4	12725	2.0	20.7	14.9	0.2780	15.0	0.0417	2.2	0.14	263.7	5.6	249.0	33.2	113.4	352.4	263.7	5.6
351.3	83170	1.5	19.4	3.1	0.2975	3.1	0.0418	0.7	0.23	263.9	1.9	264.4	7.3	269.0	70.1	263.9	1.9
296.4	73541	1.9	19.4	3.1	0.2967	3.3	0.0418	1.0	0.31	264.0	2.7	263.9	7.6	263.0	71.5	264.0	2.7
228.2	66640	1.3	19.3	5.8	0.2982	6.6	0.0418	3.1	0.47	264.1	8.0	265.0	15.4	273.1	133.7	264.1	8.0
248.5	62132	1.6	19.3	3.0	0.2982	3.5	0.0418	1.7	0.49	264.2	4.4	265.0	8.1	272.2	69.0	264.2	4.4
236.5	57924	1.8	18.4	2.6	0.3135	3.4	0.0419	2.1	0.62	264.4	5.4	276.9	8.1	383.1	59.5	264.4	5.4
197.7	14004	1.4	18.3	5.5	0.3150	5.6	0.0419	1.0	0.18	264.6	2.6	278.0	13.5	392.6	122.5	264.6	2.6
89.8	24253	1.4	19.1	12.3	0.3031	12.7	0.0419	3.2	0.25	264.7	8.3	268.9	29.9	304.8	280.3	264.7	8.3
223.8	86625	1.8	19.0	5.8	0.3049	6.1	0.0420	2.0	0.33	265.1	5.2	270.3	14.6	315.0	132.0	265.1	5.2
197.1	38445	1.1	19.5	4.9	0.2978	5.1	0.0420	1.4	0.28	265.3	3.7	264.7	11.8	259.1	111.6	265.3	3.7
115.0	20551	0.9	19.2	13.6	0.3018	14.2	0.0420	4.1	0.29	265.5	10.7	267.8	33.4	288.0	311.7	265.5	10.7
374.4	62850	1.2	19.5	1.8	0.2977	2.1	0.0421	1.0	0.48	265.6	2.6	264.6	4.8	255.7	41.8	265.6	2.6
271.0	45605	1.5	19.4	4.8	0.2997	5.0	0.0421	1.3	0.26	265.7	3.4	266.2	11.6	270.8	109.7	265.7	3.4
524.7	140976	1.4	19.4	1.8	0.3000	2.5	0.0421	1.7	0.70	266.1	4.5	266.4	5.8	269.2	40.7	266.1	4.5
260.5	20022	0.9	18.8	3.0	0.3093	5.1	0.0422	4.2	0.81	266.3	10.8	273.6	12.2	337.2	67.1	266.3	10.8

Appendix A: Cont. U/Pb detrital zircon geochronologic analyses by Laser-Ablation Multicollector ICP Mass Spectrometry

					Isotope ratios					Apparent ages (Ma)							
U (ppm)	206Pb 204Pb	U/Th	206Pb* 207Pb*	± (%)	207Pb* 235U*	± (%)	206Pb* 238U	± (%)	error corr.	206Pb* 238U*	± (Ma)	207Pb* 235U	± (Ma)	206Pb* 207Pb*	± (Ma)	**Best age (Ma)**	**± (Ma)**
SAL 1964 96-35-2 Cont.																	
139.5	28442	1.5	18.4	4.5	0.3153	5.0	0.0422	2.3	0.45	266.4	5.9	278.3	12.2	379.5	100.3	266.4	5.9
328.7	8780	1.5	19.2	2.7	0.3032	4.0	0.0422	2.9	0.73	266.7	7.7	268.9	9.5	287.6	62.2	266.7	7.7
252.8	59408	1.7	19.2	3.8	0.3030	4.3	0.0423	2.1	0.49	266.8	5.5	268.7	10.2	285.6	85.9	266.8	5.5
152.7	19309	1.2	19.3	4.8	0.3023	5.5	0.0423	2.7	0.49	267.3	7.1	268.2	12.9	276.3	109.3	267.3	7.1
224.8	13713	1.9	18.7	5.0	0.3123	5.1	0.0424	1.1	0.21	267.4	2.8	276.0	12.4	348.8	113.3	267.4	2.8
500.8	711850	2.2	19.7	1.5	0.2975	2.0	0.0424	1.3	0.64	268.0	3.3	264.4	4.6	232.8	35.0	268.0	3.3
255.5	20708	1.4	19.2	2.4	0.3059	2.9	0.0425	1.6	0.54	268.4	4.1	271.0	6.9	293.5	56.0	268.4	4.1
348.6	10377	1.0	18.9	3.4	0.3104	3.5	0.0425	1.0	0.28	268.4	2.6	274.5	8.4	326.7	76.3	268.4	2.6
110.5	7365	1.0	18.2	7.0	0.3245	7.7	0.0428	3.1	0.41	270.0	8.2	285.4	19.0	413.0	156.4	270.0	8.2
125.5	23843	1.5	19.4	6.4	0.3036	7.0	0.0428	2.7	0.39	270.1	7.1	269.2	16.4	261.5	147.3	270.1	7.1
72.1	27955	0.6	21.4	26.2	0.2770	26.6	0.0430	4.4	0.17	271.4	11.7	248.3	58.6	35.3	637.4	271.4	11.7
217.8	23357	1.1	19.3	5.1	0.3078	5.2	0.0430	0.7	0.14	271.6	1.9	272.4	12.3	279.4	117.2	271.6	1.9
148.6	45187	0.7	19.3	4.7	0.3075	4.9	0.0430	1.6	0.33	271.6	4.3	272.2	11.8	277.0	106.9	271.6	4.3
121.9	19398	1.2	19.9	7.8	0.2988	8.3	0.0431	2.9	0.35	272.3	7.8	265.5	19.5	205.7	181.3	272.3	7.8
136.6	15425	1.5	18.7	12.5	0.3187	12.7	0.0433	2.4	0.19	273.3	6.4	280.9	31.2	344.5	283.0	273.3	6.4
257.1	54632	1.4	19.3	2.7	0.3112	6.4	0.0436	5.8	0.91	275.1	15.6	275.1	15.4	275.3	61.6	275.1	15.6
73.2	31196	1.7	19.2	8.3	0.3183	11.1	0.0443	7.4	0.66	279.4	20.2	280.6	27.3	290.4	190.6	279.4	20.2
149.4	14632	0.7	19.5	4.9	0.3143	5.1	0.0444	1.2	0.24	280.3	3.4	277.5	12.4	253.7	113.8	280.3	3.4
478.7	112738	0.9	18.9	1.6	0.3475	2.3	0.0477	1.7	0.72	300.1	4.8	302.8	6.0	323.6	36.3	300.1	4.8
362.9	56436	1.9	18.3	2.5	0.4124	2.8	0.0547	1.1	0.41	343.5	3.8	350.6	8.2	397.8	56.3	343.5	3.8
217.5	91825	1.7	18.7	3.9	0.4209	4.0	0.0571	0.5	0.13	357.8	1.7	356.7	12.0	349.4	89.2	357.8	1.7
118.1	13173	1.2	17.8	5.1	0.4866	5.3	0.0630	1.4	0.27	393.8	5.5	402.6	17.6	453.8	112.9	393.8	5.5
243.5	76479	1.9	18.5	2.1	0.4684	2.9	0.0630	2.0	0.68	393.9	7.5	390.0	9.3	367.4	47.2	393.9	7.5

Appendix A: Cont. U/Pb detrital zircon geochronologic analyses by Laser-Ablation Multicollector ICP Mass Spectrometry

					Isotope ratios					Apparent ages (Ma)							
U (ppm)	206Pb 204Pb	U/Th	206Pb* 207Pb*	± (%)	207Pb* 235U*	± (%)	206Pb* 238U	± (%)	error corr.	206Pb* 238U*	± (Ma)	207Pb* 235U	± (Ma)	206Pb* 207Pb*	± (Ma)	**Best age** (Ma)	± (Ma)
SAL 1964 96-35-2 Cont.																	
458.9	74380	0.9	18.4	1.1	0.4719	3.4	0.0631	3.3	0.95	394.4	12.4	392.5	11.2	381.0	24.9	394.4	12.4
100.4	25714	1.1	16.9	4.5	0.7601	5.2	0.0931	2.6	0.51	573.6	14.4	574.0	22.7	575.8	97.1	573.6	14.4
302.9	182820	1.8	13.2	0.4	1.9192	1.0	0.1840	1.0	0.94	1088.5	9.8	1087.8	7.0	1086.3	7.3	1086.3	7.3
SAL 1695 96-36-1																	
217.9	1086	1.3	17.9	6.8	0.2802	7.3	0.0364	2.7	0.36	230.8	6.1	250.8	16.3	442.6	151.6	230.8	6.1
172.2	39620	0.8	19.8	5.9	0.2747	6.6	0.0394	3.0	0.45	249.1	7.2	246.5	14.4	221.6	135.5	249.1	7.2
96.4	27421	0.7	18.7	8.2	0.2911	8.5	0.0396	2.1	0.24	250.3	5.1	259.5	19.4	343.4	186.4	250.3	5.1
104.5	23396	0.9	21.5	9.9	0.2543	10.1	0.0396	2.0	0.20	250.3	4.9	230.0	20.7	27.9	236.9	250.3	4.9
108.8	40995	0.7	18.3	10.4	0.3009	10.8	0.0400	2.8	0.26	252.7	6.8	267.1	25.3	395.7	233.7	252.7	6.8
137.5	26761	0.7	19.8	6.0	0.2785	6.1	0.0400	1.2	0.20	253.0	3.1	249.4	13.6	216.3	139.2	253.0	3.1
132.1	30691	0.5	20.0	4.1	0.2770	4.6	0.0401	2.0	0.43	253.4	4.8	248.2	10.0	200.2	95.5	253.4	4.8
217.6	29063	1.3	20.3	4.1	0.2726	4.4	0.0401	1.7	0.38	253.5	4.2	244.7	9.6	161.6	95.7	253.5	4.2
151.7	2313	2.0	16.3	12.5	0.3399	12.6	0.0401	1.2	0.09	253.6	2.9	297.1	32.4	654.5	270.0	253.6	2.9
39.0	7660	0.7	22.0	37.2	0.2526	37.3	0.0403	2.9	0.08	254.8	7.2	228.7	76.6	-32.3	931.3	254.8	7.2
136.3	12301	0.7	20.1	10.0	0.2774	10.5	0.0404	3.1	0.30	255.1	7.8	248.6	23.1	187.2	233.7	255.1	7.8
330.3	47046	0.9	19.7	1.9	0.2832	2.1	0.0404	0.8	0.39	255.3	2.0	253.2	4.7	234.0	44.3	255.3	2.0
96.8	17183	0.7	20.1	16.0	0.2775	16.1	0.0405	2.1	0.13	255.7	5.4	248.7	35.6	182.8	374.3	255.7	5.4
185.6	80824	0.6	19.9	5.5	0.2806	5.7	0.0405	1.5	0.27	255.9	3.8	251.1	12.6	207.2	126.7	255.9	3.8
140.2	23077	0.5	19.8	8.0	0.2819	8.4	0.0405	2.5	0.30	256.0	6.3	252.1	18.8	216.6	185.9	256.0	6.3
195.3	48820	1.6	19.4	5.5	0.2887	6.3	0.0405	3.1	0.49	256.0	7.7	257.5	14.3	270.9	125.8	256.0	7.7
362.4	73889	1.3	19.3	3.6	0.2892	3.6	0.0405	0.6	0.17	256.2	1.6	257.9	8.2	273.5	81.6	256.2	1.6
160.0	26327	0.7	20.3	6.9	0.2750	7.4	0.0406	2.7	0.37	256.3	6.8	246.7	16.2	156.3	161.5	256.3	6.8
201.9	26717	0.9	19.5	4.7	0.2865	5.0	0.0406	1.8	0.35	256.5	4.4	255.8	11.3	249.6	108.2	256.5	4.4

Appendix A: Cont. U/Pb detrital zircon geochronologic analyses by Laser-Ablation Multicollector ICP Mass Spectrometry

					Isotope ratios					Apparent ages (Ma)							
U (ppm)	206Pb 204Pb	U/Th	206Pb* 207Pb*	± (%)	207Pb* 235U*	± (%)	206Pb* 238U	± (%)	error corr.	206Pb* 238U*	± (Ma)	207Pb* 235U	± (Ma)	206Pb* 207Pb*	± (Ma)	**Best age (Ma)**	± (Ma)
SAL 1695 96-36-1 Cont.																	
138.6	33170	0.8	19.8	8.2	0.2833	8.3	0.0406	1.4	0.17	256.7	3.5	253.2	18.6	221.5	189.9	256.7	3.5
180.5	42862	0.9	20.2	4.1	0.2776	4.3	0.0406	1.3	0.30	256.7	3.2	248.7	9.5	174.1	95.7	256.7	3.2
141.0	14267	0.8	18.3	8.4	0.3058	8.5	0.0407	1.3	0.15	256.9	3.2	271.0	20.3	394.3	189.3	256.9	3.2
470.6	85058	0.5	19.1	1.4	0.2937	1.5	0.0407	0.6	0.39	257.0	1.5	261.5	3.6	301.8	32.5	257.0	1.5
137.8	20933	1.7	20.4	8.8	0.2748	8.9	0.0407	1.7	0.19	257.1	4.2	246.5	19.5	147.0	205.7	257.1	4.2
277.8	99143	2.1	19.2	3.2	0.2919	3.6	0.0407	1.7	0.46	257.3	4.2	260.1	8.3	284.7	73.9	257.3	4.2
142.1	67433	0.8	20.7	4.9	0.2716	5.4	0.0407	2.2	0.41	257.4	5.6	243.9	11.7	116.4	115.6	257.4	5.6
322.3	72255	1.0	19.8	2.4	0.2837	3.1	0.0408	2.1	0.65	257.6	5.2	253.6	7.0	216.6	54.9	257.6	5.2
529.8	78370	1.3	19.4	2.2	0.2906	2.5	0.0408	1.1	0.43	257.8	2.7	259.1	5.6	270.9	51.0	257.8	2.7
154.4	27919	1.0	19.0	5.0	0.2955	5.2	0.0408	1.5	0.28	257.9	3.7	262.9	12.1	307.7	113.8	257.9	3.7
119.1	28867	1.0	20.4	8.1	0.2761	8.5	0.0408	2.6	0.31	258.0	6.5	247.5	18.6	149.2	189.0	258.0	6.5
66.7	17947	1.2	19.5	9.9	0.2898	11.1	0.0409	5.1	0.46	258.3	13.0	258.4	25.4	259.4	227.5	258.3	13.0
223.0	24697	1.0	19.2	4.0	0.2948	4.2	0.0410	1.2	0.29	258.9	3.1	262.3	9.8	293.1	92.2	258.9	3.1
74.4	23845	0.4	20.6	14.0	0.2747	14.1	0.0410	1.6	0.11	259.0	4.0	246.4	30.9	128.5	331.1	259.0	4.0
219.4	37415	1.5	19.5	3.1	0.2896	3.8	0.0410	2.1	0.56	259.1	5.3	258.3	8.6	250.8	71.8	259.1	5.3
128.2	18658	0.7	19.3	3.6	0.2940	4.0	0.0411	1.8	0.44	259.6	4.5	261.7	9.3	280.8	82.9	259.6	4.5
158.8	44546	0.9	20.2	5.3	0.2813	5.6	0.0411	1.5	0.28	259.8	3.9	251.7	12.4	176.6	124.5	259.8	3.9
145.1	31729	1.7	19.3	5.8	0.2941	6.2	0.0412	2.3	0.36	260.6	5.8	261.8	14.4	272.9	133.4	260.6	5.8
151.0	32968	0.7	20.2	6.1	0.2817	6.9	0.0413	3.4	0.48	261.0	8.6	252.0	15.5	169.7	141.9	261.0	8.6
93.2	10982	0.7	21.4	12.9	0.2673	13.1	0.0414	1.9	0.14	261.5	4.9	240.5	28.0	40.2	310.5	261.5	4.9
260.0	29262	1.0	19.7	4.2	0.2900	4.3	0.0414	0.9	0.20	261.8	2.2	258.5	9.8	229.3	97.1	261.8	2.2
129.2	38424	1.1	19.4	8.0	0.2957	8.2	0.0416	1.5	0.18	262.4	3.7	263.1	18.9	268.8	184.4	262.4	3.7
177.1	22823	1.1	19.3	3.3	0.2965	3.8	0.0416	2.0	0.53	262.5	5.2	263.6	8.9	273.9	74.9	262.5	5.2

Appendix A: Cont. U/Pb detrital zircon geochronologic analyses by Laser-Ablation Multicollector ICP Mass Spectrometry

					Isotope ratios					Apparent ages (Ma)							
U (ppm)	206Pb 204Pb	U/Th	206Pb* 207Pb*	± (%)	207Pb* 235U*	± (%)	206Pb* 238U	± (%)	error corr.	206Pb* 238U*	± (Ma)	207Pb* 235U	± (Ma)	206Pb* 207Pb*	± (Ma)	**Best age (Ma)**	**± (Ma)**
SAL 1695 96-36-1 Cont.																	
261.1	9703	0.7	18.6	7.6	0.3089	7.9	0.0417	2.4	0.30	263.1	6.1	273.4	19.0	362.3	170.6	263.1	6.1
199.3	37701	0.7	19.0	2.2	0.3029	3.1	0.0417	2.2	0.71	263.2	5.8	268.6	7.4	316.6	50.1	263.2	5.8
197.1	49719	1.4	19.6	3.4	0.2930	4.1	0.0417	2.3	0.56	263.7	5.9	260.9	9.4	236.1	77.9	263.7	5.9
338.7	7405	0.7	19.2	3.4	0.2999	5.3	0.0418	4.0	0.76	264.1	10.4	266.3	12.3	285.3	77.8	264.1	10.4
139.9	26441	0.7	19.9	6.7	0.2898	9.1	0.0419	6.2	0.68	264.7	16.1	258.4	20.8	201.4	154.9	264.7	16.1
211.8	83124	1.0	19.7	5.6	0.2933	6.0	0.0420	2.2	0.37	265.1	5.7	261.1	13.8	225.3	129.1	265.1	5.7
833.0	43528	1.6	19.3	1.3	0.3018	1.7	0.0423	1.0	0.61	266.8	2.7	267.8	3.9	276.3	30.5	266.8	2.7
94.0	47264	1.5	18.4	7.3	0.3181	8.4	0.0424	4.1	0.49	267.8	10.8	280.5	20.5	387.6	164.0	267.8	10.8
184.4	33574	0.5	19.1	5.7	0.3177	6.0	0.0441	1.9	0.32	278.3	5.2	280.2	14.7	296.1	130.1	278.3	5.2
163.2	35246	1.7	18.6	3.3	0.3296	3.8	0.0444	1.7	0.47	280.0	4.8	289.3	9.4	365.2	74.8	280.0	4.8
34.0	263	0.6	13.3	16.7	0.4782	17.4	0.0460	4.7	0.27	290.1	13.3	396.8	57.1	1077.5	337.9	290.1	13.3
165.8	27556	1.4	19.6	3.4	0.3241	4.1	0.0461	2.2	0.55	290.8	6.3	285.0	10.1	238.1	78.2	290.8	6.3
296.2	49450	2.5	18.9	2.2	0.3533	3.2	0.0485	2.3	0.71	305.2	6.7	307.2	8.4	322.3	51.1	305.2	6.7
411.3	17848	2.4	18.5	1.7	0.3915	4.2	0.0526	3.9	0.92	330.4	12.6	335.5	12.1	370.7	37.5	330.4	12.6
204.3	52097	0.9	19.0	2.7	0.3873	2.9	0.0534	0.9	0.32	335.2	3.0	332.4	8.2	312.6	62.4	335.2	3.0
684.5	70837	2.4	18.4	1.3	0.4304	2.0	0.0574	1.6	0.78	360.1	5.5	363.5	6.2	385.2	28.7	360.1	5.5
263.3	118143	2.0	18.6	2.3	0.4301	2.4	0.0579	0.6	0.27	362.8	2.2	363.3	7.2	366.1	51.3	362.8	2.2
174.8	47117	1.6	18.6	4.6	0.4322	4.7	0.0582	0.9	0.18	364.7	3.1	364.7	14.5	364.8	104.7	364.7	3.1
115.1	31585	1.3	18.9	4.9	0.4275	6.7	0.0586	4.6	0.69	367.1	16.3	361.4	20.3	325.2	110.4	367.1	16.3
219.1	62142	1.4	18.5	2.7	0.4378	3.1	0.0588	1.6	0.50	368.2	5.6	368.7	9.7	372.0	61.1	368.2	5.6
507.3	138295	2.4	18.6	1.7	0.4356	1.8	0.0589	0.6	0.32	368.9	2.1	367.1	5.6	356.2	39.0	368.9	2.1
249.1	40010	1.1	18.5	1.8	0.4400	2.6	0.0590	1.9	0.73	369.3	6.9	370.2	8.2	376.3	40.2	369.3	6.9
130.1	30182	1.3	18.8	2.9	0.4327	4.0	0.0590	2.8	0.70	369.5	10.1	365.1	12.3	337.6	64.7	369.5	10.1

Appendix A: Cont. U/Pb detrital zircon geochronologic analyses by Laser-Ablation Multicollector ICP Mass Spectrometry

					Isotope ratios					Apparent ages (Ma)							
U (ppm)	206Pb 204Pb	U/Th	206Pb* 207Pb*	± (%)	207Pb* 235U*	± (%)	206Pb* 238U	± (%)	error corr.	206Pb* 238U*	± (Ma)	207Pb* 235U	± (Ma)	206Pb* 207Pb*	± (Ma)	**Best age (Ma)**	± (Ma)
SAL 1695 96-36-1 Cont.																	
438.7	96800	1.7	18.3	1.5	0.4471	2.0	0.0592	1.3	0.64	370.7	4.6	375.3	6.3	403.5	34.2	370.7	4.6
420.4	89885	2.6	18.4	1.6	0.4725	4.1	0.0629	3.8	0.92	393.5	14.5	392.9	13.5	389.5	36.7	393.5	14.5
75.9	69111	1.3	17.7	4.0	0.5980	5.0	0.0766	3.1	0.62	476.0	14.2	475.9	19.1	475.5	87.7	476.0	14.2
89.0	25052	1.0	17.9	7.7	0.6037	7.8	0.0784	1.7	0.22	486.3	8.1	479.6	30.0	447.6	170.3	486.3	8.1
225.4	4262	1.0	17.3	2.4	0.6321	2.8	0.0791	1.5	0.54	491.0	7.1	497.4	11.0	527.1	51.9	491.0	7.1
149.3	96876	1.4	17.3	2.7	0.6381	3.2	0.0800	1.6	0.52	496.1	7.8	501.1	12.5	524.1	59.2	496.1	7.8
258.1	105419	1.2	17.4	1.3	0.6342	2.2	0.0802	1.8	0.82	497.1	8.6	498.7	8.6	506.1	27.7	497.1	8.6
153.2	53139	1.2	17.3	2.9	0.6430	3.4	0.0806	1.6	0.48	499.5	7.7	504.2	13.3	525.1	64.5	499.5	7.7
46.8	29573	1.4	17.9	3.6	0.6198	4.7	0.0806	2.9	0.62	499.7	13.9	489.7	18.1	443.1	81.0	499.7	13.9
213.5	67446	1.0	17.5	1.4	0.6370	1.5	0.0809	0.7	0.43	501.2	3.2	500.5	6.0	496.8	30.3	501.2	3.2
101.5	61153	1.1	17.4	2.4	0.6416	2.8	0.0811	1.6	0.56	502.5	7.7	503.3	11.3	507.0	51.9	502.5	7.7
172.8	53681	1.6	17.8	1.2	0.6300	1.8	0.0813	1.4	0.76	503.7	6.7	496.1	7.2	460.9	26.4	503.7	6.7
172.4	28107	0.8	17.2	3.4	0.6615	3.5	0.0827	0.8	0.24	512.3	4.0	515.5	14.0	530.0	73.5	512.3	4.0
291.9	65545	1.7	16.7	5.7	0.6865	6.5	0.0833	3.1	0.48	516.0	15.6	530.7	26.7	594.1	122.7	516.0	15.6
198.8	56665	1.5	17.4	2.5	0.6631	3.0	0.0836	1.7	0.57	517.8	8.5	516.5	12.2	510.8	54.7	517.8	8.5
229.6	53687	2.1	17.3	1.0	0.6702	1.5	0.0843	1.1	0.75	521.8	5.7	520.9	6.1	516.6	21.7	521.8	5.7
114.0	24749	1.5	17.3	3.2	0.6741	3.4	0.0844	1.0	0.30	522.2	5.2	523.2	13.9	527.5	71.2	522.2	5.2
102.4	44678	2.1	17.4	2.9	0.6715	3.1	0.0849	1.0	0.32	525.4	5.0	521.6	12.7	505.1	64.9	525.4	5.0
392.7	119195	5.3	17.2	1.1	0.6830	2.1	0.0852	1.8	0.85	527.2	9.2	528.6	8.7	534.8	24.1	527.2	9.2
216.5	113182	4.1	17.1	1.7	0.6900	1.9	0.0856	0.9	0.46	529.5	4.4	532.8	7.8	547.2	36.3	529.5	4.4
202.9	88092	2.4	14.8	12.8	0.8230	14.4	0.0886	6.6	0.46	547.2	34.7	609.7	66.3	849.6	267.7	547.2	34.7
156.3	63693	4.6	17.4	1.9	0.7195	3.6	0.0907	3.0	0.84	559.5	16.2	550.4	15.3	512.6	42.3	559.5	16.2
95.4	17097	0.9	16.9	3.3	0.7425	5.1	0.0908	3.9	0.77	560.1	20.9	563.8	22.0	579.2	70.8	560.1	20.9

Appendix A: Cont. U/Pb detrital zircon geochronologic analyses by Laser-Ablation Multicollector ICP Mass Spectrometry

					Isotope ratios					Apparent ages (Ma)							
U (ppm)	206Pb 204Pb	U/Th	206Pb* 207Pb*	± (%)	207Pb* 235U*	± (%)	206Pb* 238U	± (%)	error corr.	206Pb* 238U*	± (Ma)	207Pb* 235U	± (Ma)	206Pb* 207Pb*	± (Ma)	**Best age (Ma)**	**± (Ma)**
SAL 1695 96-36-1 Cont.																	
213.3	95542	2.5	16.9	1.2	0.7426	1.7	0.0912	1.2	0.73	562.8	6.7	563.9	7.5	568.6	25.8	562.8	6.7
51.6	26020	0.6	16.6	5.8	0.7631	6.1	0.0921	1.9	0.31	568.0	10.3	575.8	26.9	606.6	126.2	568.0	10.3
216.0	118145	0.5	16.8	1.3	0.7818	2.1	0.0954	1.6	0.77	587.7	9.0	586.5	9.2	582.1	28.5	587.7	9.0
419.3	270653	2.1	16.8	0.7	0.7909	1.6	0.0963	1.5	0.90	592.5	8.2	591.7	7.3	588.5	15.5	592.5	8.2
216.1	118521	1.4	16.8	1.4	0.7970	1.9	0.0970	1.3	0.69	596.8	7.6	595.1	8.7	588.7	30.6	596.8	7.6
407.7	295974	5.7	15.8	3.2	0.8594	4.1	0.0982	2.6	0.63	603.7	14.7	629.8	19.0	724.6	66.9	603.7	14.7
199.5	82134	1.3	16.7	1.2	0.8169	1.7	0.0987	1.2	0.70	607.0	6.8	606.3	7.7	603.7	26.2	607.0	6.8
555.8	164875	13.5	16.7	0.5	0.8204	0.8	0.0992	0.6	0.77	609.9	3.5	608.3	3.6	602.4	10.9	609.9	3.5
489.7	240962	3.3	16.3	0.6	0.8720	2.1	0.1032	2.0	0.96	633.3	12.3	636.7	10.1	648.6	13.1	633.3	12.3
348.8	13472	3.0	15.8	3.6	0.9055	3.6	0.1040	0.6	0.18	637.8	3.9	654.7	17.4	713.0	75.6	637.8	3.9
631.4	106273	1.3	16.4	0.4	0.8872	1.4	0.1056	1.3	0.95	646.9	8.2	644.8	6.7	637.7	9.2	646.9	8.2
244.0	76407	1.4	14.1	0.4	1.4935	2.3	0.1528	2.2	0.98	916.4	19.1	927.7	13.9	954.8	9.0	954.8	9.0
392.2	83742	3.1	14.0	0.9	1.4530	2.5	0.1478	2.4	0.94	888.8	19.5	911.1	15.1	965.5	17.7	965.5	17.7
144.2	164658	3.2	13.9	1.2	1.5611	2.4	0.1568	2.1	0.88	939.2	18.7	954.9	15.1	991.4	23.7	991.4	23.7
263.4	63037	2.6	13.8	0.5	1.5843	1.2	0.1586	1.1	0.92	949.2	9.8	964.1	7.5	998.2	9.6	998.2	9.6
178.1	108990	1.6	13.7	1.4	1.5035	2.4	0.1496	2.0	0.81	899.0	16.6	931.8	14.9	1010.3	29.0	1010.3	29.0
327.2	418571	5.2	13.6	0.8	1.7664	2.1	0.1737	1.9	0.92	1032.3	18.6	1033.2	13.8	1035.1	17.2	1035.1	17.2
442.4	136729	7.9	13.3	0.5	1.8736	2.3	0.1808	2.3	0.98	1071.4	22.7	1071.8	15.6	1072.5	9.3	1072.5	9.3
101.8	136919	0.8	13.2	2.0	1.8500	2.7	0.1775	1.8	0.68	1053.3	17.9	1063.4	18.0	1084.3	40.4	1084.3	40.4
337.4	64503	3.1	13.2	0.6	1.9024	5.4	0.1821	5.4	0.99	1078.5	53.7	1081.9	36.2	1089.0	11.3	1089.0	11.3
156.4	58123	1.7	13.1	1.0	1.8845	2.1	0.1795	1.8	0.88	1064.0	17.9	1075.7	13.8	1099.2	19.9	1099.2	19.9
279.8	387880	1.9	13.1	0.7	1.9752	3.1	0.1876	3.0	0.98	1108.4	30.6	1107.1	20.8	1104.5	13.1	1104.5	13.1
277.9	341472	2.0	12.6	0.5	2.3050	1.3	0.2100	1.2	0.93	1228.7	13.2	1213.8	9.0	1187.4	9.2	1187.4	9.2

Appendix A: Cont. U/Pb detrital zircon geochronologic analyses by Laser-Ablation Multicollector ICP Mass Spectrometry

					Isotope ratios					Apparent ages (Ma)							
U (ppm)	206Pb 204Pb	U/Th	206Pb* 207Pb*	± (%)	207Pb* 235U*	± (%)	206Pb* 238U	± (%)	error corr.	206Pb* 238U*	± (Ma)	207Pb* 235U	± (Ma)	206Pb* 207Pb*	± (Ma)	**Best age (Ma)**	**± (Ma)**
SAL 1695 96-36-1 Cont.																	
351.9	348254	2.5	8.5	0.4	4.4122	2.3	0.2707	2.3	0.99	1544.5	31.2	1714.6	19.1	1929.2	7.0	1929.2	7.0
207.6	269358	1.0	8.3	0.2	5.5751	2.4	0.3367	2.4	1.00	1870.6	38.9	1912.3	20.7	1957.8	3.8	1957.8	3.8
104.8	304527	1.4	5.1	0.2	14.4252	2.4	0.5304	2.4	0.99	2742.9	53.3	2778.1	22.8	2803.7	4.0	2803.7	4.0
250.6	953034	1.8	3.3	0.6	26.1765	6.2	0.6206	6.2	1.00	3112.2	152.6	3353.2	60.8	3500.5	9.4	3500.5	9.4
SAL 1966 96-36-4																	
103.5	30088	1.3	19.6	16.6	0.2801	17.3	0.0398	4.9	0.28	251.8	12.0	250.7	38.5	241.0	385.8	251.8	12.0
209.0	39827	1.0	19.6	3.1	0.2980	3.5	0.0424	1.6	0.45	267.8	4.1	264.9	8.2	239.0	72.4	267.8	4.1
255.9	171828	1.1	19.8	2.8	0.2965	2.9	0.0426	0.7	0.24	269.1	1.8	263.7	6.8	215.8	66.0	269.1	1.8
207.0	48777	1.7	19.0	3.2	0.3191	3.4	0.0439	1.1	0.31	276.9	2.9	281.2	8.3	317.5	73.4	276.9	2.9
73.6	26766	1.7	19.2	9.5	0.3183	10.1	0.0443	3.5	0.34	279.6	9.5	280.6	24.8	289.1	217.6	279.6	9.5
458.9	177390	1.6	18.8	2.1	0.3823	2.3	0.0522	0.9	0.38	328.1	2.8	328.7	6.4	333.6	48.0	328.1	2.8
420.7	155838	0.6	18.7	1.6	0.3883	1.9	0.0527	0.9	0.47	331.1	2.9	333.1	5.3	347.4	37.2	331.1	2.9
126.4	42508	1.3	18.3	3.9	0.3992	4.0	0.0530	1.0	0.25	333.1	3.2	341.1	11.6	395.8	87.1	333.1	3.2
140.3	39094	1.5	18.8	6.6	0.3922	6.7	0.0534	1.1	0.17	335.1	3.6	336.0	19.1	341.9	149.4	335.1	3.6
116.2	38876	1.3	18.9	5.3	0.3894	5.4	0.0535	0.9	0.17	335.7	3.1	334.0	15.4	321.8	120.8	335.7	3.1
147.5	60673	1.9	19.3	3.5	0.3812	3.7	0.0535	1.3	0.35	335.7	4.3	327.9	10.5	272.6	80.3	335.7	4.3
329.4	149068	1.2	18.9	1.7	0.3939	2.1	0.0541	1.2	0.57	339.7	3.9	337.2	5.9	320.2	38.6	339.7	3.9
645.4	233022	1.1	18.8	0.9	0.4000	1.9	0.0545	1.7	0.89	342.0	5.8	341.6	5.6	339.2	19.8	342.0	5.8
183.1	76727	1.0	18.6	5.1	0.4042	5.3	0.0545	1.3	0.25	342.3	4.4	344.7	15.5	360.4	116.1	342.3	4.4
285.3	74044	2.0	19.0	1.7	0.3965	1.8	0.0546	0.7	0.41	343.0	2.5	339.1	5.2	312.8	37.8	343.0	2.5
214.3	40604	1.0	19.2	1.6	0.3947	1.9	0.0550	1.1	0.57	344.9	3.7	337.8	5.5	288.9	35.7	344.9	3.7
201.5	44302	1.1	18.5	1.9	0.4158	2.2	0.0557	1.1	0.50	349.6	3.7	353.0	6.5	375.4	42.7	349.6	3.7
61.7	48338	1.1	18.3	5.9	0.4465	6.5	0.0594	2.8	0.43	371.8	10.1	374.8	20.5	393.5	132.8	371.8	10.1

Appendix A: Cont. U/Pb detrital zircon geochronologic analyses by Laser-Ablation Multicollector ICP Mass Spectrometry

					Isotope ratios					Apparent ages (Ma)							
U (ppm)	206Pb 204Pb	U/Th	206Pb* 207Pb*	± (%)	207Pb* 235U*	± (%)	206Pb* 238U	± (%)	error corr.	206Pb* 238U*	± (Ma)	207Pb* 235U	± (Ma)	206Pb* 207Pb*	± (Ma)	**Best age** (Ma)	± (Ma)
SAL 1966 96-36-4 Cont.																	
302.8	18868	1.5	18.3	1.5	0.4625	1.8	0.0614	0.9	0.49	384.4	3.3	386.0	5.7	395.5	34.5	384.4	3.3
375.1	205686	2.0	17.8	0.6	0.5622	2.0	0.0726	1.9	0.95	451.9	8.2	453.0	7.2	458.4	13.9	451.9	8.2
102.7	49328	1.0	17.3	4.4	0.6217	4.6	0.0780	1.0	0.23	483.9	4.9	490.9	17.7	523.6	97.3	483.9	4.9
92.2	20957	0.7	17.9	1.9	0.6005	3.0	0.0780	2.3	0.76	484.3	10.5	477.6	11.3	445.3	43.1	484.3	10.5
91.2	68713	1.5	17.7	4.2	0.6122	4.7	0.0787	2.0	0.44	488.2	9.6	484.9	18.1	469.7	93.2	488.2	9.6
150.5	141521	1.2	17.8	2.1	0.6147	2.9	0.0792	2.0	0.69	491.3	9.4	486.5	11.0	464.0	45.5	491.3	9.4
278.1	87555	1.6	17.7	1.3	0.6189	1.7	0.0795	1.0	0.61	493.3	4.8	489.2	6.4	469.7	29.0	493.3	4.8
105.5	54273	0.9	17.4	5.4	0.6306	5.5	0.0798	1.2	0.22	494.9	5.9	496.5	21.7	503.8	118.8	494.9	5.9
434.6	262734	1.0	17.5	0.9	0.6282	1.7	0.0799	1.4	0.85	495.8	6.7	495.0	6.5	491.4	19.3	495.8	6.7
170.1	70701	1.1	17.5	2.8	0.6312	3.0	0.0800	1.1	0.37	496.2	5.4	496.8	11.9	499.8	62.2	496.2	5.4
272.7	144237	1.0	17.3	0.6	0.6371	1.0	0.0801	0.8	0.83	496.6	4.0	500.5	4.0	518.5	12.1	496.6	4.0
180.0	192764	0.8	17.2	2.0	0.6416	2.8	0.0803	2.0	0.71	497.6	9.4	503.3	11.1	529.0	43.3	497.6	9.4
59.5	38300	1.2	17.2	5.1	0.6473	5.7	0.0805	2.6	0.46	499.2	12.6	506.8	22.7	541.3	110.5	499.2	12.6
156.3	68687	1.5	17.1	2.6	0.6832	2.8	0.0849	1.0	0.35	525.3	4.9	528.7	11.4	543.3	56.6	525.3	4.9
129.8	6330	0.7	15.6	13.9	0.7530	14.0	0.0850	1.6	0.11	525.8	8.1	570.0	61.1	750.4	295.0	525.8	8.1
329.8	32816	6.0	17.2	1.5	0.6855	2.7	0.0853	2.2	0.83	527.9	11.3	530.1	11.1	539.7	32.9	527.9	11.3
14.5	16456	11.4	19.8	20.0	0.6050	20.4	0.0867	4.1	0.20	535.8	21.1	480.4	78.3	223.8	466.5	535.8	21.1
95.5	36829	3.4	17.2	1.8	0.7042	2.3	0.0876	1.5	0.65	541.4	7.8	541.3	9.7	540.6	38.7	541.4	7.8
68.9	59913	1.0	17.6	5.9	0.6863	6.1	0.0877	1.4	0.23	541.7	7.3	530.6	25.2	483.2	131.0	541.7	7.3
80.1	49029	2.0	17.9	4.8	0.6759	5.2	0.0880	1.8	0.35	543.4	9.4	524.3	21.1	441.5	107.4	543.4	9.4
18.4	8941	0.7	18.5	15.3	0.6581	15.9	0.0885	4.5	0.28	546.4	23.8	513.5	64.3	369.5	345.7	546.4	23.8
20.6	9105	0.9	18.1	21.8	0.6727	23.4	0.0885	8.3	0.36	546.6	43.7	522.3	95.7	417.7	492.6	546.6	43.7
174.4	75676	2.6	17.3	2.1	0.7081	2.2	0.0886	0.7	0.33	547.3	3.9	543.6	9.5	528.1	46.6	547.3	3.9

Appendix A: Cont. U/Pb detrital zircon geochronologic analyses by Laser-Ablation Multicollector ICP Mass Spectrometry

					Isotope ratios					Apparent ages (Ma)							
U (ppm)	206Pb 204Pb	U/Th	206Pb* 207Pb*	± (%)	207Pb* 235U*	± (%)	206Pb* 238U	± (%)	error corr.	206Pb* 238U*	± (Ma)	207Pb* 235U	± (Ma)	206Pb* 207Pb*	± (Ma)	**Best age (Ma)**	**± (Ma)**
SAL 1966 96-36-4 Cont.																	
302.2	57949	5.0	16.9	1.1	0.7271	2.2	0.0890	1.8	0.85	549.5	9.7	554.8	9.2	576.8	24.5	549.5	9.7
139.6	86420	2.5	17.1	2.8	0.7178	3.3	0.0890	1.8	0.54	549.6	9.4	549.3	14.0	548.5	60.3	549.6	9.4
616.6	687881	4.6	17.1	0.7	0.7189	1.4	0.0892	1.2	0.85	550.8	6.1	550.0	5.8	546.7	15.8	550.8	6.1
86.6	35387	2.4	16.8	3.8	0.7352	5.2	0.0894	3.6	0.69	551.8	19.0	559.6	22.5	591.4	82.3	551.8	19.0
40.4	20453	2.3	18.0	9.2	0.6850	9.8	0.0895	3.1	0.32	552.7	16.7	529.8	40.3	432.2	206.2	552.7	16.7
397.7	114911	1.1	17.1	0.6	0.7227	1.2	0.0896	1.0	0.86	553.1	5.3	552.3	4.9	548.8	12.8	553.1	5.3
268.3	14210	3.1	16.6	2.0	0.7472	2.5	0.0897	1.5	0.61	553.9	8.1	566.6	10.9	617.6	43.3	553.9	8.1
227.9	195704	57.1	17.2	1.5	0.7199	1.8	0.0898	0.9	0.49	554.2	4.6	550.6	7.6	535.6	33.9	554.2	4.6
128.2	43788	1.9	16.9	1.0	0.7376	1.4	0.0906	1.0	0.70	559.0	5.1	561.0	5.8	569.2	20.9	559.0	5.1
174.1	91452	0.6	16.8	2.2	0.7457	2.5	0.0908	1.2	0.48	560.4	6.5	565.7	11.0	587.3	48.2	560.4	6.5
266.9	636106	17.9	16.8	1.1	0.7448	1.4	0.0910	0.8	0.59	561.6	4.3	565.2	5.9	579.9	23.7	561.6	4.3
122.2	53320	2.1	17.1	1.8	0.7341	2.5	0.0912	1.8	0.71	562.4	9.8	559.0	10.9	545.0	38.9	562.4	9.8
76.5	38901	1.1	17.0	3.6	0.7399	4.2	0.0913	2.3	0.54	563.3	12.2	562.3	18.2	558.5	77.5	563.3	12.2
296.2	122541	1.4	17.0	1.8	0.7414	3.1	0.0915	2.5	0.82	564.2	13.7	563.2	13.4	559.2	38.7	564.2	13.7
21.5	14031	0.6	16.8	8.9	0.7545	9.6	0.0919	3.5	0.37	566.6	19.2	570.8	41.9	587.7	193.7	566.6	19.2
341.1	12289	55.5	16.7	1.4	0.7612	1.8	0.0920	1.2	0.66	567.5	6.5	574.7	8.0	603.6	29.6	567.5	6.5
159.8	72983	2.1	16.6	2.7	0.7669	3.3	0.0924	1.8	0.56	569.7	10.0	578.0	14.5	610.9	59.0	569.7	10.0
34.1	25856	0.8	17.4	7.8	0.7358	8.2	0.0927	2.4	0.29	571.7	13.2	560.0	35.4	512.7	172.7	571.7	13.2
748.5	239846	56.7	16.9	0.5	0.7642	0.9	0.0934	0.7	0.80	575.8	3.7	576.4	3.7	579.0	11.1	575.8	3.7
43.5	16645	0.4	17.5	8.1	0.7362	8.3	0.0936	1.8	0.21	576.7	9.8	560.2	35.8	493.7	179.2	576.7	9.8
199.0	280772	1.0	16.8	1.5	0.7686	1.8	0.0939	1.1	0.60	578.3	6.1	578.9	8.1	581.5	31.8	578.3	6.1
47.4	26113	0.3	16.5	6.1	0.7908	6.8	0.0949	2.9	0.43	584.2	16.1	591.6	30.4	620.2	132.3	584.2	16.1
58.4	31377	17.8	17.2	5.0	0.7626	5.2	0.0953	1.6	0.31	587.0	9.1	575.5	23.0	530.1	109.0	587.0	9.1

Appendix A: Cont. U/Pb detrital zircon geochronologic analyses by Laser-Ablation Multicollector ICP Mass Spectrometry

					Isotope ratios					Apparent ages (Ma)							
U (ppm)	206Pb 204Pb	U/Th	206Pb* 207Pb*	± (%)	207Pb* 235U*	± (%)	206Pb* 238U	± (%)	error corr.	206Pb* 238U*	± (Ma)	207Pb* 235U	± (Ma)	206Pb* 207Pb*	± (Ma)	**Best age** (Ma)	± (Ma)
SAL 1966 96-36-4 Cont.																	
394.7	203468	6.1	16.6	1.2	0.7939	2.6	0.0957	2.3	0.89	589.1	12.7	593.4	11.5	609.6	25.6	589.1	12.7
193.8	18558	4.5	15.5	12.7	0.8579	13.3	0.0963	4.0	0.30	592.5	22.6	629.0	62.6	762.4	269.0	592.5	22.6
368.0	396129	15.3	16.7	1.2	0.7964	1.4	0.0965	0.7	0.50	593.7	4.1	594.8	6.5	598.9	27.0	593.7	4.1
216.1	70166	1.1	16.6	1.7	0.8054	1.8	0.0971	0.7	0.37	597.4	3.9	599.9	8.3	609.3	36.8	597.4	3.9
106.3	55891	0.7	16.8	3.2	0.7994	3.8	0.0972	2.0	0.53	597.7	11.4	596.5	17.0	591.8	69.4	597.7	11.4
110.7	308698	1.3	16.6	2.1	0.8145	2.9	0.0984	2.0	0.69	604.7	11.7	605.0	13.4	605.9	46.1	604.7	11.7
213.7	166266	3.8	16.6	1.2	0.8203	1.5	0.0989	1.0	0.64	608.1	5.6	608.2	7.0	608.6	25.4	608.1	5.6
196.7	160004	2.9	16.1	1.5	0.8596	1.9	0.1005	1.3	0.65	617.5	7.4	629.9	9.1	674.5	31.6	617.5	7.4
218.7	115494	4.7	16.6	1.8	0.8394	4.8	0.1011	4.5	0.93	620.8	26.3	618.8	22.2	611.5	38.7	620.8	26.3
232.6	310887	0.9	16.3	0.8	0.8594	2.8	0.1017	2.7	0.96	624.5	16.1	629.8	13.2	648.8	16.6	624.5	16.1
207.4	139714	0.9	16.4	2.5	0.8687	2.7	0.1033	1.0	0.36	633.7	5.9	634.9	12.9	638.8	54.7	633.7	5.9
49.5	35725	1.2	16.1	8.9	0.9145	9.1	0.1071	1.6	0.18	655.8	10.1	659.4	44.1	671.9	191.5	655.8	10.1
277.5	145210	3.6	16.4	1.3	0.9160	2.0	0.1089	1.6	0.78	666.6	10.0	660.2	9.8	638.5	27.2	666.6	10.0
289.3	179062	3.4	16.2	1.2	0.9459	1.6	0.1109	1.1	0.69	678.2	7.3	676.0	8.1	668.5	25.2	678.2	7.3
236.4	39576	2.8	15.5	1.8	1.0241	3.2	0.1151	2.7	0.83	702.3	17.8	716.0	16.6	758.9	38.2	702.3	17.8
177.2	57512	5.7	15.4	2.3	1.0282	4.6	0.1151	4.0	0.87	702.4	26.8	718.0	23.9	767.2	48.9	702.4	26.8
73.4	38194	1.6	15.9	3.9	1.0128	4.3	0.1170	1.8	0.42	713.0	12.0	710.3	21.8	701.7	82.5	713.0	12.0
193.0	159905	1.1	14.9	0.8	1.1881	1.5	0.1284	1.3	0.83	778.7	9.4	795.1	8.5	841.3	17.7	778.7	9.4
218.0	168644	2.2	14.6	0.9	1.2270	3.2	0.1302	3.1	0.96	789.3	23.0	813.0	17.9	878.4	17.7	789.3	23.0
92.5	83594	1.0	15.3	3.2	1.1736	3.6	0.1304	1.5	0.42	790.3	11.2	788.4	19.5	782.7	67.7	790.3	11.2
369.8	13093	5.3	14.2	2.8	1.3651	3.3	0.1403	1.7	0.52	846.6	13.6	874.1	19.4	944.3	58.0	846.6	13.6
244.1	101251	4.0	14.4	1.7	1.3499	2.2	0.1415	1.5	0.66	852.9	11.7	867.5	12.9	904.9	34.2	852.9	11.7
264.4	249920	1.8	14.5	0.5	1.3570	2.9	0.1424	2.9	0.99	858.3	23.0	870.6	17.0	902.0	10.2	858.3	23.0

Appendix A: Cont. U/Pb detrital zircon geochronologic analyses by Laser-Ablation Multicollector ICP Mass Spectrometry

					Isotope ratios					Apparent ages (Ma)							
U (ppm)	206Pb 204Pb	U/Th	206Pb* 207Pb*	± (%)	207Pb* 235U*	± (%)	206Pb* 238U	± (%)	error corr.	206Pb* 238U*	± (Ma)	207Pb* 235U	± (Ma)	206Pb* 207Pb*	± (Ma)	**Best age** (Ma)	± (Ma)
SAL 1966 96-36-4 Cont.																	
125.6	109479	0.3	14.4	1.5	1.3689	4.4	0.1434	4.1	0.94	864.1	33.5	875.7	25.8	905.1	31.0	864.1	33.5
281.7	30309	2.7	14.6	1.2	1.4170	4.9	0.1503	4.7	0.97	902.5	39.7	896.1	28.9	880.3	24.3	902.5	39.7
285.7	231387	2.3	14.0	0.6	1.5535	1.8	0.1574	1.7	0.94	942.3	14.5	951.9	10.9	974.1	12.5	974.1	12.5
135.3	103516	2.3	13.9	1.6	1.5371	2.3	0.1551	1.6	0.70	929.6	13.6	945.4	13.9	982.2	32.9	982.2	32.9
128.9	83733	2.7	13.9	2.2	1.3855	6.0	0.1395	5.6	0.93	842.0	43.9	882.8	35.3	986.4	45.2	986.4	45.2
178.0	360333	4.0	13.8	1.1	1.6198	1.6	0.1616	1.2	0.76	965.5	11.0	977.9	10.2	1005.8	21.7	1005.8	21.7
514.9	8011	4.6	13.6	2.2	1.5023	5.1	0.1485	4.7	0.91	892.7	39.0	931.3	31.4	1023.9	43.5	1023.9	43.5
39.2	30732	1.6	13.6	3.0	1.7904	4.3	0.1764	3.1	0.73	1047.5	30.2	1042.0	28.0	1030.4	59.8	1030.4	59.8
219.9	32195	2.0	13.5	0.8	1.7312	1.3	0.1701	1.1	0.82	1012.6	10.3	1020.2	8.7	1036.5	15.6	1036.5	15.6
112.8	123739	2.5	13.4	2.0	1.7414	2.7	0.1696	1.9	0.69	1010.2	17.5	1024.0	17.5	1053.7	39.5	1053.7	39.5
171.2	226114	4.6	13.4	1.3	1.6179	2.2	0.1574	1.8	0.80	942.4	15.4	977.2	13.7	1056.2	26.0	1056.2	26.0
127.5	129721	1.2	13.4	0.9	1.8263	3.7	0.1776	3.5	0.97	1053.7	34.4	1054.9	24.0	1057.6	18.6	1057.6	18.6
65.4	46091	1.7	13.4	2.0	1.8510	2.9	0.1796	2.1	0.73	1065.0	20.5	1063.8	18.9	1061.5	39.5	1061.5	39.5
62.4	46100	1.2	13.2	2.1	1.8627	2.9	0.1783	2.0	0.70	1057.8	19.6	1067.9	19.0	1088.7	41.5	1088.7	41.5
54.3	4828	1.9	13.2	3.3	1.8242	5.5	0.1743	4.4	0.80	1035.5	42.4	1054.2	36.3	1093.0	66.4	1093.0	66.4
386.6	90168	2.1	13.1	0.3	1.9530	1.3	0.1856	1.3	0.98	1097.3	12.7	1099.5	8.7	1103.8	5.7	1103.8	5.7
128.1	114692	1.6	13.1	0.4	1.9476	3.6	0.1843	3.6	0.99	1090.7	35.7	1097.6	24.0	1111.4	8.3	1111.4	8.3
152.1	189080	1.4	12.3	0.8	2.3549	3.4	0.2107	3.3	0.97	1232.4	37.4	1229.0	24.4	1223.2	15.6	1223.2	15.6
86.8	79886	1.5	12.2	1.6	2.3763	3.1	0.2110	2.7	0.87	1234.1	30.4	1235.5	22.3	1237.9	30.5	1237.9	30.5
125.6	124347	1.7	12.2	1.0	2.3340	4.1	0.2068	4.0	0.97	1211.9	43.9	1222.7	29.0	1241.8	18.8	1241.8	18.8
371.4	492388	1.5	10.2	0.2	3.7956	1.8	0.2805	1.7	1.00	1594.1	24.7	1591.8	14.1	1588.8	3.3	1588.8	3.3
269.4	66181	0.9	9.6	0.2	4.1945	1.9	0.2912	1.9	1.00	1647.6	27.7	1672.9	15.7	1704.8	3.4	1704.8	3.4
129.7	186291	0.7	9.2	0.4	4.3331	1.8	0.2879	1.8	0.97	1630.8	25.7	1699.7	15.2	1785.7	7.9	1785.7	7.9

Appendix A: Cont. U/Pb detrital zircon geochronologic analyses by Laser-Ablation Multicollector ICP Mass Spectrometry

					Isotope ratios					Apparent ages (Ma)							
U (ppm)	206Pb 204Pb	U/Th	206Pb* 207Pb*	± (%)	207Pb* 235U*	± (%)	206Pb* 238U	± (%)	error corr.	206Pb* 238U*	± (Ma)	207Pb* 235U	± (Ma)	206Pb* 207Pb*	± (Ma)	**Best age** (Ma)	**±** (Ma)
SAL 1966 96-36-4 Cont.																	
75.3	46417	1.2	8.7	0.5	4.4538	1.9	0.2816	1.8	0.96	1599.3	25.5	1722.4	15.6	1875.5	9.6	1875.5	9.6
176.3	19216	1.0	7.7	0.3	6.4612	1.2	0.3611	1.2	0.96	1987.6	20.3	2040.6	10.8	2094.7	5.8	2094.7	5.8
142.6	279175	1.2	5.4	0.3	12.8992	1.2	0.5059	1.2	0.97	2639.1	25.8	2672.3	11.6	2697.5	5.1	2697.5	5.1
51.9	173838	2.2	4.1	0.4	20.7164	4.5	0.6227	4.5	1.00	3120.5	110.5	3125.4	43.5	3128.6	6.5	3128.6	6.5

Appendix B: U/Pb and (U-Th)/He age data for selected zircons in East and West Antarctica *=analyses from *Schilling* [2010].

Sample number	Site Name	Th/U (atomic)	U (ppm)	Th (ppm)	eU (ppm)	ZHe Age Pick (Ma)	Upper Error (Ma)	Lower Error (Ma)	U/Pb age (Ma)	Error (Ma)	Th/U from U/Pb	Shape
1611-5	AG	0.33	298.58	97.33	321.46	462.59	44.45	44.45	565.42	5.00	0.32	Irregular
1611-34	AG	0.22	234.95	51.31	247.01	162.28	16.35	16.35	566.74	25.79	0.28	Irregular
1611-6	AG	0.11	309.55	31.88	317.04	419.29	41.18	41.18	565.41	10.73	0.01	Irregular
1611-31	AG	0.12	49.73	5.63	51.05	356.36	35.78	35.78	557.92	15.62	0.01	Irregular
1611-51	AG	0.32	194.29	60.00	208.39	178.40	20.28	20.28	565.37	4.42	0.42	Irregular
1654-2*	BG	0.51	193.12	95.26	215.51	175.58	51.13	25.57	530.32	5.80	0.49	Irregular
1654-10*	BG	0.73	206.28	147.68	240.99	154.33	40.12	20.06	246.50	6.36	0.58	Irregular
1654-12*	BG	0.72	79.09	55.24	92.07	146.44	6.48	36.89	595.08	5.06	0.80	Euhedral
1654-4	BG	0.27	462.84	124.05	492.00	140.41	22.34	22.34	479.06	31.30	0.41	Irregular
1654-17	BG	0.11	306.30	33.55	314.18	144.07	16.88	16.88	568.32	24.81	0.09	Irregular
1776-16	BIS	0.57	29.03	16.06	32.81	95.15	12.14	12.14	579.81	6.71	0.55	Irregular
1775-22	BIS	0.94	40.92	37.34	49.70	181.17	21.54	21.54	571.02	5.46	1.11	Irregular
1776-33	BIS	0.38	196.94	73.64	214.24	230.40	25.96	25.96	466.07	8.45	0.39	Irregular
1776-2	BIS	0.37	141.89	51.34	153.95	296.46	56.63	56.63	534.30	17.49	0.50	Irregular
BN-35	BN	0.34	127.10	41.70	136.89	322.76	37.88	37.88	574.88	20.70	1.00	Irregular
BN-46	BN	0.71	116.15	79.85	134.92	157.71	22.32	22.32	577.66	22.58	1.84	Irregular
BN-61	BN	0.90	67.91	59.88	81.98	185.57	20.00	20.00	560.15	9.27	1.04	Irregular
BN-81	BN	0.96	295.43	276.99	360.52	152.67	30.64	30.64	579.21	18.89	1.76	Irregular
BR-2	BN rock	0.75	213.65	156.59	250.44	143.56	16.19	16.19	517.60	16.88	0.94	Irregular
BR-7	BN rock	0.55	7335.89	3952.59	8264.75	176.93	26.19	26.19	555.65	9.35	0.48	Irregular
1694-3*	DN	0.24	257.03	61.20	271.41	168.13	3.02	30.07	589.30	4.56	0.60	Euhedral
1694-9*	DN	0.55	316.72	170.32	356.74	160.90	28.75	14.38	524.24	7.05	0.51	Irregular
1694-14*	DN	0.40	417.63	163.93	456.16	169.97	2.87	32.90	257.78	1.49	0.34	Euhedral

Appendix B: Cont. U/Pb and (U-Th)/He age data for selected zircons in East and West Antarctica *=analyses from *Schilling* [2010].

Sample number	Site Name	Th/U (atomic)	U (ppm)	Th (ppm)	eU (ppm)	ZHe Age Pick (Ma)	Upper Error (Ma)	Lower Error (Ma)	U/Pb age (Ma)	Error (Ma)	Th/U from U/Pb	Shape
1694-18*	DN	0.55	263.34	142.31	296.79	145.27	48.26	24.13	1056.84	96.90	0.71	Irregular
1694-23*	DN	0.40	220.70	85.20	240.72	170.12	43.56	21.78	528.64	4.62	0.31	Irregular
1695-3	DN	0.89	128.90	112.13	155.25	127.83	16.36	16.36	600.93	5.82	0.80	Irregular
1695-109	DN	0.69	15.09	10.14	17.48	154.77	18.04	18.04	560.47	15.56	0.37	Irregular
1700-1	KH	0.66	93.08	59.96	107.17	175.92	23.71	23.71	521.50	3.01	0.17	Irregular
1700-44	KH	0.25	231.87	56.24	245.09	155.39	20.01	20.01	545.47	10.57	0.32	Irregular
1700-45	KH	0.18	350.23	61.80	364.75	155.04	15.00	15.00	534.48	3.44	0.33	Irregular
1771-19*	KIS	0.48	261.64	121.87	290.28	240.49	4.22	39.60	511.95	9.10	0.55	Euhedral
1771-30*	KIS	0.30	203.85	59.77	217.90	352.34	80.94	40.47	1099.77	68.25	0.26	Irregular
1771-66*	KIS	0.08	220.63	17.27	224.69	314.69	6.53	57.44	1022.34	38.88	0.12	Euhedral
1772-19*	KIS	0.62	164.23	99.38	187.59	160.35	31.17	15.58	488.49	13.69	0.48	Irregular
1772-37*	KIS	0.41	139.81	55.36	152.82	118.96	22.79	11.40	558.34	5.40	0.41	Irregular
1773-5*	KIS	0.28	240.82	65.63	256.24	183.24	46.94	23.47	1114.95	22.80	0.35	Irregular
1773-102	KIS	0.28	285.27	79.21	303.88	183.92	21.47	21.47	513.41	5.53	0.39	Irregular
1773-10	KIS	0.24	158.24	36.66	166.86	157.58	21.13	21.13	728.85	18.26	0.03	Irregular
1773-98	KIS	0.61	189.56	112.94	216.10	262.84	35.56	35.56	520.10	13.84	0.37	Irregular
1773-60	KIS	0.38	108.65	40.41	118.14	322.94	6.15	6.15	497.86	5.32	0.40	Euhedral
1773-48	KIS	0.17	427.05	69.86	443.46	178.72	37.92	37.92	498.55	6.43	0.01	Irregular
1771-27	KIS	0.74	142.87	103.36	167.16	145.42	21.45	21.45	544.65	23.45	1.23	Irregular
1771-133	KIS	0.18	196.18	34.70	204.33	189.70	3.62	3.62	506.87	17.35	0.16	Euhedral
1771-105	KIS	0.47	138.78	63.17	153.63	219.35	24.95	24.95	551.84	6.61	0.47	Irregular
1583-2	LW	0.28	137.80	38.11	146.75	160.00	16.47	16.47	590.98	6.03	0.18	Irregular
1583-7	LW	3.55	25.88	89.56	46.92	376.82	36.11	36.11	547.61	13.88	2.37	Irregular

Appendix B: Cont. U/Pb and (U-Th)/He age data for selected zircons in East and West Antarctica *=analyses from *Schilling* [2010].

Sample number	Site Name	Th/U (atomic)	U (ppm)	Th (ppm)	eU (ppm)	ZHe Age Pick (Ma)	Upper Error (Ma)	Lower Error (Ma)	U/Pb age (Ma)	Error (Ma)	Th/U from U/Pb	Shape
1583-8	LW	0.37	212.50	77.68	230.76	147.25	17.92	17.92	554.52	18.96	0.45	Irregular
1583-9	LW	0.78	143.39	108.79	168.96	487.04	43.67	43.67	606.44	22.18	0.85	Irregular
1583-10	LW	0.46	196.19	87.40	216.73	155.34	15.07	15.07	532.80	2.91	0.71	Irregular
1583-11	LW	0.57	48.42	27.12	54.79	219.24	23.16	23.16	547.49	15.75	0.75	Irregular
1583-15	LW	0.92	135.51	121.61	164.09	532.18	60.65	60.65	561.13	5.80	0.76	Irregular
1583-17	LW	0.49	141.79	67.78	157.71	345.36	35.73	35.73	574.90	5.98	0.84	Irregular
1940-12	MA	1.34	69.89	91.59	91.42	183.58	17.77	17.77	562.68	14.57	1.18	Irregular
1940-21	MA	0.87	152.33	129.25	182.70	139.62	16.27	16.27	581.82	3.01	0.87	Irregular
1942-36	MA	0.65	240.48	151.35	276.05	169.09	16.86	16.86	595.34	7.29	0.90	Irregular
1942-53	MA	0.44	118.63	50.32	130.46	170.77	21.15	21.15	593.32	16.47	1.02	Irregular
1942-66	MA	0.27	676.34	176.33	717.78	159.05	16.52	16.52	596.33	5.77	0.37	Irregular
MA3B1-3	MA rock	0.19	302.76	57.43	316.25	156.47	14.93	14.93	537.67	4.45	0.04	Irregular
MA3B1-34	MA rock	0.82	121.85	97.31	144.72	157.83	15.97	15.97	585.02	21.27	0.41	Irregular
MA3B1-105	MA rock	0.31	46.72	13.95	50.00	131.14	12.11	12.11	583.29	27.95	1.28	Irregular
MA3B1-120	MA rock	0.32	101.43	32.07	108.96	169.88	16.45	16.45	585.89	4.57	0.52	Irregular
1690-7*	MH	2.04	149.19	296.49	218.87	161.40	51.15	25.58	559.56	5.04	2.17	Irregular
1690-17*	MH	0.39	116.77	44.51	127.23	164.18	32.10	16.05	488.20	7.15	0.57	Irregular
1690-20*	MH	0.29	279.06	78.12	297.42	145.86	46.62	23.31	967.61	5.93	0.42	Irregular
1691-2*	MH	0.85	103.94	85.96	124.14	153.19	3.69	33.36	275.83	3.02	0.62	Euhedral
1691-6*	MH	0.23	214.64	47.67	225.84	140.08	33.57	16.78	534.73	4.46	0.61	Irregular
1691-13*	MH	0.32	978.76	307.16	1050.94	147.12	41.24	20.62	599.55	6.76	0.17	Irregular
1945-13	MH	1.11	28.11	30.36	35.24	168.06	16.34	16.34	555.23	9.49	0.81	Irregular
1946-7	MH	0.51	162.78	81.30	181.88	143.81	17.70	17.70	496.93	4.35	0.39	Irregular

Appendix B: Cont. U/Pb and (U-Th)/He age data for selected zircons in East and West Antarctica *=analyses from *Schilling* [2010].

Sample number	Site Name	Th/U (atomic)	U (ppm)	Th (ppm)	eU (ppm)	ZHe Age Pick (Ma)	Upper Error (Ma)	Lower Error (Ma)	U/Pb age (Ma)	Error (Ma)	Th/U from U/Pb	Shape
1690-23	MH	0.35	416.93	142.19	450.34	115.09	14.87	14.87	489.85	5.38	0.34	Irregular
1690-7	MH	1.11	92.20	99.63	115.61	132.75	18.94	18.94	1186.25	56.92	1.62	Irregular
1690-84	MH	0.35	237.57	80.65	256.53	144.73	22.45	22.45	560.35	16.10	1.58	Irregular
1905-14	MH	0.10	285.67	26.52	291.90	151.79	16.91	16.91	597.55	8.74	0.58	Irregular
1905-13	MH	0.39	277.69	105.67	302.52	153.54	16.15	16.15	3110.50	8.13	0.66	Irregular
1906-36	MH	0.91	17.08	15.07	20.62	176.60	18.75	18.75	563.39	4.71	0.08	Irregular
1907-37	MH	0.55	94.41	51.03	106.40	163.49	20.90	20.90	561.84	9.12	0.29	Irregular
1907-41	MH	0.89	64.02	55.46	77.05	134.27	22.67	22.67	564.52	4.45	0.58	Irregular
1911-23	MH	0.62	135.18	81.93	154.43	168.55	16.72	16.72	583.90	5.65	0.76	Irregular
1911-37	MH	0.87	75.94	64.62	91.12	146.93	16.78	16.78	531.15	21.30	0.06	Irregular
MH6B-4	MH	1.05	104.16	106.78	129.25	140.14	18.20	18.20	569.83	7.97	1.20	Irregular
MH106-41	MH rock	0.42	53.76	22.07	58.95	151.69	11.73	11.73	554.85	41.02	0.21	Irregular
MH106-88	MH rock	0.70	210.37	143.77	244.15	125.92	12.19	12.19	530.04	13.43	0.93	Irregular
MH106-126	MH rock	0.35	251.06	84.60	270.94	151.56	23.29	23.29	548.42	8.96	0.05	Irregular
1616-24	MR	0.03	551.99	18.05	556.23	354.77	30.09	30.09	558.33	12.64	0.03	Irregular
1616-60	MR	1.49	38.40	55.79	51.51	375.02	33.39	33.39	574.89	12.53	1.47	Irregular
1616-73	MR	0.57	26.19	14.54	29.61	450.95	39.73	39.73	556.60	4.68	0.65	Irregular
1616-2	MR	0.38	237.66	88.88	258.55	380.45	32.97	32.97	590.72	5.62	0.28	Irregular
1616-4	MR	0.67	80.00	52.45	92.33	449.17	41.25	41.25	581.27	10.02	0.89	Irregular
1616-6	MR	0.23	89.93	19.77	94.58	371.26	46.67	46.67	593.95	20.70	0.25	Irregular
1616-7	MR	1.05	245.77	252.42	305.09	267.30	34.27	34.27	595.14	5.27	0.36	Irregular
1616-9	MR	0.73	34.69	24.59	40.47	124.96	12.29	12.29	564.02	12.92	0.61	Irregular
1616-10	MR	0.12	1316.08	156.42	1352.84	74.39	6.59	6.59	559.98	3.16	0.02	Irregular

Appendix B: Cont. U/Pb and (U-Th)/He age data for selected zircons in East and West Antarctica *=analyses from *Schilling* [2010].

Sample number	Site Name	Th/U (atomic)	U (ppm)	Th (ppm)	eU (ppm)	ZHe Age Pick (Ma)	Upper Error (Ma)	Lower Error (Ma)	U/Pb age (Ma)	Error (Ma)	Th/U from U/Pb	Shape
1616-20	MR	0.62	40.77	24.67	46.57	323.17	35.69	35.69	568.83	5.26	0.63	Irregular
1616-63	MR	0.25	166.07	40.52	175.59	403.06	40.35	40.35	612.80	59.12	0.25	Irregular
1616-69	MR	2.49	15.67	38.09	24.62	448.78	37.90	37.90	578.55	12.31	1.93	Irregular
1616-70	MR	0.32	255.06	79.03	273.63	640.28	80.39	80.39	601.60	3.04	0.25	Irregular
1616-72	MR	0.18	199.79	34.42	207.88	717.47	149.18	149.18	538.50	3.79	0.01	Irregular
1616-74	MR	0.20	234.06	46.71	245.03	441.21	36.62	36.62	614.04	5.69	0.18	Irregular
1660-6*	SN	0.52	315.54	159.37	352.99	336.85	6.97	70.09	1033.96	42.65	0.56	Euhedral
1659-2	SN	0.44	244.77	104.72	269.38	328.68	62.23	62.23	550.12	5.27	0.13	Irregular
1659-13	SN	0.69	90.47	61.03	104.81	308.03	43.99	43.99	530.62	3.77	0.56	Irregular
1659-38	SN	0.59	118.92	68.14	134.93	292.38	41.98	41.98	534.91	2.57	0.45	Irregular
1659-73	SN	0.15	536.74	79.18	555.35	250.07	40.08	40.08	1057.15	51.56	0.14	Irregular
1744-20*	WIS	0.21	214.24	44.37	224.67	76.29	17.89	8.94	528.08	19.57	0.43	Irregular
1744-21*	WIS	0.08	288.50	23.04	293.91	335.25	118.81	59.41	1035.68	75.98	0.21	Irregular
1744-26*	WIS	0.34	219.05	72.56	236.11	199.09	60.61	30.30	580.39	38.91	0.67	Irregular
1744-35*	WIS	0.24	443.87	102.79	468.02	98.42	29.40	14.70	1048.38	74.02	0.34	Irregular
1755-41*	WIS	0.20	545.39	105.24	570.12	157.13	2.78	35.84	1010.02	62.09	0.77	Euhedral
1755-44*	WIS	1.28	277.79	347.80	359.52	271.58	59.40	29.70	536.74	13.44	0.97	Irregular
1755-63	WIS	0.63	77.16	47.59	88.34	164.05	33.92	33.92	507.62	11.23	0.63	Irregular
1755-54	WIS	0.69	116.29	78.52	134.74	339.23	36.79	36.79	507.35	16.10	0.74	Irregular

Appendix C: $^{40}Ar/^{39}Ar$ age data for selected samples. The ‘internal ± age' is from the error on the mass spectrometer, and the 'total ± age' is the 1 sigma error taking into account the error on the J value which was used in creating the ^{39}Ar.

Sample	Run ID	Ca/K	Cl/K	Mol 39Ar	%40Ar*	Age (Ma)	Internal ± Age	Total ± Age
SAL 1755 WIS								
1755 hb	14655-05A	15.89206	0.03216	0.013	55.8	468.52	3.83	6.05
1755 hb	14655-07A	11.31193	0.08621	0.005	84	471.67	3.62	5.94
1755 hb	14655-02A	10.91837	0.07417	0.007	95.5	477.04	3.14	5.71
1755 hb	14655-06A	11.64332	0.04089	0.007	90.2	479.33	2.58	5.44
1755 hb	14655-03A	9.51529	0.06725	0.01	97.1	484.92	2.40	5.41
1755 hb	14655-01A	6.82191	0.02941	0.075	98.7	484.99	0.97	4.95
1755 hb	14655-13A	9.37619	0.02402	0.014	98.2	486.75	2.09	5.30
1755 hb	14655-08A	9.30206	0.04515	0.008	88.2	493.02	2.67	5.61
1755 hb	14655-12A	12.7074	0.06145	0.012	94.3	493.63	2.22	5.41
SAL 1579 LW-Bt								
1579 hb	14656-17A	15.18412	-0.03452	0.001	66.5	489.54	10.29	11.39
1579 hb	14656-12A	31.38183	0.04069	0.007	94.1	529.17	3.16	6.17
1579 hb	14656-20A	6.18215	0.01679	0.012	97.4	595.06	2.65	6.52
1579 hb	14656-06A	11.41902	0.11708	0.008	99	719.41	3.33	7.93
1579 hb	14656-09A	7.24814	0.05084	0.007	98.8	1222.34	6.61	13.90
1579 hb	14656-11A	10.20847	0.02781	0.012	79.7	1288.26	5.34	13.94
1579 hb	14656-23A	7.79101	0.12024	0.008	96.1	1386.19	6.54	15.33
1579 hb	14656-18A	5.30238	0.07434	0.014	97.1	1438.22	4.79	15.16
1579 hb	14656-24A	12.11975	0.09885	0.004	97.8	1515.73	10.76	18.59
SAL 1614 MR-At								
1614 hb	14657-12A	7.42332	0.02587	0.022	92.3	492.44	1.77	5.23
1614 hb	14657-19A	9.1978	0.0667	0.013	93.7	507.92	2.35	5.60
1614 hb	14657-27A	10.92619	0.09149	0.01	97.2	510.12	2.32	5.60
1614 hb	14657-10A	13.47111	0.02796	0.022	92.9	510.90	1.89	5.45
1614 hb	14657-07A	8.1271	0.06897	0.012	98.9	511.28	2.25	5.59
1614 hb	14657-22A	18.95553	0.0905	0.006	79	513.12	3.97	6.49
1614 hb	14657-11A	8.64333	0.05172	0.022	98.6	516.73	1.65	5.42

Appendix C: Cont. $^{40}Ar/^{39}Ar$ age data for selected samples.

Sample	Run ID	Ca/K	Cl/K	Mol 39Ar	%40Ar*	Age (Ma)	Internal ± Age	Total ± Age
SAL 1614 MR-At								
1614 hb	14657-01A	14.72744	0.07402	0.009	96.2	519.24	2.47	5.75
1614 hb	14657-02A	35.70892	0.03492	0.011	96.5	519.84	2.59	5.81
1614 hb	14657-08A	10.22521	0.03048	0.026	98.8	521.25	1.58	5.45
1614 hb	14657-23A	7.21942	0.06135	0.032	95.1	521.91	1.56	5.45
1614 hb	14657-14A	11.18951	0.0286	0.007	93.4	534.09	3.18	6.22
1614 hb	14657-03A	9.18432	0.02117	0.012	97.6	534.75	2.47	5.89
1614 hb	14657-26A	13.38213	0.04646	0.009	95.5	535.56	2.76	6.03
1614 hb	14657-24A	13.38799	0.10408	0.009	93.3	548.55	2.85	6.18
1614 hb	14657-05A	11.50413	0.07385	0.016	95.7	548.86	2.25	5.93
1614 hb	14657-15A	11.43833	0.14416	0.009	96.1	551.25	2.83	6.19
1614 hb	14657-09A	17.08584	0.04554	0.002	93.1	560.78	7.08	9.03
1614 hb	14657-20A	11.1941	0.08419	0.011	93.2	564.43	2.84	6.32
1614 hb	14657-16A	9.5721	0.03714	0.001	93.6	578.24	15.39	16.44
1614 hb	14657-18A	7.69594	0.10512	0.003	73.1	681.65	6.87	9.68
1614 hb	14657-06A	6.58918	0.36541	0.001	36.1	934.00	27.41	28.95
1614 hb	14657-13A	15.1229	0.09167	0.003	85.9	1046.39	9.43	14.09
1614 hb	14657-17A	17.17501	0.07131	0.008	92.9	1390.88	6.20	15.23
SAL 1611 AG-Ct								
1611 hb	14658-16A	23.45652	0.0412	0.013	97	488.47	2.06	5.30
1611 hb	14658-10A	9.15314	0.01521	0.086	99.6	512.36	1.03	5.23
1611 hb	14658-12A	27.87801	0.1655	0.017	89.4	515.90	2.22	5.61
1611 hb	14658-19A	7.33633	0.05047	0.017	96.7	516.97	1.93	5.52
1611 hb	14658-24A	10.40354	0.04385	0.025	97.3	521.50	1.66	5.47
1611 hb	14658-25A	10.38064	0.04804	0.009	86.9	532.19	2.72	5.97
1611 hb	14658-03A	11.14795	0.03312	0.042	98.1	535.71	1.27	5.51
1611 hb	14658-01A	10.89719	0.01736	0.085	98.4	543.62	1.09	5.54
1611 hb	14658-11A	9.96997	0.02764	0.024	94.6	546.67	1.90	5.79
1611 hb	14658-07A	7.54146	0.0538	0.114	97.4	548.50	0.98	5.57

Appendix C: Cont. $^{40}Ar/^{39}Ar$ age data for selected samples.

Sample	Run ID	Ca/K	Cl/K	Mol 39Ar	%40Ar*	Age (Ma)	Internal ± Age	Total ± Age
SAL 1611 AG-Ct								
1611 hb	14658-13A	10.3106	0.0396	0.045	97.3	564.98	1.34	5.81
1611 hb	14658-14A	8.49751	0.02727	0.022	96.7	569.52	1.91	6.01
1611 hb	14658-04A	6.6889	0.01717	0.136	93.3	570.91	1.17	5.83
1611 hb	14658-02A	12.17559	0.04768	0.07	96.9	575.57	1.22	5.88
1611 hb	14658-06A	9.55174	0.02919	0.055	93.9	577.79	1.36	5.93
1611 hb	14658-17A	10.4645	0.09829	0.101	97.1	590.75	1.10	6.01
1611 hb	14658-23A	9.85397	0.10839	0.006	63.4	591.12	5.00	7.74
1611 hb	14658-21A	7.71951	0.03034	0.04	98.5	594.85	1.50	6.14
1611 hb	14658-08A	7.4751	0.02637	0.026	98.6	608.64	1.76	6.34
1611 hb	14658-15A	10.69569	0.066	0.078	95.2	635.96	1.35	6.50
1611 hb	14658-09A	13.08622	0.02222	0.05	85.3	657.58	1.85	6.83
1611 hb	14658-22A	7.06551	0.05592	0.016	94.6	657.97	2.46	7.02
1611 hb	14658-26A	10.10361	0.055	0.007	93.4	735.62	4.21	8.48

Appendix D: Calculations to determine temporal variability of till ZHe ages with in the Ross/Pan-African U/Pb population (450-600 Ma). ZHe ages were subdivided based on all Ross Orogeny grains were subdivided based on 'old' (550-600 Ma) versus 'young' (460-550 Ma grains). ZHe ages were selected if their errors included ages between 115-200 Ma even if the 'age pick' age was >200 Ma or <115 Ma.

"Young grains"

ZHe age (Ma)	ZHe upper error (Ma)	ZHe lower error (Ma)	Site	U/Pb age (Ma)	U/Pb error (Ma)	ZHe age + upper error (Ma)	ZHe age - lower error (Ma)
Young' grains							
115.09	14.87	14.87	MH	489.85	5.38	129.96	100.21
143.81	17.70	17.70	MH	496.93	4.35	161.51	126.11
140.41	22.34	22.34	BG	479.06	31.30	162.75	118.07
146.93	16.78	16.78	MH	531.15	21.30	163.71	130.14
145.42	21.45	21.45	KIS	544.65	23.45	166.87	123.97
155.04	15.00	15.00	KH	534.48	3.44	170.03	140.04
155.34	15.07	15.07	LW	532.80	2.91	170.41	140.26
140.08	33.57	16.78	MH	534.73	4.46	173.64	123.29
155.39	20.01	20.01	KH	545.47	10.57	175.40	135.38
160.90	28.75	14.38	DN	524.24	7.05	189.66	146.53
160.35	31.17	15.58	KIS	488.49	13.69	191.52	144.76
189.70	3.62	3.62	KIS	506.87	17.35	193.32	186.08
164.18	32.10	16.05	MH	488.20	7.15	196.28	148.13
164.05	33.92	33.92	WIS	507.62	11.23	197.97	130.13
175.92	23.71	23.71	KH	521.50	3.01	199.63	152.21
183.92	21.47	21.47	KIS	513.41	5.53	205.39	162.45
170.12	43.56	21.78	DN	528.64	4.62	213.68	148.34
178.72	37.92	37.92	KIS	498.55	6.43	216.64	140.80
175.58	51.13	25.57	BG	530.32	5.80	226.71	150.01
219.24	23.16	23.16	LW	547.49	15.75	242.41	196.08
240.49	4.22	39.60	KIS	511.95	9.10	244.71	200.88

Mean (Ma)= 165.746
Standard Deviation (Ma)= 27.608
Median (Ma)= 160.904

Appendix D: cont.

"Old grains"

ZHe age (Ma)	ZHe upper error (Ma)	ZHe lower error (Ma)	Site	U/Pb age (Ma)	U/Pb error (Ma)	ZHe age + upper error (Ma)	ZHe age - lower error (Ma)
124.96	12.29	12.29	MR	564.02	12.92	137.25	112.67
118.96	22.79	11.40	KIS	558.34	5.40	141.76	107.57
127.83	16.36	16.36	DN	600.93	5.82	144.19	111.47
146.44	6.48	36.89	BG	595.08	5.06	152.92	109.55
139.62	16.27	16.27	MA	581.82	3.01	155.89	123.35
134.27	22.67	22.67	MH	564.52	4.45	156.94	111.60
140.14	18.20	18.20	MH	569.83	7.97	158.34	121.93
144.07	16.88	16.88	BG	568.32	24.81	160.95	127.18
147.25	17.92	17.92	LW	554.52	18.96	165.17	129.34
144.73	22.45	22.45	MH	560.35	16.10	167.17	122.28
151.79	16.91	16.91	MH	597.55	8.74	168.70	134.88
168.13	3.02	30.07	DN	589.30	4.56	171.16	138.06
154.77	18.04	18.04	DN	560.47	15.56	172.81	136.72
159.05	16.52	16.52	MA	596.33	5.77	175.57	142.53
160.00	16.47	16.47	LW	590.98	6.03	176.47	143.52
162.28	16.35	16.35	AG	566.74	25.79	178.63	145.93
157.71	22.32	22.32	BN	577.66	22.58	180.03	135.39
152.67	30.64	30.64	BN	579.21	18.89	183.30	122.03
163.49	20.90	20.90	MH	561.84	9.12	184.39	142.60
168.06	16.34	16.34	MH	555.23	9.49	184.40	151.72
168.55	16.72	16.72	MH	583.90	5.65	185.27	151.83
169.09	16.86	16.86	MA	595.34	7.29	185.96	152.23
147.12	41.24	20.62	MH	599.55	6.76	188.37	126.50
170.77	21.15	21.15	MA	593.32	16.47	191.92	149.61
176.60	18.75	18.75	MH	563.39	4.71	195.35	157.84
178.40	20.28	20.28	AG	565.37	4.42	198.68	158.12
183.58	17.77	17.77	MA	562.68	14.57	201.35	165.80
181.17	21.54	21.54	BIS	571.02	5.46	202.71	159.63
185.57	20.00	20.00	BN	560.15	9.27	205.57	165.57
161.40	51.15	25.58	MH	559.56	5.04	212.55	135.83
219.35	24.95	24.95	KIS	551.84	6.61	244.30	194.40
199.09	60.61	30.30	WIS	580.39	38.91	259.70	168.79

Mean (Ma)= 159.59
Standard Deviation (Ma)= 21.4869
Median (Ma)= 159.524

Appendix E: E-A: Geological map of the Scott Glacier region. Green circle indicate the sites selected for AFT analysis including the Fission Wall and Mount Griffith. [*Fitzgerald and Stump*, 1997]. E-B: AFT profile for Mount Griffith and the Fission Wall (modified from Stump and Fitzgerald, 1992) compared to elevation [*Fitzgerald and Stump*, 1997]. E-C: Geologic map of the Nimrod and Beardmore Glaciers from *Fitzgerald* (1994). Green circle indicates sites selected for AFT analysis in the Beardmore Glacier area. E-D: AFT profile for samples east and west of Beardmore Glacier [*Fitzgerald*, 1994]. Projected ZHe ages are based on these two sites and calculations are listed on following pages.

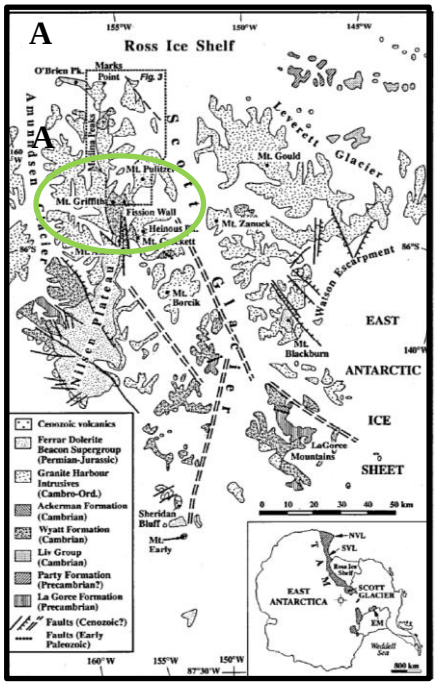

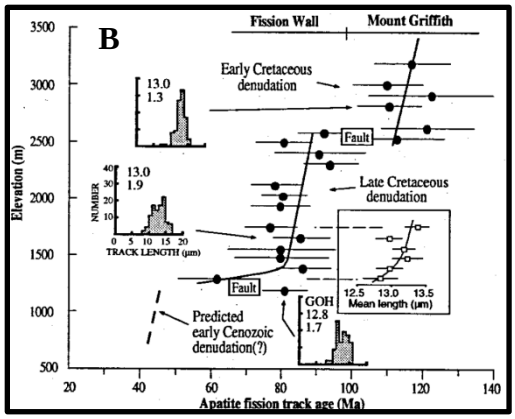

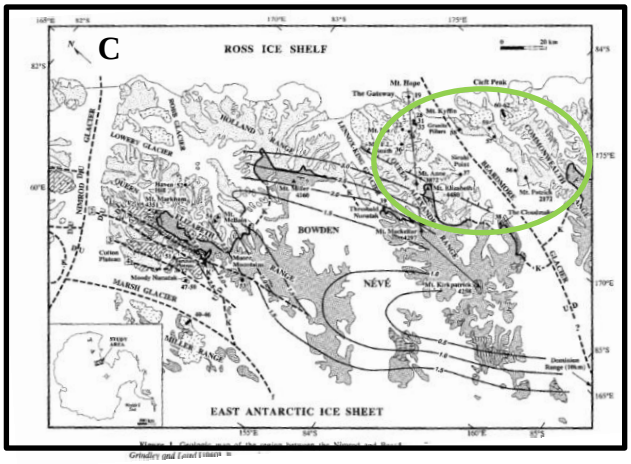

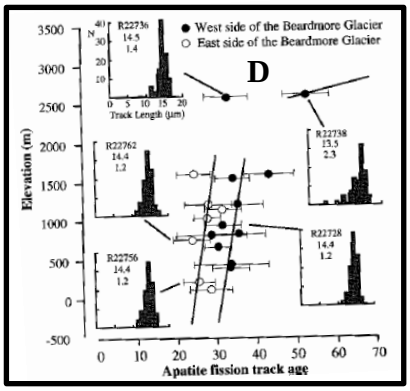

Appendix E: Cont.

1. Beardmore Glacier: West Side
    a. Slope was calculated based on AFT age versus elevation
        i. Two 'points' were chosen to derive slope
        (38 Ma, 1.75 km)
        (30 Ma, -.3 km)
        ii. Slope = (1.75-(-.3) km)/(38-30 Ma)
        =1 km/3.9 Ma
    b. If assuming minimum uplift (1.6 km)
        i. 1.6 km/ X Ma=1 km/ 3.9 Ma
            1. 1.6 km of uplift takes 6.24 Ma
            2. ZHe ages would be reset
                a. At time:
                    i. Minimum: 30 Ma+6.24 Ma= 36.24 Ma
                    Maximum: 38 Ma + 6.24 Ma = 44.24 Ma
    c. If assuming maximum uplift (4.4 km)
        i. 4.4 km/ X Ma=1 km/ 3.9 Ma
            1. 4.4 km of uplift takes 17.16 Ma
            2. ZHe ages would be reset
                a. At times:
                    i. Minimum: 30 Ma+17.16 Ma=47.16Ma
                    ii. Maximum: 38 Ma + 17.16 Ma = 55.16 Ma
    d. If ZHe ages were reset at same time as AFT, the ZHe ages would fall between 36.24-55.16 Ma
2. Beardmore Glacier: East Side
    a. Slope was calculated based on AFT age versus elevation
        i. Two 'points' were chosen to derive slope
        (30 Ma, 1.8 km)
        (24 Ma, -.3 km)
        ii. Slope = (2.6-1.4 km)/(30-24 Ma)
        =1 km/5 Ma
    b. If assuming minimum uplift (1.6 km)
        i. 1.6 km/ X Ma=1 km/ 5 Ma
            1. 1.6 km of uplift takes 8 Ma
            2. ZHe ages would be reset
                a. At times:
                    i. Minimum: 24 Ma+8 Ma=32 Ma
                    ii. Maximum: 30 Ma + 8 Ma = 38 Ma
    c. If assuming maximum uplift (4.4 km)
        i. 4.4 km/ X Ma=1 km/ 5 Ma
            1. 4.4 km of uplift takes 22 Ma
            2. ZHe ages would be reset
                a. At times:
                    i. Minimum: 24 Ma+22 Ma=46 Ma
                    ii. Maximum: 30 Ma + 22 Ma = 52 Ma
    d. If ZHe ages were reset at same time as AFT, the ZHe ages would fall between 32-52 Ma

3. AFT closure temperature: 90-120°C
   ZHe closure temperature: 160-200°C
   Assuming geothermal gradient of 25°C/km
   AFT is reset at crustal depths 3.6-4.8 km
   ZHe is reset at crustal depths 6.4-8 km
   Difference of depths range from 1.6 km (absolute minimum) to 4.4 (absolute maximum)
4. Mt. Griffith [*Fitzgerald and Stump*, 1997]
   a. Slope was calculated based on AFT age versus elevation
      i. Two 'points' were chosen to derive slope
         (120 Ma, 3.4 km)
         (116 Ma, 2.475 km)
      ii. Slope = (3.4-2.475 km)/(120-116 Ma)
         =1 km/4.32 Ma
   b. If assuming minimum uplift (1.6 km)
      i. 1.6 km/ X Ma=1 km/ 4.32 Ma
         1. 1.6 km of uplift takes 6.912 Ma
         2. ZHe ages would be reset
            a. At times:
               i. Minimum: 116 Ma+6.912 Ma=122.912 Ma
                  Maximum: 120 Ma + 6.912 Ma = 126.912 Ma
   c. If assuming maximum uplift (4.4 km)
      i. 4.4 km/ X Ma=1 km/ 4.32 Ma
         1. 4.4 km of uplift takes 19.008 Ma
         2. ZHe ages would be reset
            a. At times:
               i. Minimum: 116 Ma+19.008 Ma=135.008 Ma
               ii. Maximum: 120 Ma + 19.008 Ma = 139.008 Ma
   d. If ZHe ages were reset at same time as AFT, the ZHe ages would fall between 122.912-139.008 Ma
5. Fission Wall [*Fitzgerald and Stump*, 1997]
   a. Slope was calculated based on AFT age versus elevation
      i. Two 'points' were chosen to derive slope
         (90 Ma, 2.6 km)
         (80 Ma, 1.4 km)
      ii. Slope = (2.6-1.4 km)/(90-80 Ma)
         =1 km/8.3 Ma
   b. If assuming minimum uplift (1.6 km)
      i. 1.6 km/ X Ma=1 km/ 8.3 Ma
         1. 1.6 km of uplift takes 13.28 Ma
         2. ZHe ages would be reset
            a. At times:
               i. Minimum: 80 Ma+13.28 Ma=93.28 Ma
               ii. Maximum: 90 Ma + 13.28 Ma = 103.28 Ma
   c. If assuming maximum uplift (4.4 km)
      i. 4.4 km/ X Ma=1 km/ 8.3 Ma
         1. 4.4 km of uplift takes 36.52 Ma
         2. ZHe ages would be reset
            a. At times:
               i. Minimum: 80 Ma+36.52Ma=116.52 Ma
               ii. Maximum: 90 Ma + 36.52 Ma = 126.52 Ma
   d. If ZHe ages were reset at same time as AFT, the ZHe ages would fall between 93.28-126.52 Ma

References Cited

Alley, R. B. (1989), Water-pressure coupling of sliding and bed deformation: I. Water system, *Journal of Glaciology, 35(119),* 108-118.

Alley, R. B., D. D. Blankenship, C. R. Bentley, and S. T. Rooney (1986), Deformation of till beneath Ice Stream-B, West Antarctica, *Nature, 322*, 57-59, doi: 10.1038/322057a0.

Alley, R. B., K. M. Cuffey, E. B. Evenson, J. C. Strasser, D. E. Lawson, and G. J. Larson (1997), How glaciers entrain and transport basal sediment, Physical constraints, *Quaternary Science Reviews, 16(9),* 1017-1038, doi:10.1016/S02773791(97)00034-6.

Alley, R. B., P. U. Clark, P. Huybrechts, and I. Joughin (2005), Ice-Sheet and Sea-Level Changes, *Science, 310(5747),* 456-460.

Anandakrishnan, S., D. D. Blankenship, R. B. Alley, and P. L. Stoffa (1998), Influence of subglacial geology on the position of a West Antarctic ice stream from seismic observations, *Nature, 394*, 62-65, doi: 10.1038/27889.

Anderson, J. B. (1999), Antarctic Marine Geology, Cambridge University Press, New York, New York.

Anderson, J. M. (1979), The geology of the Taylor Group, Beacon Supergroup, Byrd Glacier area, Antarctica, *New Zealand Antarctic Record, 2*, 6-11.

Bader, N. A. (2013), Provenance of the ice cored moraine tills at Mt. Achernar, Law Glacier, Antarctica, M.S. Thesis, Dept. of Earth Science, IUPUI, Indianapolis, Indiana.

Bahati, G., and J. F. Natukunda (2010), Status of geothermal exploration and development in Uganda, Presented at Short Course IV on Exploration for Geothermal Resources, organized by UNU-GTP, KenGen and GDC, at Lake Naivasha, Kenya, November 1-22, 2009.

Ballance, P. F., and W. A. Watters (2002), Hydrothermal alteration, contact metamorphism, and authigenesis in Ferrar Supergroup and Beacon Supergroup Rocks, Carapace Nunatak, Allan Hills, and Coombs Hills, Victoria Land, Antarctica, New Zealand *Journal of Geology and Geophysics, 45(1)*, 71-84, doi: 10.1080/00288306.2002.9514960.

Bamber, J. L., R. E. M. Riva, B. L. A Vermeersen, and A. M. LeBrocq (2009), Reassessment of the Potential Sea-level Rise from a collapse of the West Antarctic Ice Sheet, *Science, 324(5929),* 901-903.

Barrett, P. J. (1966), Petrology of some Beacon rocks between the Axel Heiberg and Shackleton glaciers, Queen Maud Range, Antarctica, *Journal of Sedimentary Petrology, 36*, 794-805.

Barrett, P. J. (1991), The Devonian to Triassic Beacon Supergroup of the Transantarctic Mountains and correlatives in other parts of America, in The Geology of Antarctica, Monogr. on Geol. and Geophys., vol. 17, edited by R. J.Tingey, pp. 120-152, Oxford Univ. Press, Oxford, U. K.

Barrett, P. J., F. J. Davey, W. U. Ehrmann, M. J. Hambrey, R. Jarrard, J. J. M. van der Meer, J. Raine, A. P. Roberts, F. Talarico, and D. K. Watkins (2000), Studies from the Cape Roberts Project, Ross Sea, Antarctica, Scientific Results of CRP-2/2A, Parts I and II, *Terra Antartica, 7(4/5).*

Barrett, P. J., C. A. Ricci, C. J. Bucker, F. J. Davey, W. U. Ehrmann, M. G. Laird, J. J. M. van der Meer, J. I. Raine, J. L. Smellie, F. Talarico, M. R. A. Thomson, K. L. Verosub, and G. Villa (2001), Studies from the CapeRoberts Project, Ross Sea, Antarctica, Scientific Report of CRP-3, Parts I and II. *Terra Antartica, 8 (3/4).*

Bell, R. E., M. Studinger, G. Karner, C. A. Finn, and D. D. Blankenship (2006), Identifying major sedimentary basins beneath the West Antarctica Ice Sheet from aeromagnetic data analysis, in Contributions to Global Earth Sciences, edited by D. K. Fütterer, D. Damaske, G. Kleinschmidt and F. Tessensohn, pp. 117-122, Springer-Verlag, Berlin Heidelberg, New York, New York.

Bentley, C. R., N. Lord, and C. Liu (1998), Radar reflections reveal a wet bed beneath stagnant Ice Stream C and a frozen bed beneath ridge BC, West Antarctica, *Journal of Glaciology, 44(146),* 149-156, doi: 10.1144/GSL.SP.2000.176.01.17.

Bernet, M., and G. Reinhard (2005), Diagenetic history of Triassic sandstone from the Beacon Supergroup in central Victoria Land, Antarctica, *New Zealand Journal of Geology and Geophysics, 48(3),* 447-458, doi:10.1080/00288306.2005.9515125.

Bialas, R. W., W. R. Buck, M. Studinger, and P. G. Fitzgerald (2007), Plateau collapse model for the Transantarctic Mountains West Antarctic Rift System, Insights from numerical experiments, *Geology, 35(8),* 687-690, doi: 10.1130/G23825A.1.

Black, L. P., S. L. Kamo, C. M. Allen, D. W. Davis, J. N. Aleinikoff, J. W. Valley, R. Mundil, I. H. Campbell, R. J. Korsch, I. S. Williams, and C. Foudoulis (2004), Improved $^{206}Pb/^{238}U$ microprobe geochronology by the monitoring of a trace-element-related matrix effect; SHRIMP, ID-TIMS, ELA-ICP-MS and oxygen isotope documentation for a series of zircon standards, *Chemical Geology, 205*, 115-140, doi: 10.1016/j.chemgeo.2004.01.003.

Blankenship, D. D., C. R. Bentley, S. T. Rooney, and R. B. Alley (1986), Seismic measurements reveal a saturated porous layer beneath an active Antarctic ice stream, *Nature, 322*, 54-57, doi: 10.1038/322054a0.

Bo, S., M. J. Siegert, S. M. Mudd, D. Sugden, S. Fujita, C. Xiangbin, J. Yunyun, T. Xueyuan, and L. Yuansheng (2009), The Gamburtsev Mountains and the origin and early evolution of the Antarctic Ice Sheet, *Nature, 459*, 690-693, doi: 10.1038/nature08024.

Borg, S., D. J. DePaolo, E. D. Wendlandt, and T. G. Drake (1989), Studies of granites and metamorphic rocks, Byrd Glacier area, *Antarctic Journal of the United States 24*, 19-21.

Brecke, D. M. (2007), Provenance of glacially transported material near Nimrod Glacier, East Antarctica: Evidence of the ice-covered East Antarctic Shield, M.S. Thesis, Dept. of Geological Sciences, University of Minnesota-Duluth, Duluth, Minnesota.

Bushnell, V. C. and C. Craddock (1970), Geologic Maps of Antarctica, Antarctica Map Folio Ser., Folio 12.

Capponi, G., B. Messiga, G. B. Piccardo, M. Scambelluri, G. Traverso, and R. Vannucci (1990), Metamorphic assemblages in layered amphibolites and micaschists from the Dessent Formation (Mountaineer Range, Antarctica), *Mem. Soc. Geol. Ital., 43*, 87-95.

Cherniak, D. J., and E. B. Watson (2001), Pb diffusion in zircon, *Chemical Geology, 172(1)*, 5-24, doi:10.1016/S0009-2541(00)00233-3.

Clark, P. U. (1987), Subglacial sediment dispersal and till composition, *Journal of Geology, 95*, 527-541.

Collinson, J. W., J. L. Isbell, D. H. Elliot, M. F. Miller, and J. M. G. Miller (1994), Permian-Triassic Transantarctic Basin, in Permian-Triassic Basins and Foldbelts along the Panthalassan margin of Gondwanaland, edited by J.J. Veevers, and C. McA. Powell, Geological Society of America Memoir, vol. 184, pp. 173-222, Boulder, Colorado.

Cox, S. E., S. N. Thomson, P. W. Reiners, S. R. Hemming, and T. van de Flierdt (2010), Extremely low long-term erosion rates around the Gamburtsev Mountains in interior East Antarctica, *Geophysical Research Letters, 37(22)*, doi: 10.1029/2010GL045106.

Coxall, H. K., and P. N. Pearson (2007), The Eocene-Oligocene transition, in Deep time perspectives on climate change: marrying the signal from computer models and biological proxies, The Micropaleontology Society Special Publications, edited by M. Williams, A. M. Hayward, F. J. Gregory, and D. N. Schmidt, pp. 351-387, The Geological Society, Bath, United Kingdom.

Crookes, W. (1879), Contributions to Molecular Physics in High Vacua, *Philosophical Transactions of the Royal Society, 170*, 641-642.

Cuffey, K. M., H. Conway, A. M. Gades, B. Hallet, R. Lorrain, J. P. Severinghaus, E. J. Steig, B. Vaughn, and J. W. C. White (2000), Entrainment at cold glacier bed, *Geology, 28*, 351-354, doi: 10.1130/0091-7613(2000)28<351:EACGB>2.0.CO;2.

Dahl, P. S. (1996), The effects of composition on retentivity of argon and oxygen in hornblende and related amphiboles: A field-tested empirical model, *Geochimica et Cosmochimica Acta, 60(19)*, 3687-3700, doi:10.1016/0016-7037(96)00170-6.

Dalrymple, E., C. Alexander, Jr., M.A. Lanphere, and G. P. Kraker (1981), Irradiation of Samples for 40Ar/39Ar Dating Using the Geological Survey TRIGA Reactor, Geological Survey Professional Paper, 1176, United States Government printing Office, Washington, D.C.

Davis, M. B., and D. Blankenship (2006), Geology of the Scott-Reedy Glaciers Area, Southern Transantarctic Mountains, Antarctica, GSA Map Series MCH093F, The Geological Society of America, Boulder, Colorado.

DeConto, R. M., and D. Pollard (2003), Rapid Cenozoic glaciation of Antarctica induced by declining atmospheric CO2, *Nature, 421*, 245-249, doi: 10.1038/nature01290.

Dits, T. M. (2013), Uncovering East Antarctic bedrock and ice sheet dynamics using till provenance of Mount Howe Blue Ice Moraines, Scott Glacier, M.S. Thesis, Dept. of Earth Science, IUPUI, Indianapolis, Indiana.

Doumani, G. A., and V. H. Minshew (1965), General geology of the Mount Weaver area, Queen Maud Mountains, Antarctica, in Geology and Paleontology of the Antarctic, Antarct. Res. Ser., vol. 6, edited by B. Hadley, pp. 127-139, AGU, Washington, D.C., doi:10.1029/AR006p0127.

Ehlers, J., and P. L. Gibbard (2004), Quaternary Glaciations: South America, Asia, Africa, Australasia, Antarctica, in Developments in Quaternary Science, part II, edited by J. Rose, Elsevier Science.

Elliot, D. H. (1975), Gondwana basins of Antarctica, in Gondwana Geology, edited by D.S.W. Campbell, Australian National University Press, pp. 493-536, Canberra, Australia.

Elliot, D. H. (1985), Physical Geography-Geological Evolution, in Key environments-Antarctica, edited by W.N. Bonner, and D.W.H. Walton, Pergamon Press, Oxford, United Kingdom, p. 39-61.

Elliot, D. H. (1992), Jurassic magmatism and tectonism associated with Gondwanaland break-up: an Antarctic perspective, in Magmatism and the causes of continental break-up, edited by B.C. Storey, T. Alabaster, and R.J. Pankhurst, Geological Society, London Special Publications, vol. 68, pp. 165-184, doi: 10.1144/GSL.SP.1992.068.01.11.

Elliot, D. H., and C. M. Fanning (2008), Detrital zircons from upper Permian and lower Triassic Victoria Group sanstones, Shackleton Glacier region, Antarctica: Evidence for multiple sources along the Gondwana plate margin, *Gondwana Research, 13(2),* 259-274, doi: 10.1016/j.gr.2007.05.003.

Elliot, D. H., and T. H. Fleming (2008), Physical volcanology and geological relationships of the Jurassic Ferrar Large Igneous Province, *Antarctica, J. Volcanol. Geotherm. Res., 172*, 20-37, doi:10.1016/j.jvolgeores.2006.02.016.

Elliot, D. H., and T. H. Fleming (2004), Occurrence and Dispersal of Magmas in the Jurassic Ferrar Large Igneous Province, Antarctica, *Gondwana Research, 7(1),* 223-237, doi: 10.1016/S1342-937X(05)70322-1.

Encarnación, J., T. H. Fleming, D. H. Elliot, and J. V. Eales (1996), Synchronous emplacement of Ferrar and Karoo dolerites and the early breakup of Gondwana, *Geology, 24(6),* 535-538, doi: 10.1130/0091-7613(1996)024<0535:SEOFAK> 2.3.CO;2.

Engelhardt, H., N. Humphrey, B. Kamb, and M. Fahnestock (1990), Physical conditions at the base of a fast moving Antarctic ice stream, *Science, 248(4951)*, 57-59, doi: 10.1126/science.248.4951.57.

Farley K. A., R. A. Wolf, and L. T. Silver (1996), The effects of long alpha-stopping distances on (U-Th)/He ages, *Geochim. Cosmochim. Acta, 60(21),* 4223-4229, doi: 10.1016/S0016-7037(96)00193-7.

Faure, G., and T. M. Mensing, (2010), The Transantarctic Mountains: Rocks, Ice, Meteorites and Water, Springer, Dordrecht, Heidelberg, London, New York.

Fitzgerald P. G. (1992), The Transantarctic Mountains of southern Victoria Land: the application of apatite fission track analysis to a rift shoulder uplift, *Tectonics, 11*, 634-662, doi: 10.1029/91TC02495.

Fitzgerald, P. G. (1994), Thermochronologic constraints on post-Paleozoic tectonic evolution of the central Transantarctic Mountains, Antarctica, *Tectonics, 13*, 818-836, doi:10.1029/94TC00595.

Fitzgerald, P. G. (2001), Apatite fission track ages associated with the altered igneous intrusive in beacon sandstone near the base of CRP-3, Victoria Land Basin, Antarctica, Terra Antartica, Bremerhaven, *Pangaea, 8(4)*, 585-592.

Fitzgerald, P. G. (2002), Tectonics and landscape evolution of the Antarctic plate since the breakup of Gondwana, with an emphasis on the West Antarctic Rift System and the Transantarctic Mountains, *R. Soc. N. Z. Bull., 35*, 453-469.

Fitzgerald, P. G., and A. J. W. Gleadow (1988), Fission track geochronology, tectonics and structure of the Transantarctic Mountains in Northern Victoria Land, Antarctica, *Isotope Geoscience, 73*, 169-198.

Fitzgerald, P. G., and E. Stump (1991), Early Cretaceous uplift in the Ellsworth Mountains of West Antarctica, *Science, 254(5028)*, 92-94, doi: 10.1126/science.254.5028.92.

Fitzgerald, P. G., and E. Stump (1997), Cretaceous and Cenozoic episodic denudation of the Transantarctic Mountains, Antarctica: new constraints from apatite fission track thermochronology in the Scott Glacier region, *Journal of Geophysical Research, 102(B4)*, 7747-7765 doi: 10.1029/96JB03898.

Fitzgerald, P. G., and S. L. Baldwin (2007), Thermochronologic constraints on Jurassic rift flank denudation in the Thiel Mountains, Antarctica, in Antarctica: A keystone in a Changing World - Online Proceedings of the 10th ISAES, edited by A. K. Cooper and C. R. Raymond et al., USGS Open-File Report 2007-1047, Short Research Paper 044, 4 p.; doi:10.3133/of2007-1047.srp044.

Fleming, T. H., A. Heimann, K. A. Foland, and D. H. Elliot (1997), $^{40}Ar/^{39}Ar$ geochronology of Ferrar Dolerite sills from the Transantarctic Mountains, Antarctica: Implications for the age and origin of the Ferrar magmatic province, *Geological Society of America Bulletin, 109(5)*, 533-546, doi:10.1130/00167606(1997)109<0533:AAGOFD>2.3.CO;2.

Fretwell, P., H. D. Pritchard, D. G. Vaughan, J. L. Bamber, N. E. Barrand, R. Bell, C. Bianchi, R. G. Bingham, D. D. Blankenship, G. Casassa, G. Catania, D. Callens, H. Conway, A. J. Cook, H. F. J. Corr, D. Damaske, V. Damm, F. Ferraccioli, R. Forsberg, S. Fujita, P. Gogineni, J. A. Griggs, R. C. A. Hindmarsh, P. Holmlund, J. W. Holt, R. W. Jacobel, A. Jenkins, W. Jokat, T. Jordan, E. C. King, J. Kohler, W. Krabill, M. Riger-Kusk, K. A. Langley, G. Leitchenkov, C. Leuschen, B. P. Luyendyk, K. Matsuoka, Y. Nogi, O. A. Nost, S. V. Popov, E. Rignot, D. M. Rippin, A. Riviera, J. Roberts, N. Ross, M. J. Siegert, A. M. Smith, D. Steinhage, M. Studinger, B. Sun, B. K. Tinto, B. C. Welch, D. A. Young, C. Xiangbin, and A. Zirizzotti, A, Bedmap2: improved ice bed, surface and thickness datasets for Antarctica, *The Cryosphere Discuss., 6*, 4305-4361, doi:10.5194/tcd-6-4305-2012, 2012.

Gehrels, G. E. (2000), Introduction to detrital zircon studies of Paleozoic and Triassic strata in western Nevada and northern California, in Paleozoic and Triassic Paleogeography and Tectonics of Western Nevada and Northern California, edited by M. J. Soreghan, and G.E. Gehrels, Geol. Soc. Am. Spec. Pap., vol. 347, pp.1-17,

Gehrels, G. (2012), Detrital zircon U-Pb geochronology: current methods and new opportunities. In: Busby, C., Azor, A. (Eds.), Tectonics of Sedimentary Basins: Recent Advances. Blackwell Publishing, 47-62, doi: 10.1002/9781444347166.ch2.

Gehrels, G., V. Valencia, and A. Pullen (2006), Detrital zircon geochronology by laser-ablation multicollector ICPMS at the Arizona Laserchron Center, in Geochronology: Emerging Opportunities, Paleontological Society Papers, edited by T. Olszewski vol. 12, pp. 67-76, The Paleontology Society, Philadelphia, Pennsylvania.

Gehrels, G., V. Valencia, J. Ruiz (2008), Enhanced precision, accuracy, efficiency, and spatial resolution of U/Pb ages by laser ablation-multicollector-inductively coupled plasma-mass spectrometry, *Geochemistry, Geophysics, Geosystems, 9(3)*, doi: 10.1029/2007GC001805.

Gleadow, A. J. W., and P. G. Fitzgerald (1987), Tectonic history and structure of the Transantarctic Mountains: New evidence from fission track dating in the Dry Valleys area of southern Victoria Land, *Earth and Planetary Science Letters, 82*, 1-14.

Goldsmith, A. S., D. F. Stockli, E. J. Pujols, C. P. Marshall (2012), The Effects of Radiation Damage as Measured by Raman Spectroscopy on Apparent (U-Th)/He Ages and He Diffusion in Zircon, GSA.

Goodge, J. W. (2007), Metamorphism in the Ross orogen and its bearing on Gondwana margin tectonics, in Convergent Margin Terranes and Associated Regions: A Tribute to W.G. Ernst, edited by M. Cloos, W. D. Carlson, M. C. Gilbert, J. G. Liou, and S. S. Sorensen, Geological Society of America Special Paper, 419, 185-203, doi: 10.1130/2006.2419(10).

Goodge, J. W. and C. M. Fanning (2002), Precambrian crustal history of the Nimrod Group, central Transantarctic Mountains: in Antarctica at the Close of a Millenium, edited by J. Gamble and D. A. Skinner, Wellington, Royal Society of New Zealand Bulletin 35, Proceedings of the 8th, International Symposium on Antarctic Earth Science, 43-50.

Goodge, J. W. and C. A. Finn (2010), Glimpses of East Antarctica: Aeromagnetic and satellite magnetic view from the central Transantarctic Mountains of East Antarctica, *Journal of Geophysical Research, 115(B9)*, 22, doi: 10.1029/2009JB006890.

Goodge, J. W., I. S. Williams, and P. Myrow (2004), Provenance of Neoproterozoic and lower Paleozoic siliciclastic rocks of the central Ross Orogen, Antarctica: Detrital record of rift-, passive- and active-margin sedimentation, *Geological Society of America Bulletin, 116(9),* 1253-1279, doi 10.1130/B25347.1.

Goodge, J. W., J. D. Vervoort, C. M. Fanning, D. M. Brecke, G. L. Farmer, I. S. Willians, P. M. Myrow, D. J. DePaolo (2008), A Positive Test of East Antarctica-Laurentia Juxtaposition Within the Rodinia Supercontinent, *Science, 321(5886)*, 235-240, doi: 10.1126/science.1159189.

Goodge, J., M. Fanning, D. Brecke, K. Licht, E. Palmer (2010), Continuation of the Laurentian Grenville province across the Ross Sea margin of Antarctica, Journal of *Geology, 118(6)*, 601-619, doi: 10.1086/656385.

Goodge, J. W., C. M. Fanning, M. D. Norman, V. C. Bennett (2012), Temporal, isotopic and spatial relations of Early Paleozoic Gondwana-margin arc magmatism, central Transtantarctic Mountains, Antarctica, *Journal of Petrology, 53(10)*, 2027-2065, doi: 10.1093/petrology/egs043.

Grindley, G. W. (1963), The Geology of the Queen Alexandra Range, Beardmore Glacier, Ross Dependency, Antarctica; with notes on the correlation of Gondwana Sequences, New Zealand Geological Survey, Department of Scientific and Industrial Research, Lower Hutt, Second Special Antarctic Issue, 6(5), 307-347.

Grove, M., and T. M. Harrison (1996), 40Ar diffusion in Fe-rich biotite, *American Mineralogist, 81*, 940-951.

Gunn, B. M., and G. Warren (1962), Geology of Victoria Land between the Mawson and Mulock Glaciers, Antarctica, *N. Z.J. Geol. Geophys., 5*, 407-426, doi:10.1080/00288306.1962.10420097.

Hambrey, M. J. (2002), Historical review of drilling in the western Ross Sea, in Future Antarctic Margin Drilling, edited by D. M. Harwood, L. Lacy, and R. H. Levy, Developing a Science Plan for McMurdo Sound in ANDRILL Science Management Office (SMO) Contribution 1, University of Nebraska-Lincoln, Lincoln, Nebraska.

Hames W. E. and S. A. Bowring (1994), An empirical evaluation of the argon diffusion geometry in muscovite, *Earth and Planetary Science Letters, 124(1-4)*, 161-169, doi: 10.1016/0012-821X(94)00079-4.

Hanchar, J. M. and C. F. Miller (1993), Zircon zonation patterns as revealed by cathodoluminescence and backscattered electron images: Implications for interpretation of complex crustal histories, *Chemical Geology, 110(1-3)*, 1-13, doi: 10.1016/0009-2541(93)90244-D.

Harrison, T. M. (1982), Diffusion of ^{40}Ar in hornblende, *Contributions to Mineralogy and Petrology, 78(3)*, 324-331, doi: 10.1007/BF00398927.

Harrison, T.M., I. Duncan, and I. McDougall (1985), Diffusion of ^{40}Ar in biotite: Temperature, pressure and compositional effects, *Geochimica et Cosmochimica Acta, 49(11)*, 2461-2468, doi: 10.1016/0016-7037(85)90246-7.

Harwood, D. M., L. Lacy, and R. H. Levy, (Eds). (2002), Future Antarctic Margin Drilling: Developing a Science Plan for McMurdo Sound. ANDRILL Science Management Office (SMO) Contribution 1, University of Nebraska-Lincoln, Lincoln, NE, pp. 301.

Hoffman, P. F. (1991), Did the breakout of Laurentia turn Gondwanaland inside-out? *Science, 252(5011)*, 1409-1412, doi: 10.1126/science.252.5011.1409.

Hoskin, P. W. O., and Black, L .P (2000), Metamorphic zircon formation by solid state recrystallization of protolith igneous zircon, *Journal of Metamorphic Geology*, *18*, 423-439.

Hourigan, J. K., P. W. Reiners, and M. T. Brandon (2005), U-Th zonation-dependent alpha-ejection in (U-Th)/He chronometry, *Geochimica et Cosmochimica Acta, 69(13)*, doi: 10.1016/j.gca.2005.01.024

Isbell, J. L. (1999), The Kukri Erosion Surface; a reassessment of its relationship to rocks of the Beacon Supergroup in the central Transantarctic Mountains, Antarctica, *Antarctic Science, 11(2)*, 226-236, doi: 10.1017/S0954102099000292.

Iverson, N. R., and D. J. Semmens (1995), Intrusion of ice into porous media by regelation: A mechanism of sediment entrainment by glaciers, *Journal of Geophysical Research, 100(B7)*, doi: 10.1029/95JB00043.

Jacobel, R. W., T. A. Scambos, C. F. Raymond, and A. M. Gades (1996), Changes in the configuration of ice stream flow from the West Antarctic Ice Sheet, *Journal of Geophysical Research, 101(B3)*, 5499-5504, doi: 10.1029/95JB03735.

Jacobs, J., C. M. Fanning, F. Henjes-Kunst, M. Olesch, and H. J. Paech (1998), Continuation of the Mozambique Belt into East Antarctica: Grenville-age metamorphism and polyphase Pan-African high-grade events in central Dronning Maud Land, *Journal of Geology, 106(4)*, 385-406, doi: 10.1086/516031.

Jaeger, J. C. (1957), The temperature in the neighborhood of a cooling intrusive sheet, *Am. Journal. Sci., 255(4)*, 306-318, doi: 10.2475/ajs.255.4.306.

Jamieson, S. S. R. and D. E. Sugden (2007), Landscape evolution of Antarctica, in Antarctica: A Keystone in a Changing World-Online Proceedings for the 10th International Symposium on Antarctic Earth Sciences, edited by A. K. Cooper et al., U.S. Geol. Surv. Open File Rep., 2007-1047.

Jezek, K., X. Wu, P. Gogineni, E. Rodríguez, A. Freeman, F. Rodriguez-Morales, and C. D. Clark (2011), Radar images of the bed of the Greenland Ice Sheet, *Geophys. Res. Lett., 38*, doi:10.1029/2010GL045519

Joughin, I., and R. B. Alley (2011), Stability of the West Antarctic ice sheet in a warming world, *Nature Geoscience, 4*, 506-513, doi: 10.1038/ngeo1194.

Kamb, B. (2000), Basal zone of the West Antarctic ice streams and its role in lubrication of their rapid motion, in The West Antarctic Ice Sheet: Behavior and Environment, Antarct. Res. Ser., vol. 77, edited by R. B. Alley and R. A. Bindschadler, pp. 157-199, AGU, Washington, D. C.

Kennett, J. P., and N. F. Exon (2004), Paleoceanographic evolution of the Tasmanian Seaway and its climatic implications, in Cenozoic Southern Ocean: Tectonics, Sedimentation, and Climate Change Between Australia and Antarctica, edited by N. F. Exon, J. P. Kennett, and M. J. Malone, Geophysical Monograph, The American Geophysical Union, Washington, D.C., pp. 345-367.

Ketcham, R. A., R. A. Donelick, and W. D. Carlson (1999), Variability of apatite fission-track annealing kinetics: III. Extrapolation to geological time scales, *American Mineralogist, 84*, 1235-1255.

Kramer, K. (2008), Provenance Study of Reedy Glacier and West Antarctic Ice Stream Tills, M.S. Thesis, Dept. of Earth Sciences, IUPUI, Indianapolis, Indiana.

Kröner , A. and R. J. Stern (2004), Pan-African Orogeny. Encyclopedia of Geology, 1, Elsevier, Amsterdam, pp 1-12.

Kyle, P. R., D. H. Elliot, and J. F. Sutter (1980), Jurassic Ferrar Supergroup tholeiites from the Transantarctic Mountains, Antarctica, and their relationship to the initial fragmentation of Gondwana, Ohio State University, Institue of Polar Studies, 394, Columbus, Ohio.

Laslett, G. M., P. F. Green, I. R. Duddy, and A. J. W. Gleadow (1987), Thermal annealing of fission track in apatite, 2. A quantitative analysis, *Chem. Geol., 65*, 1-13.

Lawrence, J. F., van Wijk, J. W., and Driscoll, N. W. (2007), Tectonic implications for uplift of the Transantarctic Mountains, International Symposium on Antarctic Earth Sciences, 1-4.

Lawver, L. A., L. M. Gahagan, and I. W. D. Dalziel (1998), A tight fit-Early Mesozoic Gondwana: a plate tectonic perspective. Origin and evolution of continents. Memoirs of the National Institute of Polar Research, Special Issue, Tokyo, National Institute of Polar Research, 214-229.

Li, Z. X., S. V Bogdanova, A. S. Collins, A. Davidson, B. De Waele, R. E. Ernst, I. C. W. Fitzsimons, R. A. Fuck, D. P. Gladkochub, J. Jacobs, K. E. Karlstrom, S. Lul, L.M. Natapov, V. Pease, S. A. Pisarevsky, K. Thrane and V. Vernikovsky (2008), Assembly, configuration, and break-up history of Rodinia: A synthesis, *Precambrian Research, 160(1-2)*, 179-210, doi: 10.1016/j.precamres.2007.04.021.

Licht, K. J., and E. F. Palmer (2013), Erosion and transport by Byrd Glacier, Antarctica during the Last Glacial Maximum, *Quaternary Science Reviews, 62*, 32-48, doi: 10.1016/j.quascirev.2012.11.017.

Licht, K. J., J. R. Lederer, and R. J., Swope (2005), Provenance of LGM glacial till (sand fraction) across the Ross Embayment, Antarctica, *Quaternary Science Reviews 24(12-13)*, 1499-1520, doi: 10.1016/j.quascirev.2004.10.017.

Lythe, M. B., and D. G. Vaughan (2001), BEDMAP: A new ice thickness and subglacial topographic model of Antarctica, *Journal of Geophysical Research, Solid Earth, 106(B6)*, 11335-11351, doi: 10.1029/2000JB900449.

Marshall, D. J. (1988), Cathodoluminescence of Geological Materials, Unwin-Hyman, Boston, Massachusetts.

Miller, S. R., P. G. Fitzgerald, and S. L. Baldwin (2010), Cenozoic range-front faulting and development of the Transantarctic Mountains near Cape Surprise, Antarctica: Thermochronologic and geomorphologic constraints, *Tectonics, 29*, TC1003, doi:10.1029/2009TC002457.

Mukasa, S. B., and I. W. D. Dalziel (2000), Marie Byrd Land, West Antarctica: Evolution of Gondwana's Pacific margin constrained by zircon U-Pb geochronology and feldspar common-Pb isotopic compositions, *Geological Society of America Bulletin, 112(4)*, 611-627, doi: 10.1130/00167606(2000)112<611:MBLWAE>2.0.CO;2.

Naish, T. R., K. J. Woolfe, P. J. Barrett, G. S. Wilson, C. Atkins, S. M. Bohaty, C. Bucker, M. Claps, F. J. Davey, G. Dunbar, A. Dunn, C. R. Fielding, F. Florindo, M. J. Hannah, D. M. Harwood, D. K. Watkins, S. Henrys, L. A. Krissek, M. Lavelle, J. van der Meer, W. C. McIntosh, F. Niessen, S. Passchier, R. D. Powell, A. P. Roberts, L. Sagnotti, R. P. Scherer, C. P. Strong, F. Talarico, K. L. Verosub, G. Villa, P-N. Webb, and T. Wonik (2001), Orbitally induced oscillations in the east Antarctic ice sheet at the Oligocene/Miocene boundary: Direct evidence from Antarctic margin drilling, *Nature, 413*, 719-723, doi: 10.1038/35099534.

Naish, T., R. Powell, R. Levy, G. Wilson, R. Scherer, F. Talarico, L. Krissek, F. Niessen, M. Pompilio, T. Wilson, L. Carter, R. DeConto, P. Huybers, R. McKay, D. Pollard, J. Ross, D. Winter, P. Barrett, G. Browne, R. Cody, E. Cowan, J. Crampton, G. Dunbar1, N. Dunbar, F. Florindo, C. Gebhardt, I. Graham, M. Hannah1, D. Hansaraj, D. Harwood, D. Helling, S. Henrys, L. Hinnov, G. Kuhn, P. Kyle, A. Läufer, P. Maffioli, D. Magens, K. Mandernack, W. McIntosh, C. Millan, R. Morin, C. Ohneiser, T. Paulsen, D. Persico, I. Raine, J. Reed, C. Riesselman, L. Sagnotti, D. Schmitt, C. Sjunneskog, P. Strong, M. Taviani, S. Vogel, T. Wilch and T. Williams (2009), Obliquity-paced Pliocene West Antarctic ice sheet oscillations, *Nature, 458*, 322-328, doi:10.1038/nature07867.

Orloff, J. (1997), Handbook of Charged Particle Optics, CRC Press, Boca Raton, Florida.
Palmer, E. F. (2008), Rock, Till, and Ice: A provenance study of the Byrd Glacier and central and western Ross Sea, Antarctica, M.S. Thesis, Dept. of Earth Sciences, IUPUI, Indianapolis, Indiana.
Palmer, E. F., K. J. Licht, R. J. Swope, and S. R. Hemming (2012), Nunatak moraines as a repository of what lies beneath the East Antarctic ice sheet, *Geological Society of America Special papers, 487*, 97-104, doi: 10.1130/2012.2487(05).
Pankhurst, R. J., S. D. Weaver, J. D. Bradshaw, B. C. Storey, and T. R. Ireland (1998), Geochronology and geochemistry of pre-Jurrassic superterranes in Marie Byrd Land, Antarctica, *Journal of Geophysical Research, 1033(B2)*, 2529-2547, doi: 10.1029/97JB02605.
Paulsen, T., J. Encarnación, V. A. Valencia, V. A., J. M. Roti Roti, and C. Rasoazanamparany (2011), Detrital U-Pb zircon analysis of an Eocene McMurdo Erratic sandstone, McMurdo Sound, Antarctica, *New Zealand Journal of Geology and Geophysics, 54(3)*, 353-360, doi: 10.1080/00288306.2011.582123.
Peters, L. E., S. Anandakrishnan, R. B. Alley, J. P. Winberry, D. E. Voigt, A. M. Smith, and D. L. Morse (2006), Subglacial sediments as a control on the onset and location of two Siple Coast ice streams, West Antarctica, *Journal of Geophysical Research, 111(B1)*, doi:10.1029/2005JB003766.
Pierce, E. L., T. Williams, T. van de Flierdt, S. R. Hemming, and S. L. Goldstein, S.A. Brachfeld (2011), Characterizing the sediment provenance of East Antarctica's weak underbelly: the Aurora and Wilkes subglacial basins, *Paleoceanography, 26(4)*, doi: 10.1029/2011PA002127.
Pollard, D., and R. M. DeConto (2009), Modeling West Antarctic ice sheet growth and collapse through the past five million years, *Nature, 458*, 329-332, doi:10.1038/nature07809.
Poller U., J. Huth, P. Hoppe, and I. S. Williams (2001), REE, U, Th, and Hf distribution in zircon from Western Carpathian Variscan granitoids: a combined cathodoluminescence and ion microprobe study, *American Journal of Science, 301*, 858-876.
Prebble, J. G., J. I. Raine, P. J. Barrett, and M. J. Hannah (2006), Vegetation and climate from two Oligocene glacioeustatic sedimentary cycles (31 and 24 Ma) cored by the Cape Roberts Project, Victoria Land Basin, Antarctica, *Palaeogeography, Palaeoclimatology, Palaeoecology, 231(1-2)*, 41-57, doi: 10.1016/j.palaeo.2005.07.025.
Price, S. F., R. A. Bindschadler, C. L. Hulbe, and L. R. Joughin (2001), Post-stagnation behaviour in the upstream regions of Ice Stream C, West Antarctica, *Journal of Glaciology, 47(157)*, 283-294.
Rahl, J. M., P. W. Reiners, I. H. Campbell, S. Nicolescu, and C. M. Allen (2003), Combined single-grain (U-Th)/He and U/Pb dating of detrital zircons from the Navajo Sandstone, *Utah Geol., 31*, 761-764, doi:10.1130/G19653.1.128.
Reiners, P.W. (2005), Zircon (U-Th)/He Thermochronometry, in Thermochronology, Reviews in Mineralogy and Geochemistry, edited by P. W. Reiners, P.W. and T. A. Ehlers, 58, 151-176, Mineralogical Society of America Geochemical Society.

Reiners, P.W., K. A. Farley, and H. J. Hickes (2002), He diffusion and (U-Th)/He thermochronometry of zircon: initial results from Fish Canyon Tuff and Gold Butte, *Tectonophysics, 349*, 297-308, doi: 10.1016/S0040-1951(02)00058-6.

Reiners, P. W., T. L. Spell, S. Nicolescu, and K. A. Zannetti (2004), Zircon (U-Th)/He thermochronometry: He diffusion and comparions with 40Ar/39Ar dating, *Geochimica et Cosmochimica Acta, 68(8)*, 1857-1887, doi: doi:10.1016/j.gca.2003.10.021.

Reiners, P. W., T. A. Ehlers, and P. K. Zeitler (2005), Past, Present, and future of Thermochronology, in Thermochronology, Reviews in Mineralogy and Geochemistry, 58, edited by P. W. Reiners and T. A. Ehlers, pp. 1-18.

Rignot, E., and R. H. Thomas (2002), Mass Balance of Polar Ice Sheets, *Science 297(5586)*, 1502-1506, doi: 10.1126/science.1073888.

Robbins, G. A. (1972), Radiogenic argon diffusion in muscovite under hydrothermal conditions, M.S. thesis, Brown University, Providence, Rhode Island, Brown University.

Roy, M., T. van de Flierdt, S. R. Hemming, and S. L. Goldstein (2007), $^{40}Ar/^{39}Ar$ ages of hornblende grains and bulk Sm/Nd isotopes of circum-Antarctic glacio-marine sediment: implications for sediment provenance in the southern ocean, *Chemical Geology, 244(3)*, 507-519, doi:10.1016/j.chemgeo.2007.07.017.

Samson S. D., and E. C. Alexander (1987), Calibration of the interlaboratory $^{40}Ar/^{39}Ar$ dating standard, MMhb1, *Chem. Geol., 66*, 27-34.

Schilling, A. (2010), Reconstructing past Antarctic ice flow paths in the Ross Embayment, Antarctica using sand petrography, particle size and detrital zircon provenance, M.S. Thesis, Dept. of Earth Sciences, IUPUI, Indianapolis, Indiana.

Schmidt, D. L., and P. D. Rowley (1986), Continental rifting and transform faulting along the Jurassic Transantarctic rift, Antarctica, *Tectonics, 5(2)*, 279-291 doi: 10.1029/TC005i002p00279.

Schmitz, M. D., and S. A. Bowring (2001), U-Pb zircon and titanite systematics of the Fish Canyon Tuff: an assessment of high-precision U-Pb geochronology and its application to young volcanic rocks, *Geochimica et Cosmochimica Acta, 65(15)*, 2571-2587, doi: 10.1016/S0016-7037(01)00616-0.

Siddoway, C. S. (2008), Tectonics of the West Antarctica Rift System: New light on the history and dynamics of distributed intracontinental extension, in Antarctica: A Keystone in a Changing World, edited by A. K., Cooper, P. J. Barrett, H. Stagg, B. Storey, E. Stump, W. Wise and the 10th ISAES editorial team (eds), Proceedings of the 10th International Symposium on Antarctica Earth Sciences: Washington, D. C., The National Academies Press. pp. 91-114, doi: 10.3133/of2007-1047.kp09.

Skinner, D. N. B., and J. Ricker (1968), The geology of the region between the Mauson and Priestley Glaciers, northern Victoria Land, Antarctica, Part 1-Basement metasedimentary and igneous rocks, *N.Z.J. Geol. Geophysics., 11*, 1009-1040.

Stacey, J. S., and J. D. Kramers (1975), Approximation of terrestrial lead isotope evolution by a two-stage model, *Earth Planetary Science Letters, 26(2)*, 207-221, doi: 10.1016/0012-821X(75)90088-6.

Steiger, R. H., and E. Jager (1977), Subcommission on geochronology: Convention on the use of decay constants in geo- and cosmochronology, *Earth and Planetary Science Letters, 36*, 359-362.

Stern, T. A., and U. S. ten Brink (1989), Flexural uplift of the Transantarctic Mountains, *Journal of Geophysical Research, 94(B8)*, 10315-10330, doi: 10.1029/JB094iB08p10315.

Stern, T. A., A. K. Baxter, and P.J. Barrett (2005), Isostatic rebound due to glacial erosion within the Transantarctic Mountains, *Geology, 33*, 221-224, doi: 10.1130/G21068.1.

Stearns, L. A., and G. Hamilton (2005), A new velocity map for Byrd Glacier, East Antarctica, from sequential ASTER satellite imagery, *Annals of Glaciology, 41*, 71-76.

Stearns, L. A., B. E. Smith, and G. S. Hamilton (2008), Increased flow speed on a large East Antarctic outlet glacier caused by subglacial floods, *Nature Geoscience, 1*, 827-831, doi: 10.1038/ngeo356.

Studinger, M., R. E. Bell, W. R. Buck, G. D. Karner, and D. D. Blankenship (2004), Sub-ice geology inland of the Transantarctic Mountains in light of new aerogeophysical data, *Earth and Planetary Science Letters, 220(3-4)*, 391-408, doi: 10.1016/S0012-821X(04)00066-4.

Stump, E., G. Gehrels, F. Talarico, and R. Carosi (2007), Constraints from detrital zircons geochronology on the early deformation of the Ross Orogeny, Transantarctic Mountains, Antarctica: U.S Geological Survey and The National Academies, USGS of-2007-1047, Extended Abstract 166.

Stump, E., and P. G. Fitzgerald (1992), Episodic uplift of the Transantarctic Mountains, *Geology, 20*, 161-164.

Stump, E. (1995), The Ross Orogen of the Transantarctic Mountains, Cambridge University Press, New York, New York.

Tessensohn, F., and R. Wörner (1991), The Ross Sea Rift System: Structures, evolution and analogues, in Geological Evolution of Antarctica Thompson, edited by M. R. A. Crame and J. W. Thompson, pp. 273-277, Cambridge Univ. Press, New York.

Thiel, E. C. (1959), Oversnow traverse programs, Byrd and Ellsworth Stations, Antarctica, 1957-1958, Seismology, gravity and magnetism, American Geographical Society, 141 p.

Thomson, S. N., P. W., Reiners, S. R., Hemming, and G. E. Gehrels (2013), The contribution of glacial erosion to shaping the hidden East Antarctic landscape, *Nature Geoscience, 6,* 203-207, doi:10.1038/ngeo1722.

Turner, F. J. (1981), Metamorphic petrology: Mineralogical and Field Aspects, 2nd edition, McGraw-Hill Book Co., New York, New York.

van de Flierdt, T., S. R. Hemming, S. L. Goldstein, G. E. Gehrels, and S Cox (2008), A case for the pan-African origin of the Gamburtsev Mountains, *Geophysical Research Letters, 35*, doi:10.1029/2008GL035564.

Vavra, G., R. Schmid, and D. Gebauer (1999), Internal morphology, habit and U-Th-Pb microanalysis of amphibolite-to-granulite facies zircons: geochronology of the Ivrea Zone (southern Alps), *Contributions to Mineralogy and Petrology, 134*, 380-404.

Veevers, J. J. (2003), Pan-African is Pan-Gondwanaland: oblique convergence drives rotation during 650-500 Ma assembly, *Geology, 31*, 501-504.

Vermeesch, P. (2004), How many grains are needed for a provenance study? *Earth And Planetary Science Letters, 224(3-4)*, 441-451, doi: 10.1016/j.epsl.2004.05.037.

Wheildon J., P. Morgan, K. H. William, T. R. Evans, and C. A. Swanberg (1994), Heat flow in the Kenya rift zone, *Tectonophysics, 236(1-4)*, 131-149, doi: 10.1016/0040-1951(94)90173-2.

Whillans, I. M., and W. A. Cassidy (1983), Catch a falling star; meteorites and old ice, *Science, 222(4619)*, 55-57.

Williams, T., T.van de Flierdt, E. Chung, M. Roy, S. R. Hemming, and S. L. Goldstein, (2010), Major Miocene changes in East Antarctica ice sheet dynamics revealed by iceberg provenance, *Earth and Planetary Science Letters, 290,* 351-361.

Wilson, T. J. (1992), Mesozoic and Cenozoic kinematic evolution of the Transantarctic Mountains, in Recent progress in Antarctic Earth Science, edited by Y. Yoshida, Terra Scientific, Tokyo, Japan.

Winberry, P. L., and S. Anandakrishnan (2004), Crustal structure of the West Antarctic rift system and Marie Byrd Land hotspot, *Geology, 32(11)*, 977-980, doi: 10.1130/G20768.1.

Zachos, J., M. Pagani, L. Sloan, E. Thomas, and K. Billups (2001), Trends, Rhythms, and Aberrations in Global Climate 65 Ma to Present, *Science, 292*, 686-693.

Curriculum Vitae

BETHANY MARIE WELKE

Education

September 2013	Master of Science in Geology Indiana University Indiana University-Purdue University, Indianapolis Indianapolis, IN Master's Thesis: "Double Dating detrital zircons from till in the Ross Embayment, Antarctica" Advisor: Dr. Kathy Licht
May 2011	Bachelor of Science in Letters and Science Major: Geoscience University of Wisconsin-Madison Madison, WI Study abroad: June-July 2009 Cegrí-International Centre for Higher Learning**:** Granada, Spain

Academic Experience

- Teaching assistant for G120-Physical Geology Laboratory at Indiana University-Purdue University
- AAPG Imperial Barrel Award Program: Exploration Potential of Nova Scotia Sub-basin
- Wasatch-Uinta Field Camp: 6 week capstone field course
- White Lake Canada field trip: 1 week mapping course in Ontario, Canada
- Senior Thesis: "A sedimentological approach to determine the sensitivity of the Greenland Ice Sheet to climate"
    - Advisor: Dr. Anders Carlson

Employment

Sept. 2010-June 2011	University of Wisconsin-Madison Quaternary and Paleoclimate Research: Cosmogenics Supervisor: Dr. Anders Carlson Madison, WI Duties: Crushing and sieving rock samples, mineral separation using Franz Magnetic Barrier, etching minerals using H_3PO_4, HCl and HF/HNO_3

May 2010-Sept. 2010	University of Wisconsin-Madison Quaternary and Paleoclimate Research: Terrestrial and Marine Sediment Supervisor: Dr. Anders Carlson Madison, WI Duties: Isolating grain sizes from two ocean cores off the coast of Greenland

Awards

- Geological Society of America Graduate Research Grant
- IUPUI School of Science Graduate Student Council Grant
- IUPUI Educational Enhancement Grant
- Wasatch-Uinta Field Camp Scholarship

Abstracts

- **Welke, B**., Hennessy, A., and Licht, K., 2012. Double dating in the Ross Embayment, Antarctica, Graduate research presentation abstract at 2012, American Geophysical Union: San Francisco, CA, 2012.
- Winsor, K., Carlson, A.E., Klinkhammer, J.P., Hoffman, J.S., **Welke, B**., 2012: Near-surface Ocean Temperatures South of 3 Greenland over the Past 400,000 Years: American Geophysical Union, San Francisco, CA, 2012.
- Reyes, A., Carlson, A.E., Beard, B., Winsor, K., Ullman, D.J., Hatfield, R.G., Stoner, J.S., **Welke, B**., 2012: Sr-Nd-Pb Isotope 4 Composition of Erik Drift Silt as a Proxy for South Greenland Ice Sheet Retreat during the Last Five Interglaciations: American Geophysical Union, San Francisco, CA, 2012.

Skills

- Operating systems: Advanced skills in a variety of Windows and Mac operating systems
- Software: Microsoft Office suites (advanced), Adobe Acrobat and Photoshop (advanced), ESRI ArcGIS (intermediate), ENVI (beginner), PAST (advanced), SigmaPlot (intermediate), Grapher (advanced)
- Additional languages: Spanish (Intermediate levels of speech, comprehension, reading and writing ability)

Professional Affaliations

- Geological Society of America
- American Association of Petroleum Geologists
- American Geophysical Union

Service

- March 2013: Volunteer for the Curiosity, Confidence, Challenge: a conference designed to support girls' interest in science, technology, engineering, and math
- November 2012: Hosted Weebelos (Boy Scouts) to IUPUI: taught basic geology and helped the students work on various geology activities to earn their geology badge
- June 2012: Volunteer for the Transantarctic Mountains Camp (TAM camp) workshop
- September 2011-August 2012: IUPUI Heath & Wellness Team Graduate Student Representative
- September 2011-August 2012: IUPUI School of Science Earth Science Graduate Student Representative
- September 2011-August 2012: IUPUI Graduate and Professional Student Government Representative